5-2010

Robotic Simulation of Disc Arthroplasty Surgery: Influence of Surgical Placement on Motion Segment Dynamics

Braham K. Dhillon
University of Tennessee Health Science Center

Robotic Simulation of Disc Arthroplasty Surgery: Influence of Surgical Placement on Motion Segment Dynamics

DOI
10.21007/etd.cghs.2010.0069

ROBOTIC SIMULATION OF DISC ARTHROPLASTY SURGERY: INFLUENCE OF SURGICAL PLACEMENT ON MOTION SEGMENT DYNAMICS

A Thesis
Presented for
The Graduate Studies Council
The University of Tennessee
Health Science Center

In Partial Fulfillment
Of the Requirements for the Degree
Master of Science
In the Joint Graduate Program in Biomedical Engineering and Imaging
From The University of Tennessee
and
The University of Memphis

By
Braham K. Dhillon
May 2010

DEDICATION

In appreciation of my loving grandmother
Gurbachan Kaur Dhillon

ACKNOWLEDGEMENTS

To my researcher advisor, Dr. Brain P. Kelly, I extend my deepest gratitude and respect. His experience, motivation, and patience allowed me to uncover my potential as a researcher and engineer. In addition, I would like to thank my committee members, Dr. Denis J. DiAngelo and Dr. Gladius Lewis. Their feedback and recommendations are a reflection of their interest in the subject matter and superb perception. Furthermore, I am indebted to Dr. Rudolf Bertagnoli, whose clinical experience and expertise with total disc replacement devices made this work possible.

I would also like to recognize the Biomechanics Tissue Testing Laboratory, especially my colleague Daniel M. Wido. He has contributed to this work in a number of invaluable ways, from tissue preparation and testing to designing a testing protocol.

The Medical Education & Research Institute and Synthes Spine are acknowledged for their assistance in the use of the surgical facility and use of surgical instrumentation, respectively.

On a personal note, I would like to express thanks to my beloved parents, Sukhdev S. Dhillon and Parminder R. Dhillon. Their support, love, and guidance throughout my life have made me the person that I am. To my loving sister, Bira, and comical brother, Bamu, I would like to express gratitude for keeping me inspired and motivated. Lastly, I would like to thank my family and friends for all the unknown ways in which they have contributed.

ABSTRACT

A variety of total disc replacement (TDR) designs exist for the treatment of disc pathologies. A key design parameter for a constrained ball and socket device is the location of the fixed center of rotation (COR). A previous study demonstrated that intact motion segment unit (MSU) mechanics and range of motion (ROM) were sensitive to the location of a prescribed sagittal plane rotational axis. Mal-alignment between the implant COR and the COR of the MSU may lead to an overloaded or over constrained condition.

Two paradigms exist for the placement of a fixed COR TDR device relative to MSU anatomy: positioning the implant midline or posterior to midline. Presently, there are no data to indicate which paradigm may lead to better biomechanical/clinical outcome. This research attempts to evaluate changes in MSU mechanics and ROM as a result of variations in the size and placement of a simulated ball and socket TDR, like the ProDisc-L lumbar disc prosthesis.

Six human cadaveric lumbar MSUs, L4-L5, were tested in flexion/extension using the Spine Robot to an end load limit of 8Nm. A fixed axis protocol was used to impose a pure rotation about a desired anatomical location. The Spine Robot was programmed to rotate the MSU about the COR of the implant. Subsequently, with the MSU held rigid, the implant was removed and rotation about the implant's COR was repeated. Thereafter, simulated CORs were tested in different anatomical locations as defined by a customized grid pattern. The grid pattern consisted of 8 CORs which simulated the placement of a medium and large size constrained ball and socket device. Measurements of shear forces along the disc plane, axial force normal to the disc plane, segmental bending moment, and segmental ROM were analyzed at each grid point.

Analysis of MSU mechanics and ROM for the ProDisc-L and Simulated Implant cases revealed that the two conditions were not comparable. Transfer of tissue pretension from the implant to the Spine Robot on removal of the implant, and dynamic contact forces at the implant surfaces were the contributing factors to the differences observed.

Simulated COR testing demonstrated that the posterior tissue response was sensitive to varying placements of the simulated implant. For both implant sizes, posterior positioning of the COR required distraction of the disc space. During flexion, posterior positioning resulted in significantly higher shear and axial forces as well as a trend for reduced ROM. ROM in flexion may have been influenced by different starting positions within the neutral zone due to disc space distraction. During extension, the posterior placement of the COR reduced loading and increased rotation suggesting better alignment with, or separation of the facet joints.

This novel study was able to delineate significant differences in spinal tissue response to varying simulated sizes and placements of an ideal fixed COR TDR device. The results of this study suggested that with both implant sizes the posterior placement of the COR will tend to distract the disc space and provide significantly increased ROM in extension at the expense of increased loads on posterior ligaments in flexion.

TABLE OF CONTENTS

LIST OF TABLES

LIST OF FIGURES

LIST OF ABBREVIATIONS

ALIF	anterior lumbar interbody fusion
ALL	anterior longitudinal ligament
AP	anterior-posterior
ASD	adjacent segment disease
COR	center of rotation
DOF	degrees of freedom
FCL	facet capsular ligament
IDE	investigational device exemption
ISL	interspinous ligament
ITL	intertransverse ligament
LBP	lower back pain
LF	ligamentum flavum
MSU	motion segment unit
NA	nucleus arthroplasty
ODI	oswestry disability index
PD	proximal-distal
PDS	posterior dynamic stablization
PLL	posterior longitudinal ligament
SSL	superaspinous ligament
TDR	total disc replacement
VAS	visual analogue scale

CHAPTER 1: INTRODUCTION

Lower back pain (LBP) is a prevailing condition that will affect a majority of the population at some point in their life. A systematic review for the presence of adult back pain reported a point prevalence of 15%-30%, a 1-month prevalence of 19% to 43%, and a life-time prevalence of 60% to 70% (1). Other epidemiological studies, compiled from surveys and doctor visits, reported similar findings (2,3,4). Furthermore, these studies have shown that the presence of LBP is independent of age, sex, race; and is equal among the various social and economic division (5,6).

For most individuals suffering from LBP, the term is an all encompassing condition that presents a wide range of symptoms and pathologies, often in the absence of any clinically identifiable cause. For example, the presence of a herniated disc has been documented in individuals who have been asymptomatic for LBP, whereas persons exhibiting normal biomechanical function have reported debilitating pain. Furthermore, the lack of sensitivity and specificity of clinical tests, in addition to the unknown contributions of the natural aging process, make treatment of LBP problematic (1). Unable to determine the source of the LBP, clinicians are faced with the task of diagnosing patients according to their own theories and judgment.

For a portion of the population, LBP is a result of various pathological states whose causality has been proven by evidence-based studies. These studies have identified pathologies such as intervertebral disc herniation and degeneration, zygapophysial joint osteoarthrosis, spinal stenosis, spondylolisthesis, and segmental instability as a potential source of LBP (1). Moreover, the mechanical failure of the intervertebral disc has been identified as probable common thread among these pathologies (7,8,9). For this portion of the population, clinicians have an assortment of treatment options, ranging from conventional methodologies, such as pain medication, spinal manipulation, and steroid shots, to the more aggressive approach of surgical intervention.

Approximately 1% to 3% of people suffering with lower back pain will require surgical intervention and about 40% of those interventions will be caused by disc disruption (1,5,7). While there are several treatment options for pain due to a degenerating disc, the conventional surgical treatment remains the arthrodesis, or fusion, of the motion segment unit (10,11,12). The goal of arthrodesis is to restore the disc height and provide stability to the spine following decompression of the neural elements. While the rate of successful fusion is high, it is at the expense of potentially degenerating the discs and facet joints at the adjacent levels due to increased motion at those levels as a result of the loss of motion at the treated level (10,11,12,13,14).

To address the limitations of fusion, total disc replacement (TDR) devices have been proposed. The goal of TDRs is analogous to spinal fusion, where it aims to restore disc height and provide stability to the motion segment unit (MSU). The advantage of a TDR over spinal fusion is its potential ability to reduce or prevent adjacent level segment disc disease while preserving spinal motion at the treated level (15,16,17). However, TDR devices are in the early stages of development and research, and although clinical

and biomechanical data indicate promising results, the long term benefits of TDRs compared to fusion have not been delineated (18,19,20).

Presently, a variety of lumbar TDR designs exist and a few have undergone clinical trials within the United States. As these devices mature and come to the market, surgeons will be faced with a verity of prostheses, each based on a different biomechanical design philosophy. A key design parameter for a constrained ball and socket type device, like the ProDisc-L (Synthes Spine, West Chester, PA), is its fixed center of rotation (COR). A previous study demonstrated that the lumbar motion segment unit was highly sensitive to the anatomical location of the sagittal plane rotational axis (21). Mal-alignment between the implant COR and the inherent rotational axis of the MSU may lead to an overloaded or over-constrained condition. As such, placement of the TDR axis with respect to vertebral anatomy at the time of surgery may have a significant impact on the mechanical loading of adjacent vertebral structures and on the implant itself. Potential concerns include bone remodeling, implant subsidence, implant failure and loosening, wear debris generation, soft tissue destruction, and facet degeneration.

Currently there are no strict guidelines for the surgical placement of a TDR device. The clinical education and experience of most surgeons is to position the TDR device midline. Dr. Bertagnoli, a prominent European spine surgeon, advocates the posterior to midline positioning of the implant such that the arc of motion of the proximal vertebra is better aligned with the arc of curvature of the facet joints. Furthermore, his clinical data suggests that the posterior placement of the TDR at the time of surgery may lead to a better clinical outcome. However, there are no biomechanical studies on the effects of implant placement on motion segment dynamics that can collaborate his clinical findings.

The purpose of the current study were (1) to simulate an ideal constrained ball and socket device, like the ProDisc-L disc prosthesis, by comparing the MSU response to a fixed kinematic rotational input about the COR of the ProDisc-L implant in place and subsequently about the exact same COR with the ProDisc-L implant removed and (2) to investigate the influence of implant size and variation in the surgical placement of the fixed center of rotation of the simulated ball and socket device on lumbar segment dynamics. It is hypothesized that variations in placement of the COR with respect to lumbar vertebral anatomy will induce significant differences in segmental MSU load mechanics and ranges of motion.

CHAPTER 2: BACKGROUND

This chapter is subdivided into several sections, each of which presents relevant information related to the research. The first section introduces the anatomy of the human spinal column, providing a brief synopsis about the structure and function of the vertebrae, intervertebral disc, spinal ligaments, and muscles. The second section dwells into the kinematics of a lumbar MSU by describing the quantity and quality of spinal motion. The third section highlights spinal mechanics, where importance is given to identifying the forces and moments generated by the MSU. Thereafter, disc degeneration and the corrective surgical options available for treatment are presented. The final section describes current biomechanical testing protocols and their limitations in testing TDRs.

The Spinal Column

The human spinal column is a part of the musculoskeletal system and consists of a series of thirty-three vertebrae extending from the base of the skull to pelvic girdle. The vertebrae are organized into four distinct regions depending on their size and function: seven cervical, twelve thoracic, five lumbar, and a sacral region consisting of five fused sacrum segments and four fused coccyx segments. Excluding the first and second vertebrae of the cervical region and the fused vertebrae of the sacral region, the remaining twenty-two vertebrae are separated by an intervertebral disc.

Figure 2-1, shows an anterior, posterior, and lateral view of the adult spinal column. From a posterior view the spine appears to be vertically straight; however the lateral view reveals the spine's natural curvature. The curvature of the spine exhibits lordosis in the cervical and lumbar regions and kyphosis in the thoracic and sacral regions. These curvatures are assumed to function in the distribution of mechanical stresses and the maintenance of the global axis of the body (23). Furthermore, Figure 2-1 illustrates that the basic structure for the vertebrae does not change from the cervical to the lumbar region in the spinal column. However, there is an increase in the size and mass of the vertebrae descending caudally. The subsequent increase in size and mass of the vertebra is a mechanical adaption to the progressive increase in load to which the vertebral bodies are subjected (23). Additionally, there is a variation in the angulation of the facet joints descending caudally, where the anatomical orientation of these joints determines the pattern of movement and range of motion of the vertebrae.

As a collaborative unit, the human spinal column functions (1) to provide strength and support to the remaining structures of the body, (2) to sustain and distribute the forces placed on the spine, (3) to permit multi-axis motion for the head and trunk, and (4) to protect the nerves of the spinal cord (24). The execution and maintenance of these functions are shared among several distinguished substructures: the vertebrae, the intervertebral disc, the facet joints, muscles, and ligaments. The discussion of these substructures will be limited to the lumbar region and their role in spinal biomechanics will be thereafter addressed. Discussion on the anatomy for the other regions of the spine can be found elsewhere (23,25).

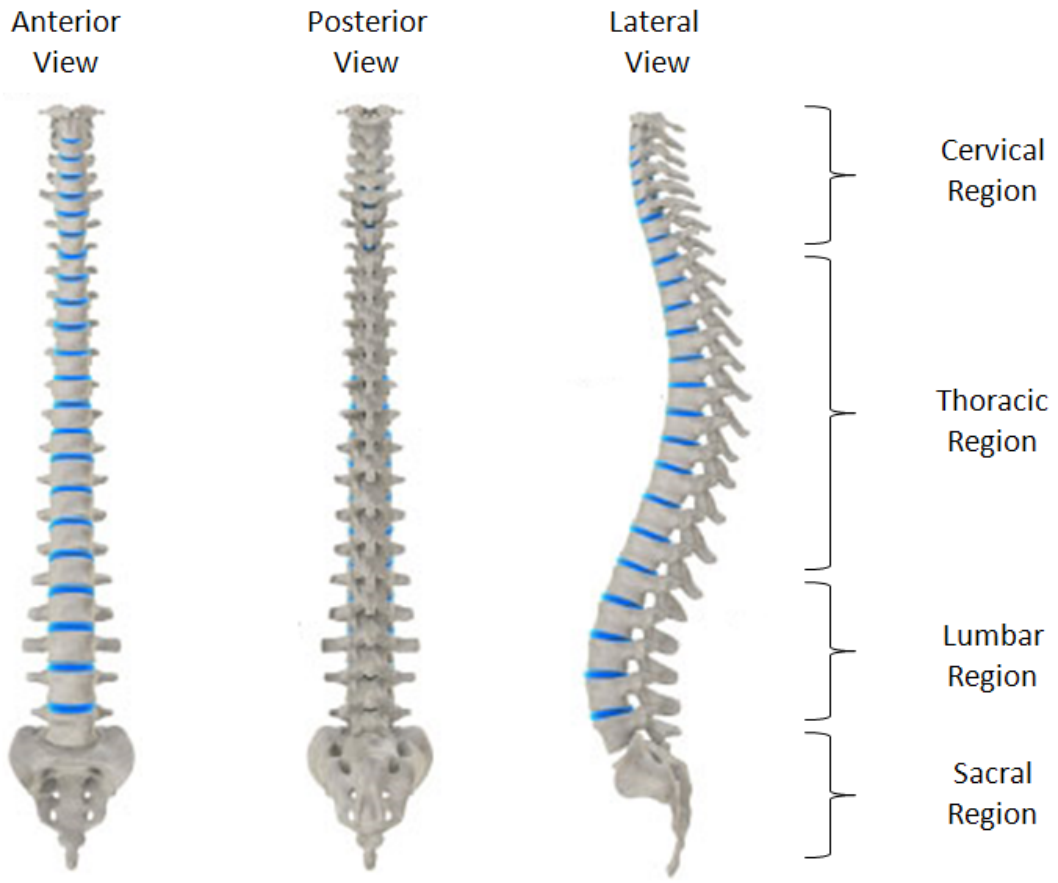

Figure 2-1: The Human Spinal Column. The anterior and posterior views suggest that the spinal column is vertically straight, with increasing vertebral thickness descending caudally. The lateral view reveals the spines natural curvature; lordosis in the cervical and lumbar regions and kyphosis in the thoracic and sacral region. [Source: Adapted with permission. Back Anatomy. http://www.bigbackpain.com/back_anatomy.html. Accessed April 23, 2010.]

The Lumbar Vertebrae

The vertebrae of the lumbar region are referenced as L1 through L5, as shown in Figure 2-2A. Two adjacent vertebrae, interspaced with an intervertebral disc, and surrounded by the paravertebral musculature comprise a motion segment unit (MSU), as shown in Figure 2-2B (23,26).

Structure

The lumbar vertebra, shown in Figure 2-3, can be divided into two separate regions. Anteriorly, the lumbar vertebra is composed of a kidney-shaped mass of bone called the vertebral body which functions as the primary load bearing structure in the spinal column. It is typically greater in width than in depth. Mean quantitative values of the vertebral dimensions are provided in Table 2-1. Structurally, the vertebral body is composed primarily of cancellous bone, a low density and strength osseous tissue but with a high surface area. Surrounding the cancellous bone is a thin, dense sheath of cortical bone. The compressive loads placed on the vertebral body are shared amongst these tissues. While mechanically stronger than the cancellous bone, the cortical bone is thought to make only a small contribution to the overall strength of the structure (23).

Posteriorly, the lumbar vertebra is comprised of various small bones, which are collectively referred to as the posterior elements. They are primarily composed of cortical bone with very little cancellous bone. The posterior elements are joined to the posterior surface of the vertebral body by two short, thick processes called the pedicles. These bones function to transmit the loads from the vertebral body to the posterior elements. Sloping caudally and midline from each of the pedicles are two broad plates called the lamina, which fuse into the spinous process, a dorsally projected wide, flat bone. Together, the pedicles and the lamina form the neural arch, which in conjunction with the vertebral body create an enclosed space termed the vertebral foramen. The vertebral foramen is a canal space in which the neural elements are housed and protected (1,23).

Projecting laterally from the junction of the pedicle and lamina is a long, flattened, rectangular bone called the transverse process. The posterior surface of this bone serves as the attachment sight for muscles and ligaments. Arising from the junction of the pedicle and lamina are two superior and two inferior articular processes, each of which bear a smooth, flat lateral surface. The superior articular processes interlock with the inferior articular process from the vertebra above to form the zygapophysial or facet joint. Similarly, the inferior articular processes interlock with the superior articular process from the vertebrae below. These joints serve to stabilize the spine by linking the vertebrae together and to control the motion patterns during bending (1,23).

Function

The facet capsular or zygapophysial joints have a unique shape and orientation which allows them to stabilize the spine. Their angulations in the sagittal plane prevent

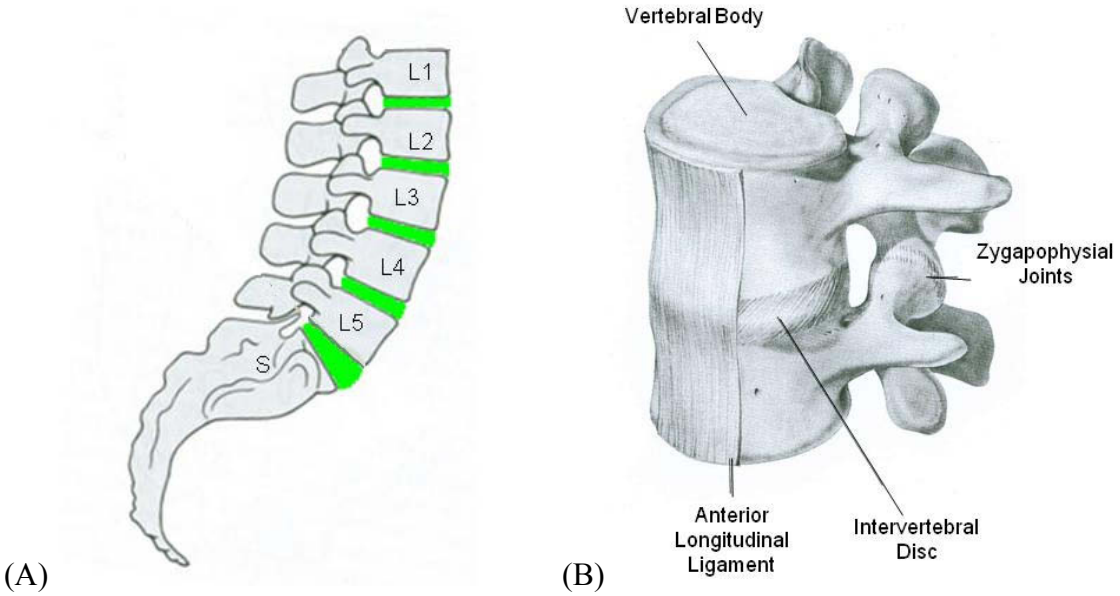

(A) (B)

Figure 2-2: The Vertebrae of the Lumbar Spine and Lumbar Motion Segment Unit. (A) The lumbar region of the human spinal column has five motion segment units, referenced from L1 to S. [Source: Adapted with permission. Adams M, Bogduk N, Burton K, and Dolan P. The Biomechanics of Back Pain. London: Elsevier Science Limited 2002; Page 133.] (B) A motion segment unit consists of two adjacent vertebral bodies, interspaced with an intervertebral disc, connective tissue, ligaments, and surrounded by the paravertebral musculature. [Source: Reprinted with permission. DePalma A. and Rothman R. The Intervertebral Disc. Philadelphia: W.B Saunders Company 1970; Page 59.]

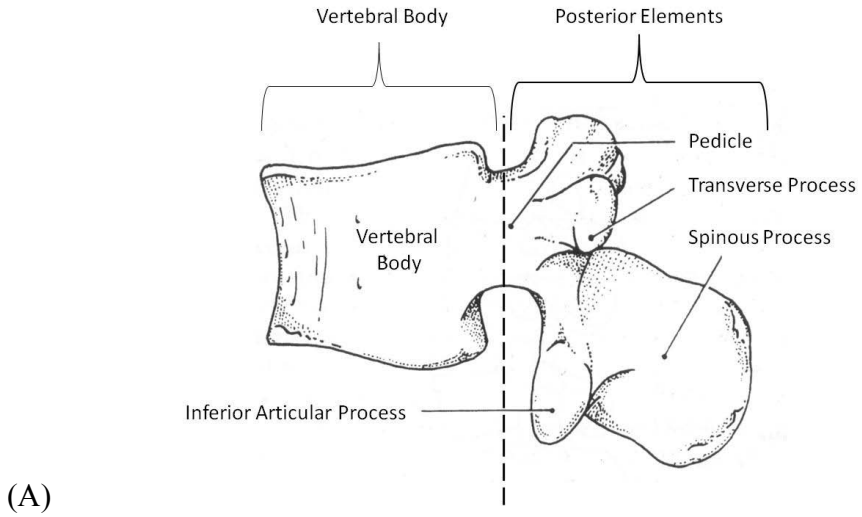

(A)

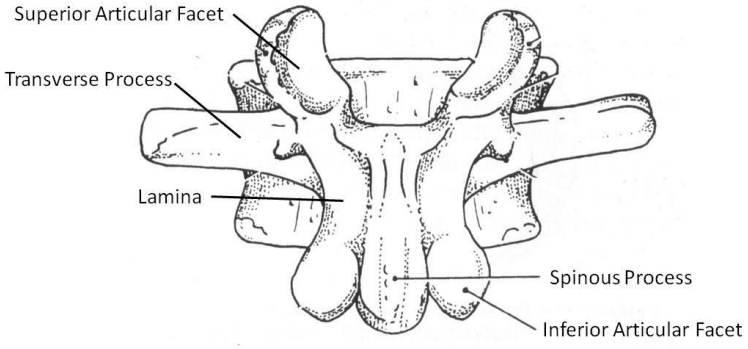

(B)

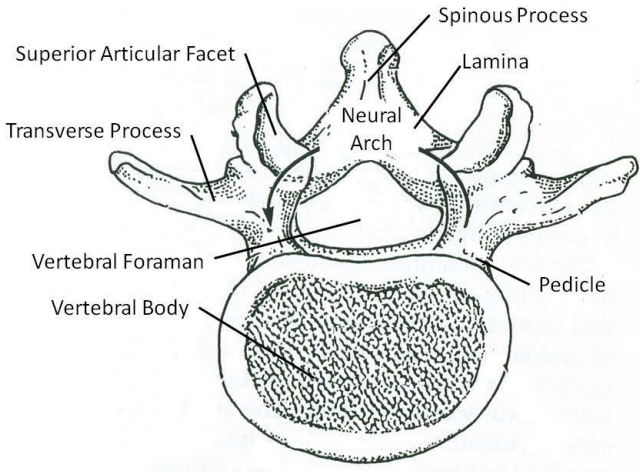

(C)

Figure 2-3: Structure of the Lumbar Vertebra. (A) Lateral view, (B) Posterior view, and (C) Inferior view. [Source: Adapted with permission. Adams M, Bogduk N, Burton K, and Dolan P. The Biomechanics of Back Pain. London: Elsevier Science Limited 2002; Page 19.]

Table 2-1: **Anthropometric Values of the Lumbar Vertebral Body.**

Vertebra	N	Parameters (mm) Means ± SD			
		A	B	C	D
L1	154	34.1±2.9	25.4±2.2	33.5±2.8	27.1±2.1
L2	157	34.7±3.0	27.2±2.0	34.4±2.9	27.0±2.1
L3	157	34.6±2.8	27.9±2.1	34.7±2.7	27.9±2.1
L4	157	34.9±2.8	27.4±2.2	34.3±2.7	27.1±2.3
L5	156	33.9±2.7	28.3±2.1	34.2±2.7	25.7±2.5

Note: N, number of measurements; A, inferior width of the vertebral body; B, anterior height of the vertebral body; C, superior width of the vertebral body; D, posterior height of the vertebral body. [Source: Adapted with permission. Gilad I and Nissan M. Sagittal Evaluation of Elemental Geometrical Dimensions of Human Vertebrae. Journal of Anatomy 1985; 143:115-120.]

excessive extension and anterior-posterior translation whereas their angulation in transverse planes prohibits excessive axial rotation and lateral bending. The orientation of the facet joints vary gradually with each lumbar level, in both the sagittal and transverse planes (1,23,28). As shown in Figure 2-4, the facet joints are relatively vertical at the L1-L2 level in the sagittal plane and become increasing more oblique descending down to the L5-S1 level (30 deg). In the transverse plane, the facet angles increase relative to the midline of vertebra. Oriented at 25 degrees at the L1-L2 level, the facet angles increase steadily to about 53 degrees at the L5-S1 level.

Figure 2-5 provides an illustration of the facet engagement in various modes of bending. In flexion the facet joints play a negligible role in resisting motion. As the vertebral body rotates, the superior facets are unopposed to travel in the proximal-distal (PD) direction. The intervertebral ligaments provide most of the resistance in flexion, with some contribution from the intervertebral disc (1,23). In extension, the facets permit motion in the PD direction, but limit its range. Excessive motion is prevented through the contact of the inferior most aspect of the facets of the upper vertebra with the lamina of the sub-adjacent vertebra. Any further extension, beyond this limit, causes the inferior facets to be deflected posteriorly as they begin rotate about the pars interarticularis. Aside from the facet joints, extension motion is restricted by contributions from the intervertebral disc and the anterior longitudinal ligament (1,23).

Resistance to lateral bending occurs via engagement of the facet joint on the ipsilateral side of the bend. This resistance is likely secondary to the influences of the intervertebral disc, but greater than the contributions of the intertransverse ligaments. It is important to note that pure lateral bending is not typically observed clinically; it is naturally coupled to axial rotation (1,23).

Axial rotation is naturally coupled to lateral bending and therefore its resistance to motion is similar to lateral bending. Axial rotation is permitted until the articulating surfaces of one facet joint engage on one side while the capsular ligaments are in tension on the contra-lateral side. For example, in right axial rotation, the facets of the left capsular joint will contact and generate compressive stresses, whereas the facets of the right capsular joint will be in tension. The contribution of facet joint in preventing axial rotation is a topic of controversy. Some researchers believe that torsion is resisted more by the bony contact of the facet surfaces than by the ligaments, while others insist that the annulus fibrosus is the primary restraint in this mode of bending (1,23).

Aside from limiting rotation, the shape and orientation of the facet joints also limit forward translation of the vertebra during excessive shear loading. The superior aspects of the facet joints on the subjacent vertebra hook and lock the inferior aspects of the joints on the superior vertebra, thereby shielding the disc from excessive shear forces and maintaining the spatial integrity of the neural arch (1,23).

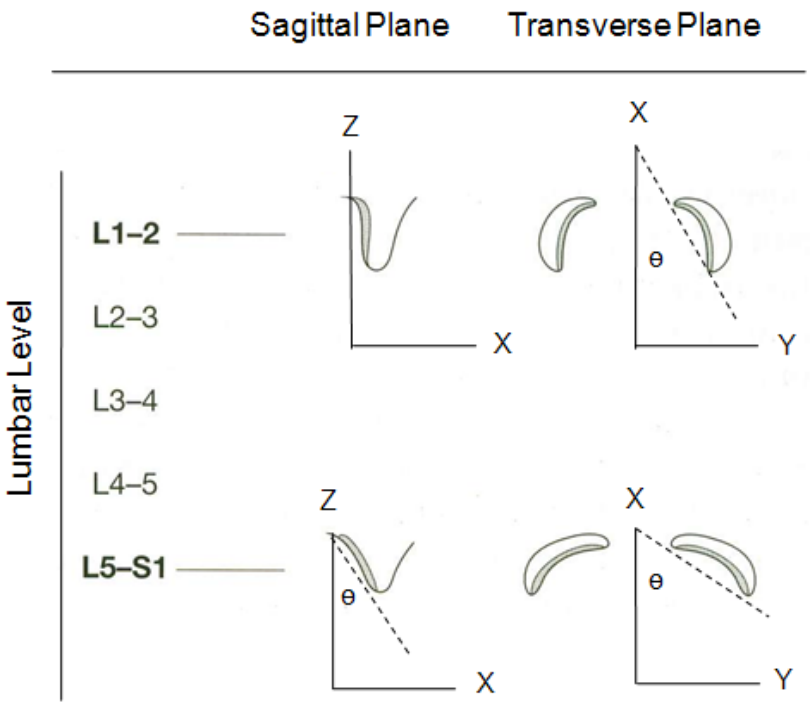

Figure 2-4: Facet Joint Angles. Facet joint angles increase descending down the vertebral column in both the sagittal and transverse planes. [Source: Reprinted with permission. Adams M, Bogduk N, Burton K, and Dolan P. The Biomechanics of Back Pain. London: Elsevier Science Limited 2002; Page 117.]

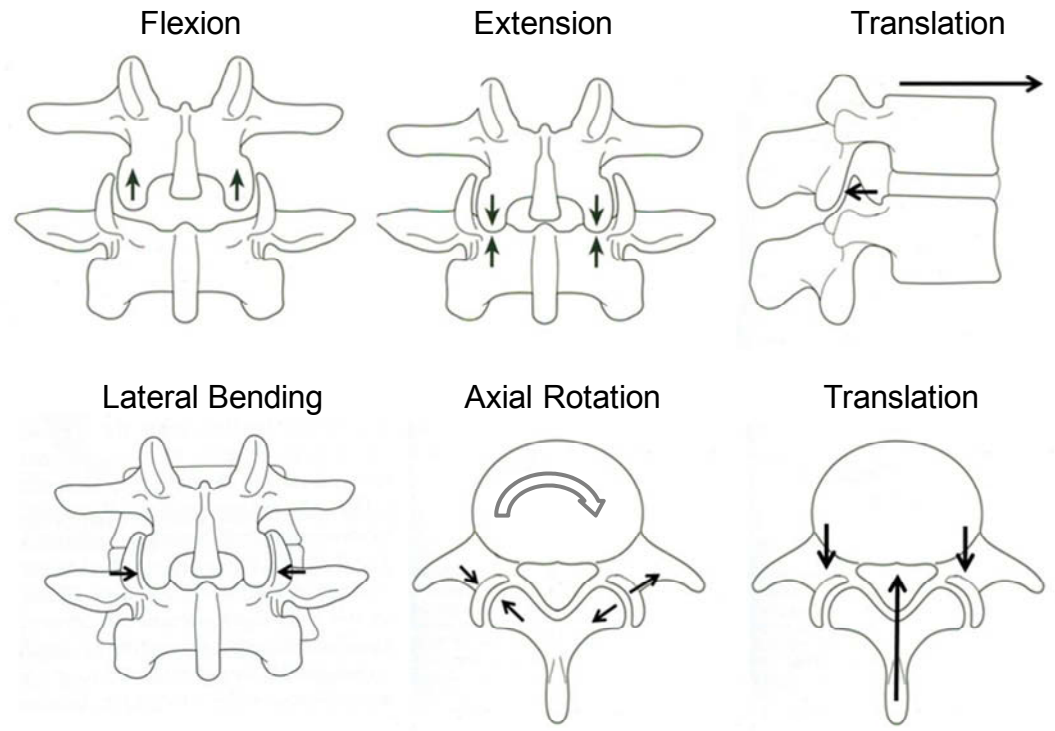

Figure 2-5: Facet Engagement in Various Modes of Bending. The engagement of the facets limit motion in different modes of bending. [Source: Adapted with permission. Adams M, Bogduk N, Burton K, and Dolan P. The Biomechanics of Back Pain. London: Elsevier Science Limited 2002; Pages 23-24.]

The Intervertebral Disc

Structure and Composition

The intervertebral disc, shown in Figure 2-6, is a viscoelastic structure located in-between adjacent vertebral bodies of the spine. In the lumbar region, the intervertebral disc accounts for 20-33% of the entire height of the vertebral column (26). Its primary function is three fold: (1) to carry and distribute the loads and forces placed on the spine, (2) to perform like a multi-axis joint that allows translational and rotational motion, and (3) to act as ligament by physically connecting the superior and inferior vertebral bodies together into a functional unit (29). The execution and maintenance of these functions of the spinal disc are shared among three distinguished substructures: the nucleus pulposus, the annulus fibrosus, and the end-plate.

The nucleus pulposus is a well hydrated, gel-like structure composed primarily of fibrous strands of proteoglycans and to a lesser extent type II collagen fibers and elastin (29). It occupies 30-50% of the disc space and is positioned slightly posterior from the center of the disc space (1,23,29). The nucleus is laterally surrounded by the annulus fibrosus and is contained superiorly and inferiorly by the cartilaginous end-plate.

Proteoglycans are heavily glycosylated proteins that are arranged into a specialized structure called aggrecans. They interact with hyaluronic acid and give rise to negatively charged aggregates. These aggregates interact with water molecules and provide the nucleus with the hydrostatic pressure needed to support vertebral loads. The collagen fibers, on the other hand, provide the nucleus with tensile strength. They are arranged randomly throughout the disc and interact with elastin to anchor nuclear tissue to bone (1,15,23).

Surrounding the nucleus pulposus are 15-25 concentric lamellae of the annulus fibrosus. The annulus fibrosus, shown in Figure 2-7, assists the nucleus in the axial support of the body weight (29,30). The lamellae rings are composed of sheets of collagen fibers; running in parallel and oriented 30 degrees from disc plane. Furthermore, the direction of the collagen fibers alternates between adjacent lamellae, forming an angle of 120 degrees between the two sheets (23,29). This structured orientation of the collagen fibers assists the disc in restricting excessive lateral translation and axial rotation.

The extracellular makeup of the annulus fibrosus is reflective of the nucleus pulposus, although to varying proportions. Maintained by fibroblast-like cells, the annulus fibrosus is primarily composed of water (65%) and proteoglycan aggrecan aggregates (20% of the dry weight) (30). Like the nucleus, the annulus has elastin fibers (10%) which are arranged radially to adhere adjacent lamellae together. Unlike the nucleus, the annulus possesses both type I and type II collagen fibers (55% of the dry weight). Type I collagen is found throughout the annulus, whereas type II collagen is restricted to the inner portions (29,30).

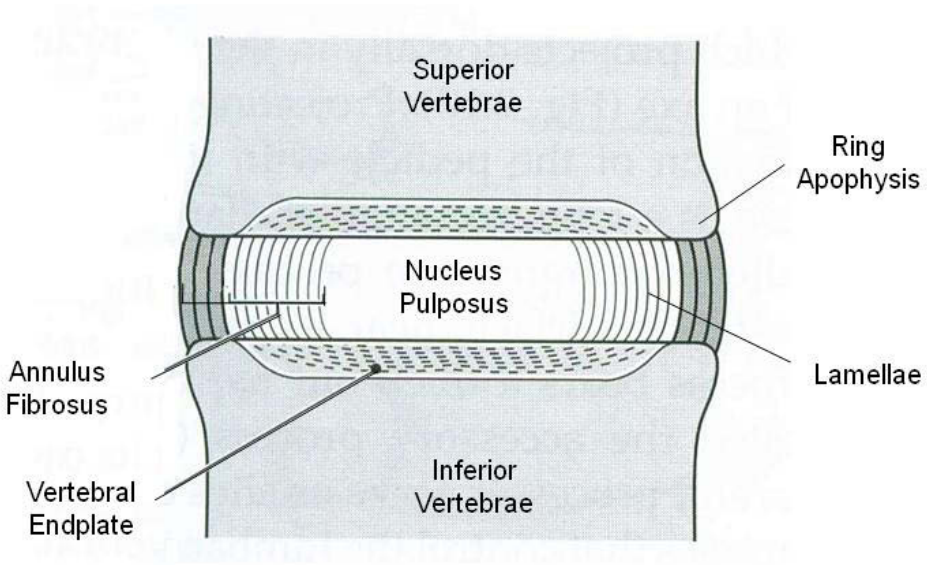

Figure 2-6: The Intervertebral Disc. The basic structure of the lumbar disc consists of the nucleus pulposus surround by the annulus fibrosus; both of which are sandwiched superior and inferiorly between the vertebral endplates. [Source: Adapted with permission. Adams M, Bogduk N, Burton K, and Dolan P. The Biomechanics of Back Pain. London: Elsevier Science Limited 2002; Page 17.]

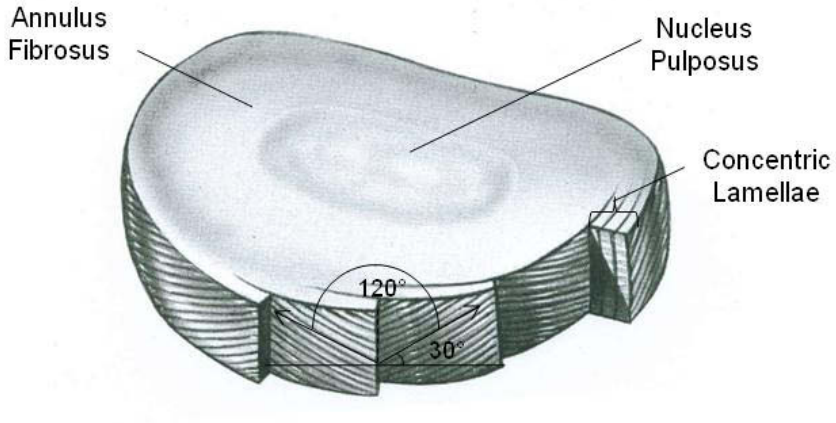

Figure 2-7: Architecture of the Annulus Fibrosus. Adjacent lamellae have collagen fibers oriented in different directions and angulated 30° relative to the horizontal datum plane. [Source: Adapted with permission. DePalma A. and Rothman R. The Intervertebral Disc. Philadelphia: W.B Saunders Company 1970; Page 13.]

The superior and inferior caps to the spinal disc are the cartilaginous end-plates. The end plates are connected to the lamellae of the annulus fibrosus and encapsulate the nucleus pulposus. The end-plates do not completely cover the vertebral disc space but leave a ring of exposed bone called ring apophysis. The ring apophysis is where the lamellae fibers of the annulus anchor to the subchondral bone (23,26,29).

The endplate is horizontal layer of hyaline cartilage that is less than 1mm in thickness and composed of the same extracellular matrix as the rest of the disc. Their collagen fibers run horizontal and parallel to the vertebral bodies and are interwoven into the annulus of the intervertebral disc (9,30).

Function

The intervertebral disc behaves as a single functional unit in limiting motion through the collaborative efforts of the nucleus pulposus and the annulus fibrosus. As shown in Figure 2-8, compressive loading of the disc reduces its height and creates an increase in the hydrostatic pressure of the nucleus. The hydrostatic pressure pushes the contents of the annulus outwards and creates a radial tensile stress in the annulus, which functions to simultaneously support the load placed on the vertebral body and resist motion (1,23,28).

The nucleus pulposus is a gelatinous structure whose unique structural properties allow it to deform easily in any direction and equalize any stresses applied to it. Due to its low rigidity, the nucleus cannot resist motion during bending; that responsibility is given to the annulus fibrosus (28).

The annulus fibrosus' functionality in resisting motion is dependent on the collagen content and fiber orientation of the comprising lamellae. The lamellae of the outer annulus are comprised primarily of type I collagen and provide the greatest resistance to motion. The lamellae of the inner annulus, composed of both type I and type II collagen fibers, function to resist high compressive loads by transmitting the hydrostatic pressure of the nucleus to the exterior annulus (1,23,31).

In flexion-extension and lateral bending, Figure 2-9, the annulus experiences a combination of mechanical stresses simultaneously (23). During bending one region of the annulus may be subjected to tension, while the opposing region is subjected to compression. The two types of loads are distributed across the disc endplate and are separated by an inflection point, the center of rotation. The tensile loads are resisted by the collagen fibers of the lamellae which cause the disc to contract; whereas the compressive loads are resisted by the stiffness properties of the lamellae (1,23).

For axial rotation, motion will be resisted via tension of annulus fibers orientated in the direction of movement. Fibers aligned opposite to the direction of the movement will become slack. However, a healthy disc rarely experiences large torsional loads during axial rotation. Before the collagen fibers of the annulus can become over strained, the facets of the neural elements become engaged and shield the disc (1).

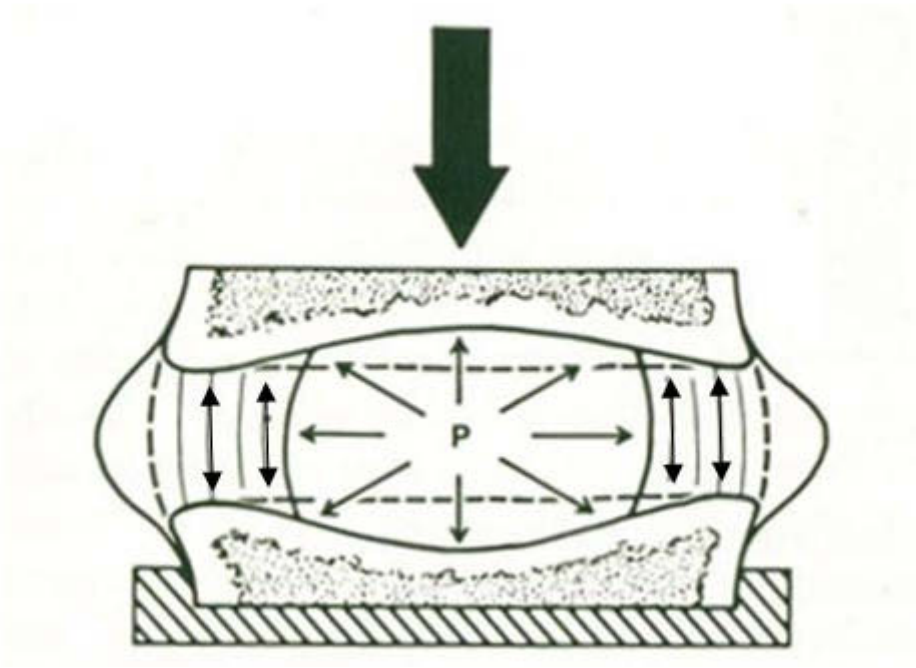

Figure 2-8: Intervertebral Disc Loading. Compression of the intervertebral disc increases the hydrostatic pressure within the nucleus, which generates tensile loads in the surrounding annulus to support the applied load. [Source: Adapted with permission. White A and Panjabi M. The Clinical Biomechanics of the Spine. New York: J.B. Lippincott Company 1990; Page 112.]

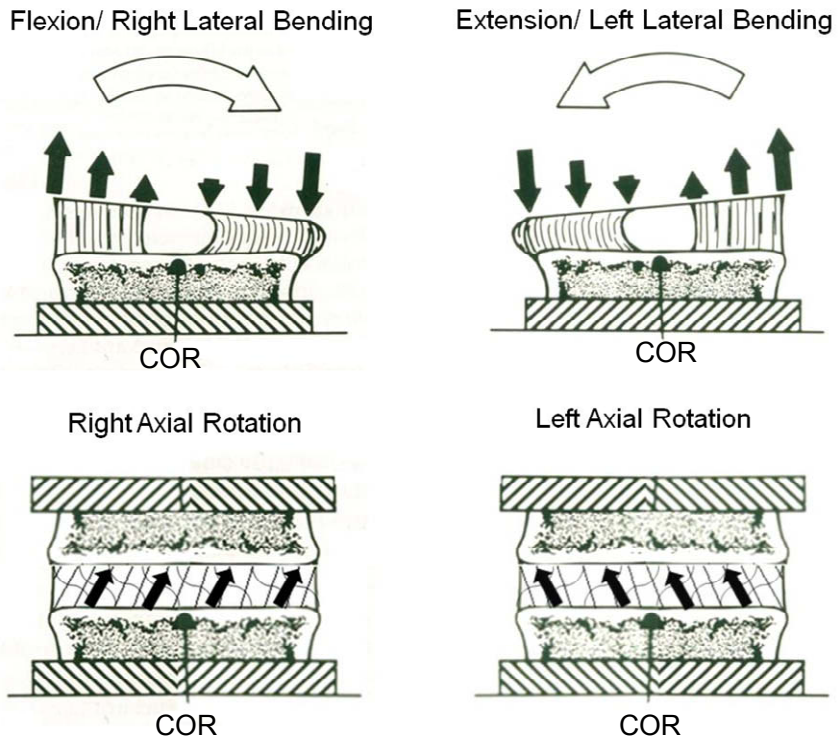

Figure 2-9: Spinal Disc Loading in Various Modes of Bending. The spinal disc experiences a combination of mechanical stresses simultaneously. Tensile and compressive loading in the sagittal and coronal plane is experienced by the disc during bending, whereas during axial rotation only the disc fibers oriented in the direction of loading experience tension. The remaining fibers are slack. [Source: Adapted with permission. White A and Panjabi M. The Clinical Biomechanics of the Spine. New York: J.B. Lippincott Company 1990; Page 112.]

Horizontal translations, both anterior-posterior and lateral, of the vertebral body will be resisted by tension developed in those fibers of the annulus that are aligned with the direction of the translation, whereas the remaining fibers will become slack. For vertical translations, all fibers, regardless of their orientation will resist separation of the vertebral bodies. However, the lumbar spine is rarely in tension due to gravitational forces and the weight of the upper torso (1,23).

Ligaments

Structure and Composition

Ligaments are uniaxial structures composed of densely packed collagen fibers. Their primary role is to provide stability to spinal structures by restricting vertebral motion to within physiological limits. When a region of the spine is subjected to tensional forces, the ligaments engage to provide tensile resistance parallel to the orientation of the fibers; however when subjected to compressive forces the spinal ligaments buckle.

Figure 2-10 shows the seven ligaments in the human spinal column. These ligaments can be divided into two ligament systems: the intrasegmental and intersegmental systems. The ligaments of the intrasegmental system hold the adjacent vertebrae together and include the ligamentum flavum, the interspinous, the intertransverse, and the facet capsular ligaments. The ligaments of the intersegmental system, which holds several vertebrae together, includes the anterior and posterior longitudinal ligaments and supraspinous ligaments.

The ligamentum flavum (LF) lines the posterior end of vertebral canal, creating a smooth protective surface for the spinal nerves. Its fibers originate from the anterior surface of the lamina of the proximal vertebra and terminate onto the posterior surface of the lamina of the vertebra below. The LF is unique among all the spinal ligaments for possessing a large quantity of elastic fibers, which do not buckle in compression. The interspinous ligaments (ISL) are thin, weak fibers that connect the opposing surfaces of the spinous processes together. The intertransverse ligaments (ITL) are thin membranous fibers intimately associated with the back muscles and are found in between the transverse processes. The facet capsular ligaments (FCL) are found surrounding the synovial joints in between the superior and inferior articular processes. These ligaments are short, taut and oriented in a plane perpendicular to the surfaces of the facets (1,23).

The anterior longitudinal ligament (ALL) descends along the anterior surface of the spine from the basioccipital region to the sacrum. Its fibers make deep firm attachments into edges of all the vertebral bodies but adhere less as the ligament spans the intervertebral discs. The posterior longitudinal ligament (PLL) runs along the posterior portion of the vertebral body. Contrary to the ALL, the PLL fibers are loosely attached to the edges of the vertebral body but are more firmly affixed to the annular fibers of the intervertebral disc. The supraspinous ligament (SSL) is a round fibrous band that originates in the ligamentum nuchae in the cervical region, descends down the tips of the spinous process, and terminates in the sacrum (1,23).

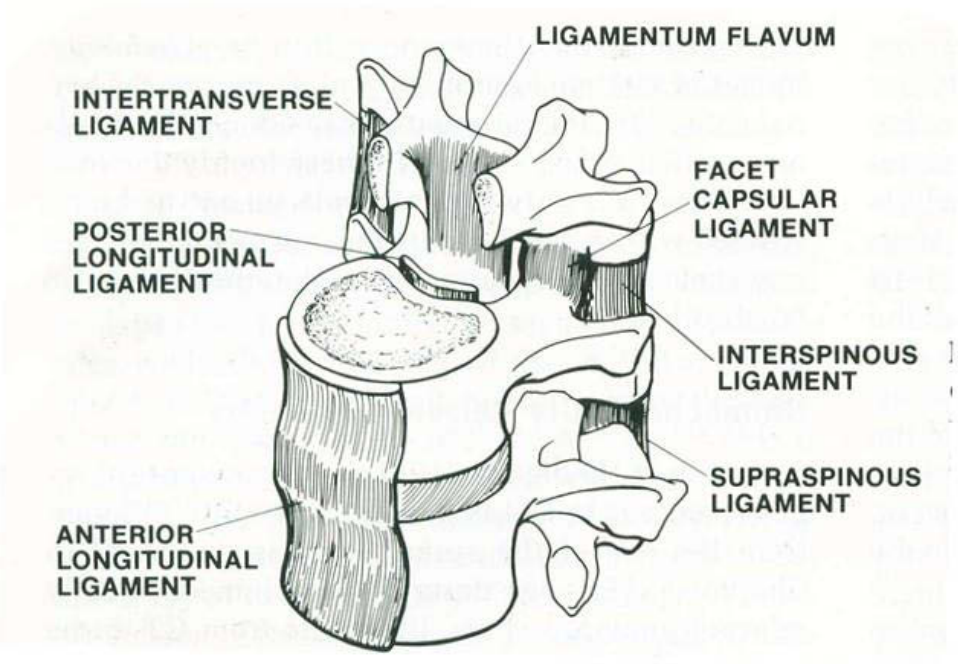

Figure 2-10: The Ligaments of the Lumbar Motion Segment Unit. The ligaments provide stability to the MSU by generating resistive tensile forces during bending. The ligaments can be divided into two groups, the intersegmental (ALL, PLL, SSL) and intrasegmental (LF, FCL, ITL, ISL) systems. **[**Source: Reprinted with permission. White A and Panjabi M. The Clinical Biomechanics of the Spine. New York: J.B. Lippincott Company 1990; Page 20.]

Function

The role of spinal ligaments in vertebral kinematics depends on their physical properties and location relative to the center of rotation of the vertebra (1,23,31). Researchers have attempted to quantify their physical properties and several studies have reported the collagen content, fiber orientation, and the cross-sectional area of various ligaments (23,28). However, this reported data should be viewed with caution because it is often difficult to isolate individual ligaments from surrounding musculature, their behavior tends to vary with vertebral body level, and the individual fiber orientation within a ligament bundle cannot be identified. The majority of the spinal ligaments are attached to various structures in the posterior elements and are orientated in the sagittal plane. The two ligaments not included in this category, the anterior and posterior longitudinal ligaments, are attached to the anterior and posterior surfaces of the vertebral body. Figure 2-11 shows the location of the spinal ligaments in reference to a hypothetical center of rotation.

The fibers of the supraspinous and interspinous ligaments are located the furthest away from the center of rotation of the spinal motion segment unit. These ligaments are known to be slack during a neutral, upright posture and have been observed to possess the greatest amount of deformation during bending (1). In fact, the large offset distance of these ligaments from the COR and high strain values provide the spine with the greatest stability in flexion during large rotations. These ligaments however show no activity during small amounts of flexion. In addition, the large moment arms of these ligaments have the mechanical advantage of providing the greatest stability to the spine with minimal compressive pre-load to the disc.

The ligamentum flavum consists of un-crimped collagen fibers and a high content of elastin. As a result, this ligament is pre-stretched in an unloaded spinal state and becomes engaged with small amount of flexion (1,23,31). While reported to have a higher tensile strength than supraspinous and interspinous ligament, the ligamentum flavum provides comparable stability to the spine as the more posterior located ligaments due to its closer proximity to the COR of the spine. In addition to providing stability in flexion, the ligamentum flavum functions to keep the vertebral foramen space intact during extension.

The posterior longitudinal ligament engages with small amounts of strain and tends to slightly preload the disc. During flexion, the PLL is marginally effective in controlling the amount of rotation due to its close proximity to the COR. However, this location does place the PLL in the ideal location to protect the spinal cord from the bulging contents of disc (1,23,31).

The anterior longitudinal ligament is reported to have the greatest tensile strength amongst all of the ligaments and predominately functions to stabilize the spine during extension. However, its proximity to the COR of the disc and to the much stronger annulus suggests that this ligaments functions secondary in resisting extension motion in the physiological range (1,23,31).

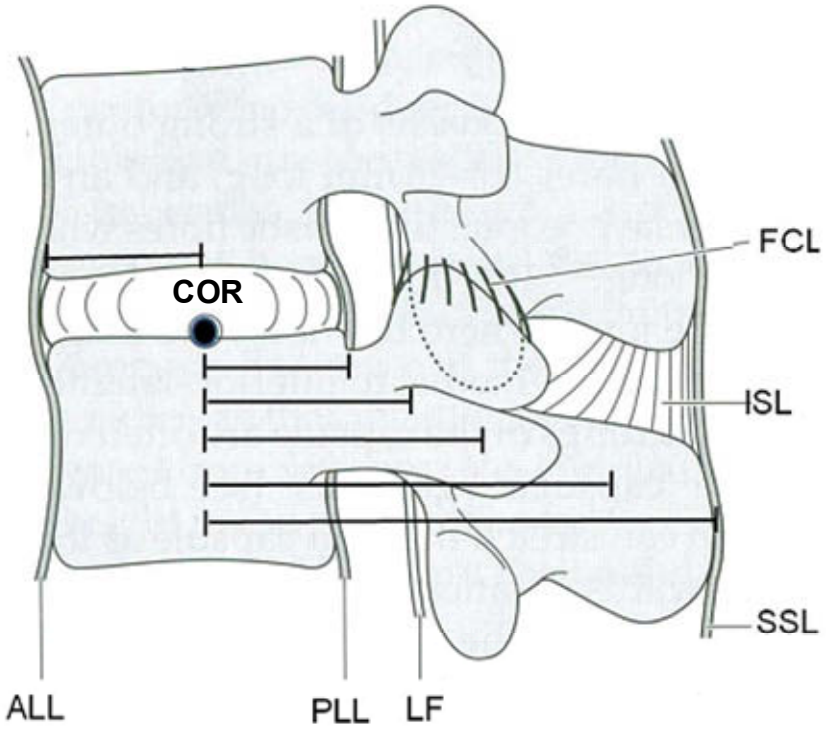

Figure 2-11: **Spinal Ligaments Location Relative to the COR.** The amount of stability a given ligament provides during bending is dependent on the collagen content, fiber orientation, cross sectional area, and location relative to the COR of the MSU. Assuming all else is equal, the greater the offset of the line of action of the ligament from the COR of the MSU, the greater the moment generated by the ligament to resist the external motion. [Source: Adapted with permission. Adams M, Bogduk N, Burton K, and Dolan P. The Biomechanics of Back Pain. London: Elsevier Science Limited 2002; Page 118.]

The facet capsular ligaments are unique in that their orientation allows them to provide stability to spine in flexion, extension, lateral bending, and axial rotation (1,23,28). These ligaments are short and strong, capable of large tensile strengths. In addition, the line of action of the FCL lies close to center of rotation, thereby allowing them to become taut with small degrees of rotation (23).

The location of intertransverse ligaments on the lateral portions of the vertebrae is indicative of their function in preventing excessive motion in lateral bending. However, their negligible cross sectional area and low tensile strength suggest that the intertransverse ligaments are too weak to provide any protection to the spine (23,28). It is theorized that the disc provides the first line of defense against excessive lateral bending, followed by contributions from the facet joints (23).

Muscles

In in vitro biomechanical studies of the human spinal column, muscle forces are typically not reproduced or simulated and hence do not contribute to the observed kinematic response of the specimen. Thus, the discussion of muscles in this section is only addressed for completeness.

A profuse amount of muscles can be found associated with the lumbar spine. However, only a small portion of those muscles are responsible for the motion and stability of the vertebrae (1). For example, the psoas major muscle fibers (Figure 2-12A), which originate from the lateral aspects of the lumbar vertebral bodies, intervertebral disc, and the transverse processes and terminate at the hip, are too close to the line of action of the lumbar vertebrae to cause any substantial movement. Their primary purpose is to flex the hip, which can exert a large compressive force on the lumbar spine. Other muscles, the quadrates lumborum, cover the anterior aspects of the transverse process and function to provide a solid a base for the action of the diaphragm. These fibers originate at the twelfth vertebrae and are joined to the ilum below.

The lumbar muscles that are the principal in controlling the movement of the lumbar vertebral column include the multifidus, longissimus thoracis, and illiocostalis lumborum (Figure 2-12B) (1). These muscle fibers originate from the spinous process, the accessory process, and transverse process, respectively. The multifidus muscle fibers are attached on either side of the spinous process and extend down into a verity of attachment sights below. The longissimus thoracis begin at each vertebral body level, just adjacent to the multifidus muscle fibers, and unite at a common tendon that is attached the ilium. The illiocostalis lumborum muscle fibers arise from the tips of the L1 to L4 transverse process and pass as flat sheets converging into the iliac spine. Collectively, the goal of these muscles is to pull down on the posterior elements and extend the lumbar spine or control the amount of flexion. Acting unilaterally, these muscles can initiate and control lateral bending.

The longissimus thoracis, pars thoracis, and illiocostalis lumborum pars thoracis span across the lumbar vertebra. Stemming from various ribs along the rib cage and

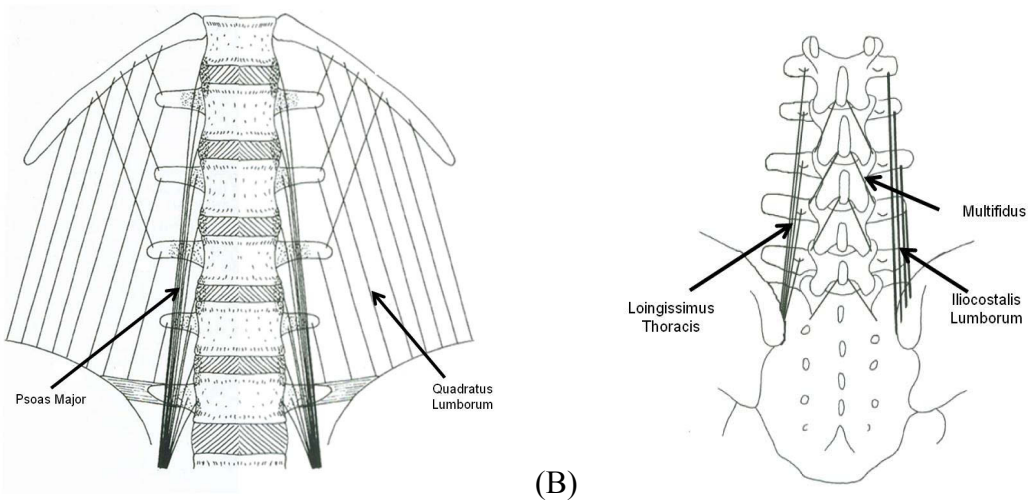

Figure 2-12: Intersegmental Spinal Muscles. (A) The psoas major and quadrates lumborum muscles do not provide stability or motion to the lumbar spine, but rather apply a compressive preload to the lower spine and aid in the flexion of the hip. (B) Muscles primarily responsible for spinal motion, by way of limiting flexion and lateral bending. [Source: Adapted from permission. Adams M, Bogduk N, Burton K, and Dolan P. The Biomechanics of Back Pain. London: Elsevier Science Limited 2002; Pages 32-34.]

ending at either the sacrum or iliac crest, these fibers aim to control the flexion of the trunk or the extension of the thorax. While, they do not act directly on the lumbar vertebrae, these muscles can exert a moment on the lumbar spine (1). Figure 2-13 provides an illustration of these muscles.

The intertransverse and interspinous muscles, located alongside to their respective ligaments are also too small and weak to cause any noticeable movement of the lumbar spine. However, they do possess an abundant amount of golgi tendons organs and are thought to aid in the proprioception of the spine (1).

Kinematics

Clinicians and researchers often assess the functionality of the lumbar spine by evaluating the vertebral motion without giving consideration to the forces that are responsible for that motion. This approach is used due to the difficulty presented in assessing the magnitude and line of action of spinal forces in vivo. With a proper understanding of a normal kinematic profile, the physiological limits, and the substructures that control it, clinicians allow themselves to better define and treat spinal abnormalities.

The lumbar spine is a highly complex structure capable of motion in all three anatomical planes (Figure 2-14). In fact, the lumbar spine can translate and rotate in each plane, thereby allowing it a total of six degrees of freedom (Figure 2-15) (23). With each motion profile there is a primary motion and an accompanying coupled motion. Primary motion is defined as the motion that is created as a result of an externally applied load. Researchers often define it as rotation in each of the principal planes. These include flexion and extension in the sagittal plane, left and right lateral bending in the coronal plane, and left and right axial rotation in the transverse plane. Coupled motion is the motion that is always associated with the primary motion and occurs due to the individual geometry of the vertebra and ligaments. For example, anterior translation is coupled with flexion and lateral bending is coupled with axial rotation. Coupled motion is normally less than the primary motion and varies depending on the lumbar vertebral level.

Primary Motion

Spinal motion measurements have been determined in vivo through the use of stereo radiographs and in vitro through cadaveric biomechanical studies (1,23,32,33-37). Table 2-2 presents the average range of motion at each spinal level for all the modes of bending from various authors. Overall, flexion range of motion (ROM) is the greatest amongst all the modes of bending. It increases slightly with decreasing vertebral level and is two to three times greater than extension ROM. Symmetry in the other two planes allows for the range of motion measurements from the right and left components of lateral bending and axial rotation to be averaged. Lateral bending shows little variation at the first three lumbar vertebral levels, with an average ROM between 6 to 8 degrees. The lower two lumbar levels, however, show a slight decrease in the range of motion. Axial rotation displays the least amount of motion amongst all the modes of bending and also

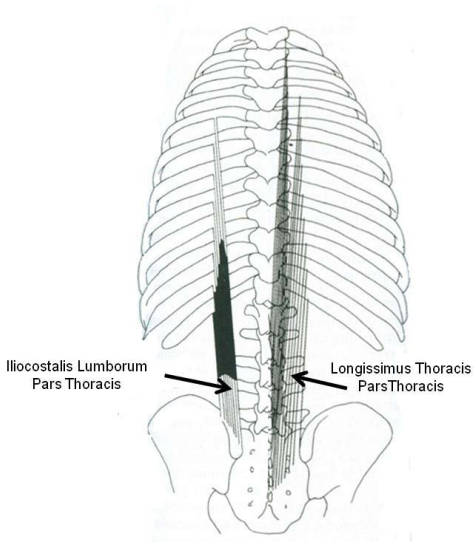

Figure 2-13: Erector Spine Muscles. These muscles span across the lumbar vertebrae and control the amount of flexion of the abdomen and extension of the thorax. [Source: Adapted with permission. Adams M, Bogduk N, Burton K, and Dolan P. The Biomechanics of Back Pain. London: Elsevier Science Limited 2002; Pages 36-37.]

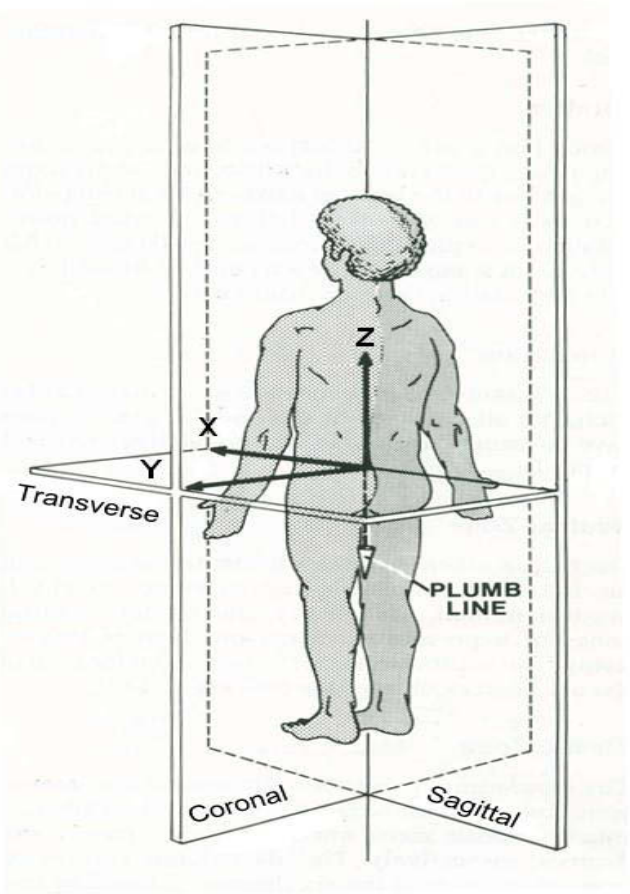

Figure 2-14: **Anatomical Planes.** The primary motion occurs in each of the anatomical plane; flexion and extension occur in the sagittal plane, lateral bending in the coronal plane, and axial rotation occurs in the transverse plane. [Source: Adapted with permission. White A and Panjabi M. The Clinical Biomechanics of the Spine. New York: J.B. Lippincott Company 1990; Page 87.]

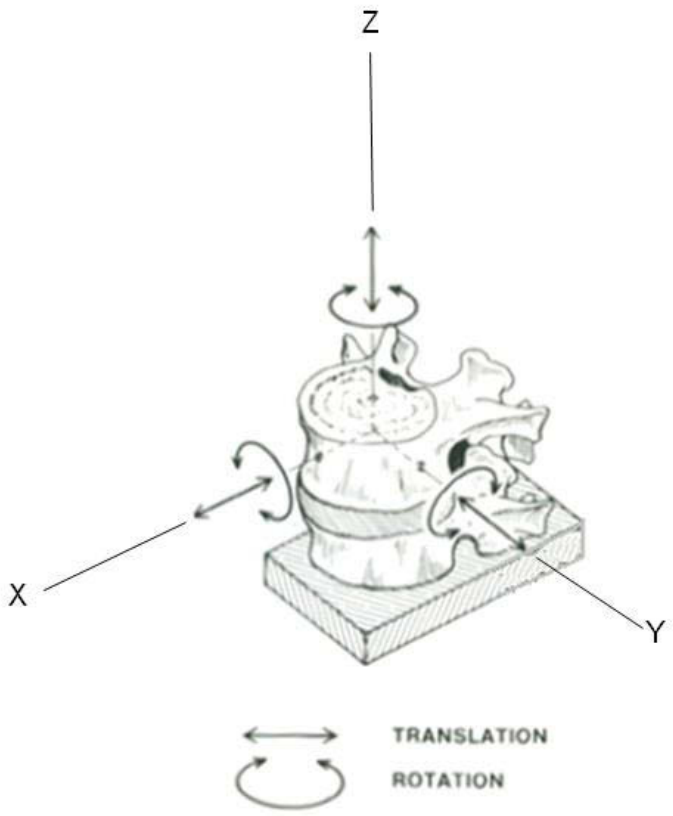

Figure 2-15: Spinal Degrees of Freedom. The lumbar spine is capable of translation and rotation in all three anatomical planes, allowing it a total of six degrees of freedom. [Source: Adapted with permission. White A and Panjabi M. The Clinical Biomechanics of the Spine. New York: J.B. Lippincott Company 1990; Page 54.]

Table 2-2: Lumbar Range of Motion at Each Spinal Level.

Mode of Bending	Spinal Level	Yamamoto*	Hayes**	Pearcey**	Dvorak**	Panjabi*	DiAngelo *
Combined Flexion and Extension (degrees)	L1-L2	10.7	7	13	11.9	11.9	7.9
	L2-L3	10.8	9	14	14.5	14.5	6.1
	L3-L4	11.2	10	13	15.3	15.3	8
	L4-L5	14.5	13	16	18.2	18.2	7.6
	L5-S1	17.8	14	14	17	17	8.9
Combined Lateral Bending (degrees)	L1-L2	4.9	-	5.5	7.9	6	7.6
	L2-L3	7	-	5.5	10.4	6	7.3
	L3-L4	5.7	-	5	12.4	8	10.2
	L4-L5	5.7	-	2.5	12.4	6	5.8
	L5-S1	5.5	-	1	9.5	3	4
Combined Axial Rotation (degrees)	L1-L2	2.1	-	1	-	2	1.9
	L2-L3	2.6	-	1	-	2	2.3
	L3-L4	2.6	-	1.5	-	2	2.9
	L4-L5	2.2	-	1.5	-	2	4.5
	L5-S1	1.3	-	0.5	-	5	2.7

Note: *In Vitro Measurements, **In Vivo Measurements. [Source: Adapted with permission. White A and Panjabi M. The Clinical Biomechanics of the Spine. New York: J.B. Lippincott Company 1990; Pages 110-111.]

shows little variation based on vertebral body level. On average axial rotation demonstrates a ROM between 1 to 3 degrees.

It is important to note that the large variations in the ROM values displayed in Table 2-2 can be attributed to differences in the end load limits of rotation, differences in ROM calculation techniques, differences in the testing methodology, and differences in the type of study conducted, in vivo or in vitro.

Coupled Motion

The amount of coupled motion depends on the vertebral body level and the posture of the lumbar spine (23,38). It is hypothesized that since the spine possesses six degrees of freedom (DOF), motion in any one direction could be coupled with motion in any of the remaining five DOF. While this is theoretically possible it is often not observed or reported; likely due to the difficulty in detecting relatively small changes. Table 2-3 describes the mean coupling pattern in all three planes with each mode of bending from biplanar radiographs of healthy individuals. The strongest coupling pattern in the lumbar region is axial rotation coupled with lateral bending. In vitro studies have reported between one to one and a half degrees of axial rotation coupled with four to six degrees of lateral bending (23,38). The direction of axial rotation coupled with lateral bending is such that the spinous process always points away from the concave side of the lateral bend. For example, left axial rotation would be coupled to left lateral bending and right axial rotation would be coupled to right lateral bending. It is important to note the coupling behavior between axial rotation and lateral bending is not equivalent to the coupling behavior between lateral bending and axial rotation. On average there is less coupled lateral bending during axial rotation.

Flexion-extension shows little to no rotational coupling behavior with either lateral bending or axial rotation. However, there is a strong translational coupling in the sagittal plane. In vivo radiographs suggest that in flexion-extension the superior vertebral body translates on average 1 to 3mm relative to the inferior vertebral body (Table 2-4) (38). The translation coupling behavior in the other planes is not quite as prominent.

Spinal Motion Measurements

Spinal motion can be described by several different terms including vertebral body rotation, translation, neutral zone, or position of the COR, and several methods exist for their quantification. For in vivo measurements, X-rays and other noninvasive image modalities (MRI, CT, and Fluoroscopy) are common. Each of these radiographic measurements is based on manual line-drawing techniques and landmark identification methods. The angle measured between the lines on each radiograph describes the relative position between adjacent vertebrae and the change in angle between flexion and extension is the measure of angular rotation. The accuracy and reproducibility of these measurements depends on variety of factors, including: image quality, patient effort,

Table 2-3: Mean Coupled Rotations in Each Mode of Bending.

Mode of Bending	Level	Rotation (degs)		
		Sagittal	Coronal	Transverse
Flexion	L1	8	-	-
	L2	10	-	-
	L3	12	-	-
	L4	13	-	-
	L5	9	-	-
Extension	L1	5	-	-
	L2	3	-	-
	L3	1	-	-
	L4	2	-	-
	L5	5	-	-
Lateral Bending	L1	2	6	0
	L2	1	6	1
	L3	1	5	1
	L4	0	3	1
	L5	2	3	0
Axial Rotation	L1	0	3	1
	L2	0	4	1
	L3	0	3	2
	L4	0	1	2
	L5	0	2	0

[Source: Adapted with permission. Bogduk N. Clinical Anatomy of the Lumbar Spine and Sacrum. Sydney: Churchill Livingstone 2005; Pages 89-90.]

Table 2-4: Mean In Vivo Coupled Translations in Flexion and Extension.

Mode of Bending	Level	Translation (mm)		
		Sagittal	Coronal	Transverse
Flexion	L1	3	0	1
	L2	2	1	1
	L3	2	1	0
	L4	2	0	0
	L5	1	0	1
Extension	L1	1	1	0
	L2	1	0	0
	L3	1	1	0
	L4	1	0	1
	L5	1	1	0

[Source: Adapted with permission. Bogduk N. Clinical Anatomy of the Lumbar Spine and Sacrum. Sydney: Churchill Livingstone 2005; Pages 89-90.]

inter-/intra- observer error, out-of-plane rotations, and mathematical algorithms (37). In vitro, optical tracking systems have been typically used with cameras to capture the motion of specific landmarks or LEDs throughout vertebral range of motion (32,37).

The accuracy, sensitivity, and specificity of radiographic tests have improved through the use of the computer-assisted methods (39). Advanced pattern reorganization and mapping algorithms are used to identify the shape, size, and density of vertebrae in each image and define a spatial relationship between one image and the next. Calculating the position of the landmarks avoids reproducibility errors commonly associated with manual methods.

Center of Rotation

Spinal motion can be described by a vertebral body's center of rotation. The COR is a hypothetical point in space about which a vertebral body undergoes pure rotation. The COR is defined by the initial and final position of the vertebral body and its magnitude of rotation, in a given plane, during the duration of the motion. Figure 2-16 describes the basic principle on how the COR measurement is determined; whether in vivo by bony landmarks on the vertebral endplates or in vitro via LED markers used in an optical tracking system.

Two landmarks are identified (points A and B) and tracked throughout the range of motion of the MSU (Θ). Points A_i and B_i represent landmarks on the endplate of the superior vertebral body prior to rotation, whereas point A_f and B_f represent the position of the landmarks after rotation. Translation vectors are drawn for each point in space (A_i to A_f and B_i to B_f) and perpendicular bisectors are constructed through their midpoints. The intersection of the bisectors at any instance in time represents the location of the COR.

Presently, there is no consensus among the research community about the exact location of the lumbar COR (23,34,36,40,41,42). However, it is believed that its location changes depending on the mode of bending, the vertebral level, and magnitude of rotation. Figure 2-17 illustrates possible COR location in each mode of bending from an assortment of authors.

White and Punjabi suggest that in flexion and extension, the COR is located within in the disc space (23). For flexion, the COR is initially positioned toward the anterior portion of the vertebral body and gradual moves anteriorly. In extension the COR behaves in the opposite manner, being initially positioned posteriorly and gradually moving posteriorly during increasing extension rotation. The finding of White and Panjabi would be similar to the works Peacy et al., Tournier et al., and Rousseau et al. if the flexion and extension COR measurements were combined (34,41,47). Other researchers, however, have concluded that in combined flexion and extension the COR is located along the posterior half of the superior endplate of the sub-adjacent vertebral body (17,36,37). These researchers likewise suggest that the COR moves anteriorly with flexion and posteriorly with extension.

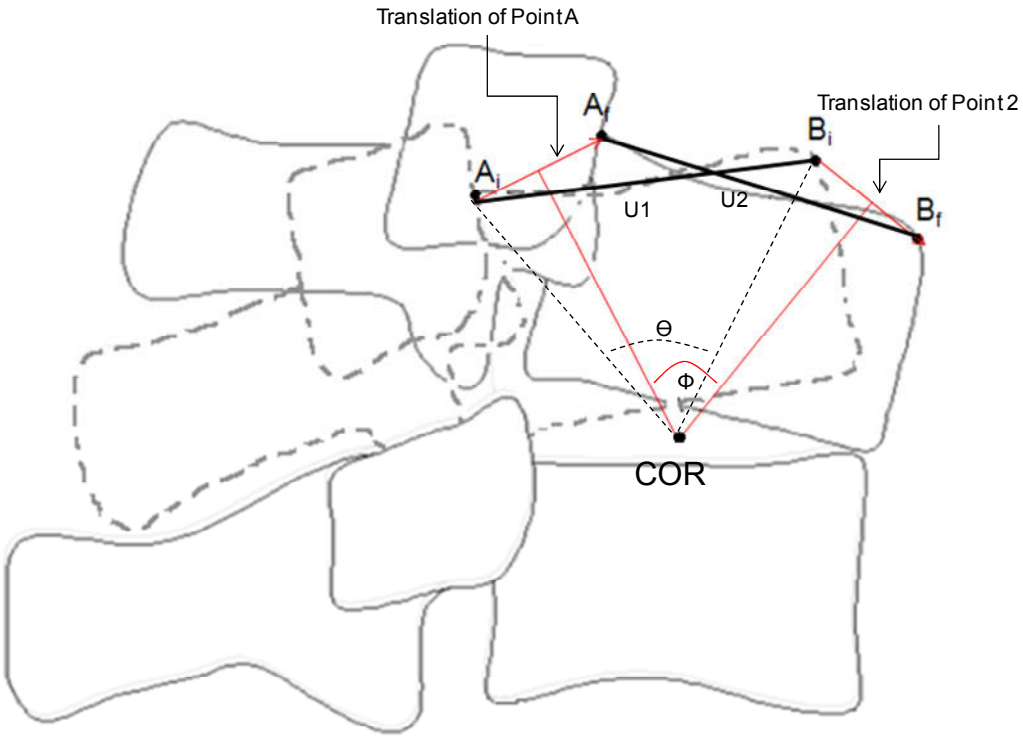

Figure 2-16: COR Calculation via Bony Landmarks. Bony landmarks (points A and B) are tracked throughout the range of motion (Θ) of the MSU. The intersection of perpendicular angle bisectors from the translation of each landmark (A_i to A_f and B_i to B_f) indentifies the location of the COR. [Source: Adapted with permission. Crisco J, Chen X, Panjabi M, et al. Optimal Marker Placement for Calculating the Instantaneous Center of Rotation. Journal of Biomechanics 1994; 27(9): 1183-1187.]

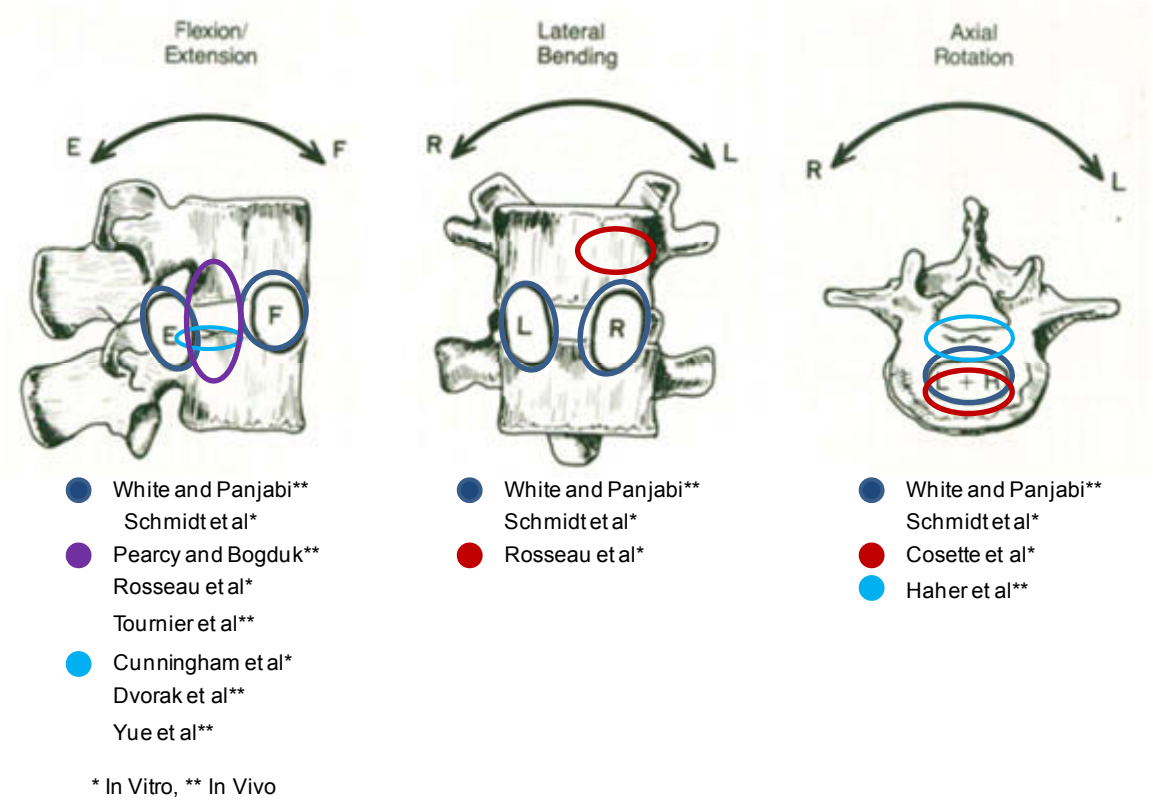

Figure 2-17: Published COR Locations. Probable locations of the COR have been identified for each mode of bending. The exact location of the COR has not been agreed upon by the research community. [Source: Adapted with permission. White A and Panjabi M. The Clinical Biomechanics of the Spine. New York: J.B. Lippincott Company 1990; Page 112.]

In lateral bending, the findings of White and Panjabi concur with the findings of Schmidt et al. in the location of the COR in the region of the intervertebral disc and the subjacent vertebral body (23,45). For left lateral bending, the COR axis is projected to lie in the right portion of the coronal bending plane and for right lateral bending it is projected to lie in the left portion. Rousseau et al. suggests that COR is initially located in the intervertebral disc but migrates to the superior vertebra on the ipsilateral side (43). While disagreeing with Rousseau et al. on the location of the COR, the analysis of Schmidt et al. does suggest the COR migrates to the ipsilateral side (45).

The location of the COR within the intervertebral disc during axial rotation has been agreed upon by several authors. However, they disagree as to where the COR is located within the disc space. Cosette et al. and Haher et al. believe that the COR is offset from the midline of the disc, whereas Schmidt et al. and White and Panjabi reported a central location (46,47). Schmidt et al. does suggest that with extreme axial rotation, the COR has the potential to migrate from the center of the intervertebral disc towards the facet joint on the contralateral side.

The reported COR locations in lateral bending and axial rotation need to be viewed with caution. Lateral bending is naturally coupled to axial rotation and vice-versa; therefore out-of-plane rotations can induce bias in the COR location when conducting planar measurements.

The lack of consensus amongst the research with respect to the location of the COR can be attributed to several factors. Deviations arise from variations in the experimental setup, instrumentation resolution, mathematical algorithms, range of motion of the subjects, and inter/intra- observer errors. The limitations in defining the location of the COR and efforts to address those limitation are discussed next.

Crisco et al. and colleagues have derived basic equations to calculate the COR from bony landmarks (44). Other, more robust equations have been derived in attempt to improve the precision and accuracy of measurements (48,49). However, despite the best efforts of researchers and clinicians the discrepancies in COR measurements made from anatomical landmarks remains high (50). Panjabi et al. investigated the errors in the measurements of COR from point markers on a moving body and suggested that small errors in the X and Y coordinates can be magnified to large errors in the calculation of the COR, approximately 30 to 50 times greater (51). Buckley et al. compared COR measurements with a commercial optical tracking system using an optimization algorithm and a direct-solve approach. This group found a 6mm error zone with the optimization algorithm compared to a 12mm error zone with the direct solve approach (52). DiAngelo et al. concluded that COR measurements were prone to large error zones depending on signal noise, resolution, and range of movement analyzed. An introduction of 0.05mm of noise had an error zone of 3mm, whereas as 0.5mm of noise had an error zone of 5 to 10mm (53).

Traditionally, clinical COR measurements have been derived by overlying or comparing full flexion-extension radiographs from which angles of rotation and COR locations are determined through manual methods. These methods have several

drawbacks. First, determining a COR measurement from full extension-flexion radiographs assumes that the location of the COR does not change throughout the ROM, which is contrary to current thinking. Taking additional radiographic images has the potential to over irradiate the patients. Furthermore, the ROM measurements are subjective to patient effort. Patients with pain will limit their motion and studies have confirmed that COR measurements from small ROM are increasingly inaccurate. For example Woltring et al. assessed that the error in COR position was inversely proportional to the amount of rotation; random error tended toward infinity when rotation tended toward zero (54). Pearcy and Bogduk et al. also reported that when flexion and extension ROM was less than 5 degrees, the measurement error in the COR could be unacceptably large (55). Lim et al. made similar conclusions when taking ROM measurements from the keel of the ProDisc in plain radiographs; concluding that at least 4.6 degrees of ROM was required to be 95% certain that any prosthesis had sagittal motion (56).

The inter- and intra-observer error remains high with COR measurements. It is difficult to consistently identify the same reference landmarks in multiple radiographs. Variations in endplate appearance are typical in radiographs due to out of plane motion and patient posture. Tournier et al. demonstrated a mean intra-observer uncertainty in COR measurements were 26% for the X value and 32% for Y value, whereas the inter-observer uncertainty was as high as 18% for the X value and 34% for the Y value (41). Other such studies have reported similar findings (57). Cakir et al. using digitized prosthesis images demonstrated that angular motion can be measured with an accuracy of ±2 degrees for the same observer and ±3 degrees for different observers (58).

The conventional manual method of determining COR measurements is laborious and time consuming. In calculating the COR, clinicians need to outline and digitize each vertebral body in all radiographs. Furthermore, for reliable results this procedure needs to be repeated multiple times (59). In attempts to marginalize the uncertainty in COR measurements and improve clinical application of this tool, sophisticated motion analysis software with pattern recognition algorithms have been developed. The software outlines each vertebral body from digital radiographic images and computes the geometric center of each vertebral body. The COR is thereafter determined and defined as an offset distance from the geometric center. A study by Zhao et al. attempted to assess the differences in motion measurements between three surgeons and Medical Metrics software as compared to electromagnetic sensors rigidly mounted to the spinous processes of cadaveric spines (60). Results indicated that the surgeons were significantly less accurate and more variable in determining the range of motion, superior vertebral body translation, and intervertebral disc height. The reported error in ROM measurements with the Medical Metrics software was 0.5±0.2 degrees as compared to 2±1 degrees for the surgeons. Even with advanced image processing software however, many of the errors and limitations associated with determining COR locations from clinical measurements described above still exist.

Spinal Mechanics

The lumbar spine experiences a combination of several complex forces in vivo. These forces are exerted through the effects of gravity, muscle and ligament activity, and externally applied loads. Presently there is no practical method to directly measure these forces. However indirect measurements can be made by comparing measurements of lumbar muscle activity and interdiscal pressures against biomechanical analyses. By understanding and documenting the contribution of these forces, clinicians can better assess the source of low back injuries and institute protective measures against them.

Sources of Spinal Forces

Gravity applies a vertical force on each part of the body in direct proportion to its mass. For the lumbar spine, this force is the additive result of the bodyweight of the head, trunk, and arms. Body posture, such as forward bend or sitting, will increase the compressive forces on the lumbar spine, whereas lying down will reduce the loads (1).

Muscles of the back and abdomen act to stabilize the lumbar spine against the influence of gravity. However, this is at the expense of the lumbar discs. The tension developed by the muscles oriented along the long axis of the lumbar spine subject the lumbar vertebrae to high compressive forces. Even during relaxed standing or sitting, muscle tension can increase the forces on the lumbar spine to approximately twice the body weight (1). During activities such as forward bending and lifting an external load, muscles need to generate much higher forces to overcome the effects of gravity acting on the upper body, thereby placing even more stress on the discs (1).

Passive tissues, such as ligaments, can sustain high tensile loads when stretched during bending. These structures store elastic energy when stretched and release it upon returning to their original length, thereby reducing the amount of work for muscles. The amount of work ligaments can perform depends on their cross-sectional area, fiber composition, and location relative to the center of rotation of the vertebra (1,23,31). The supraspinous and interspinous ligaments are weak ligaments but have long moment arms. Therefore, these ligaments are able to generate larger bending resistance with minimal compressive penalty on the disc. The ligaments of the neural elements, on the other hand, are stronger ligaments with shorter moment arms. Therefore, when engaged, these ligaments add a higher compressive load on the discs.

During the handling of external loads, the lumbar spine is subjected to loads several times greater than the weight of the external load (1). Normally, manual handling requires the upper body to move quickly and often from a stationary position. Therefore, back muscles must generate much higher tensile forces to overcome the effects of gravity. Furthermore, the bending moment generated by the upper body and the external load must be overcome by a greater extensor moment in order to lift the load. The further the center of mass of the trunk and external load is positioned away from the COR of the body, the greater the mechanical advantage required by the joints/muscles.

Forces and Moments

The culmination of all the forces on the lumbar spine can be reduced to a single resultant force acting at a point location (Figure 2-18). This resultant force, R, can be broken up into its compressive (C) and shear (S) components. The 3D component which acts perpendicular to the mid-plane of the disc is the compressive or tensile component and the other two components which act parallel to the mid-plane of the disc are the shear components. A compressive force acts to compact the vertebral bodies while a tensile force acts to pull the vertebral bodies apart. Shear forces acts to deform the object in the plane in which the force is applied.

If the resultant force is acting through the center of rotation of the lumbar spine, then there will be no accompanying bending moment. However, if the resultant force is at a point offset to the center of rotation of the lumbar spine, a net bending moment equal in magnitude to the product of the force and perpendicular moment arm is generated. The direction perpendicular to the plane in which the applying forces resides will determine the direction of the moment and therefore bending of the spine. For example the shear and compressive components of the force in Figure 2-19 will cause the lumbar spine to bend about an axis perpendicular to the page (y axis), i.e. flexion and extension in the sagittal plane.

Loads

In a standing upright individual, excluding all other forces, a 70kg individual experiences an average of 385N on the lumbar spine. Assuming a disc angle of 30 degrees below the horizontal datum for L4-L5 MSU this individual would generate 333N of compressive force and 192N of shear force. Flexing the lumbar spine initially tends to reduce lordotic curvature, thereby reducing the shear load and increasing the compressive load on the spine (1). Furthermore, flexed postures tend to place the posterior annulus and neural ligaments in tension, which tend to further load the discs in compression. On the other hand, lordotic postures and extension tend to slack these ligaments, shifting the compressive load onto the neural elements, and reducing the compressive load on the discs (1). Symmetry of the disc in the coronal and sagittal plane suggests that the spinal loads the disc experiences in lateral bending are similar to flexion. In fact, the loading profile in lateral bending follows that of flexion with the exception that the magnitudes of the loads are greater (1).

Considerably high forces are generated by the intervertebral discs to resist the external loads placed on the lumbar spinal column. Since the nucleus pulposus is highly pliable, the responsibility of transmitting and withstanding the loads falls on the annulus fibrosus. The ability of the annulus to resist loads is the greatest when the extracting force is parallel to the orientation of the annular fiber, i.e., 30 degrees relative to the horizontal axis, and weakest when the extracting force is purely vertical (23). Presently there is no consensus on the mechanical strength of the annulus, however reported values can be found in the works of Panjabi et al. and Adams et al. (1,23).

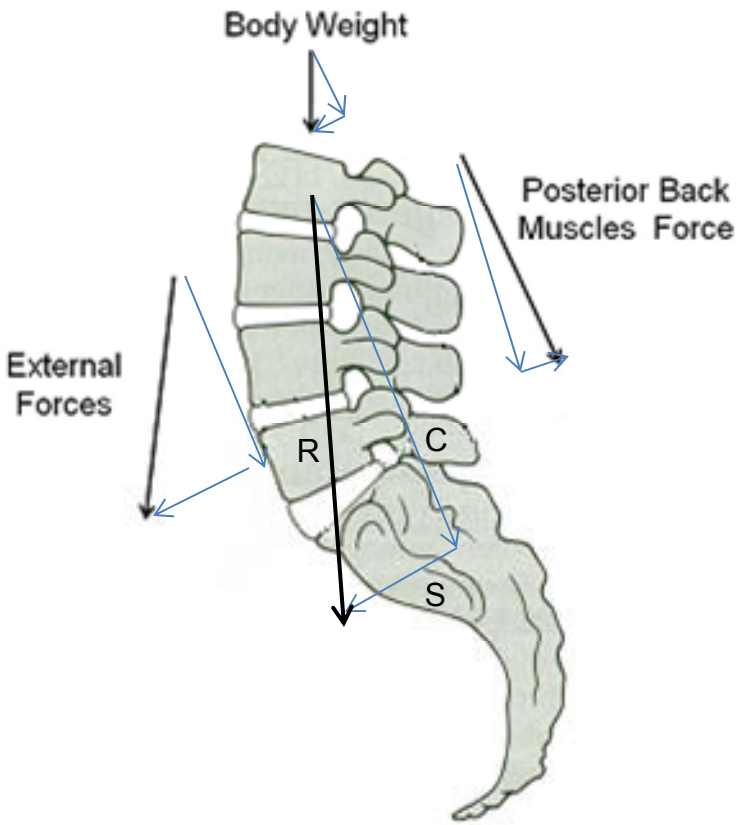

Figure 2-18: **Sources of Spinal Forces on the Lumbar Spine.** The application of all the loads experienced by the lumbar spine can be reduced into single resultant force acting at a point in space. The resultant force (R) can be resolved into its components (C and S), those acting perpendicular to the plane of the disc and those acting parallel to the plane of the disc. [Source: Adapted with permission. Adams M, Bogduk N, Burton K, and Dolan P. The Biomechanics of Back Pain. London: Elsevier Science Limited 2002; Page 133.]

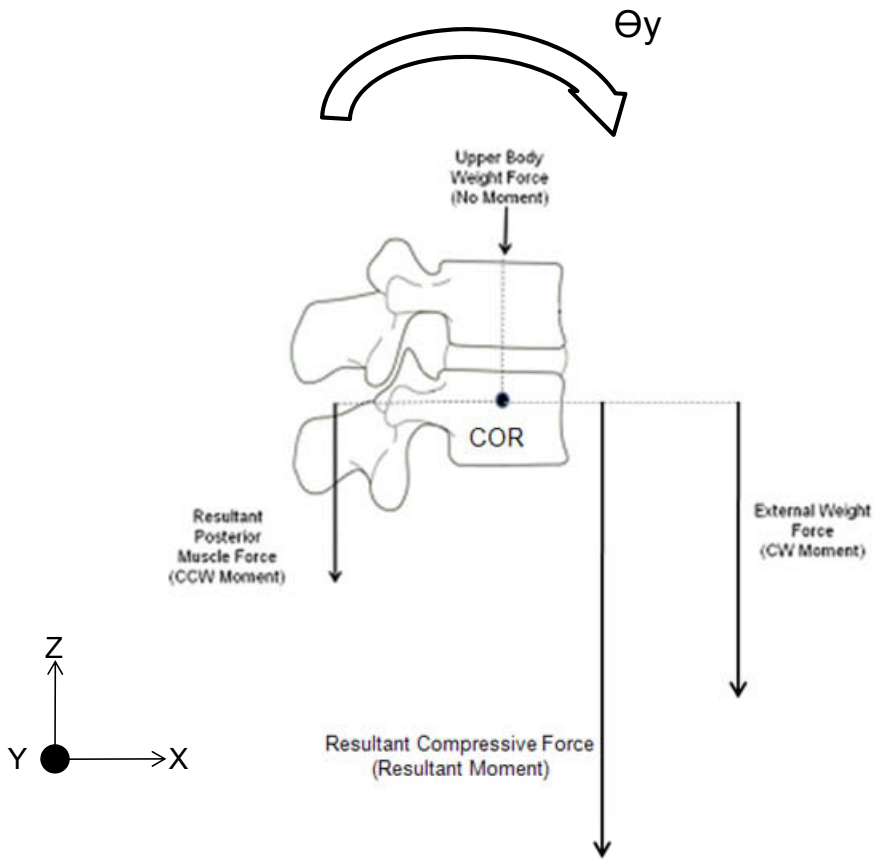

Figure 2-19: Description of Forces and Moments. Forces offset from the COR of the MSU induce a moment on the spine, whereas forces acting through the COR do not. The counterclockwise (CCW) and clockwise (CW) moments can be added to determine the magnitude and direction of a net resultant moment. [Source: Adapted with permission. Adams M, Bogduk N, Burton K, and Dolan P. The Biomechanics of Back Pain. London: Elsevier Science Limited 2002; Page 133.]

With respect to spinal ligaments it was pointed out previously that ultimate strength does not evenly correlate to their contribution in stabilizing the motion segment. A very strong ligament with a short moment arm can equally stabilize the MSU as a weak ligament with a long moment arm. To acquire a complete sense of a ligaments contribution to sustaining or resisting a load other biomechanical parameters such as, cross-sectional area, strain, stiffness and mode of bending must be analyzed. Literature values can be acquired from the works of Panjabi et al. and Adams et al., however such data should be viewed with caution because some ligaments transcend multiple levels, vary in physical properties between different levels, and can be oriented at various angles relative to the horizontal datum (1,23). Therefore, simple tensile strength tests may alter the natural line of action of the ligaments and underestimate their overall strength.

Flexibility

The human lumbar spine exhibits a non-linear, viscoelastic, and biphasic behavior that can be described by the flexibility curve (1,23). Flexibility is traditionally defined as degrees of rotation per unit of bending load. The inverse of flexibility is spinal stiffness. While both measurements are accurate in describing spinal mechanics in vitro, spinal flexibility better represents the clinical concepts of range of motion and spinal instability.

A typical flexibility curve is presented in Figure 2-20, where the dependent variable is the bending moment (Nm) and the independent variable is the rotation (degrees). The non-linearity of the curve displays that a given change in load does not give a proportional increase in rotation. Furthermore, the biphasic nature of the spine highlights the two distinct loading zones. The initial portion of spinal loading is referred to the neutral zone. This zone indicates little resistance to spinal loading, where a minimal application of a load results in a substantial rotation. The loading zone from the end of the neutral zone to the physiological load limit is referred to as the elastic zone. This zone is typically more linear and characterizes the elastic deformation of the spine.

For a perfectly elastic structure, the original shape is regained and all of the energy stored in the structure is returned. However, the spine exhibits a certain amount of inelastic behavior (Figure 2-21). The non-recovered energy, lost due to heat, between the loading and unloading curves is referred to as hysteresis energy. In addition to quantifying the amount of energy lost within the system, the loading and unloading curves suggests that a specimen's deformation when unloading is greater for the same amount of applied load then when the specimen was loaded. Another mechanical parameter of importance is the visocelastic behavior of the spine. This parameter implies that the mechanical behavior of the spine is dependent on the rate of loading, where an increased rate of loading results in a stiffer spinal construct.

Disc Degeneration and Surgical Options

Lower back pain is a result of various pathological states in the spinal column whose causality has been illuminated by evidence-based studies. These studies have identified pathologies such as intervertebral disc herniation and degeneration,

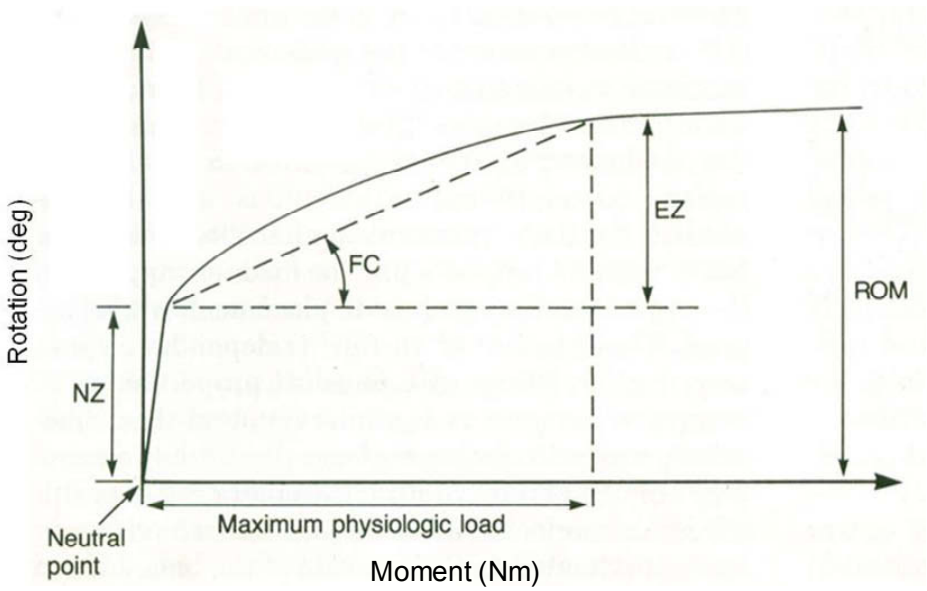

Figure 2-20: Typical Flexibility Curve. A flexibility curve describes the ability of the MSU to deform under application of a known load. The curve can be divided into two regions; the neutral zone, which shows a substantial change in rotation for a given amount of load, and the elastic zone, which is often linear and exhibits elastic deformation of the spine. **[**Source: Adapted with permission. Adams M, Bogduk N, Burton K, and Dolan P. The Biomechanics of Back Pain. London: Elsevier Science Limited 2002; Page 133.]

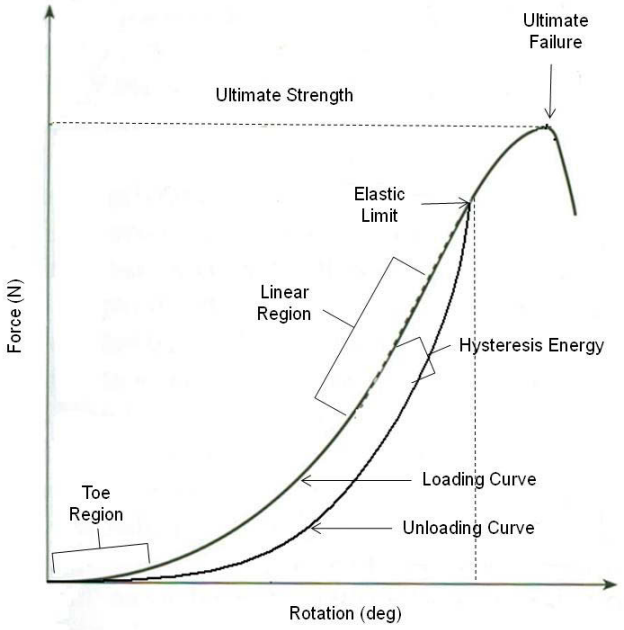

Figure 2-21: A Typical Force-Deformation Curve. A force deformation curve describes the loading and unloading behavior of a MSU, where the difference between the work of the two is the hysteresis energy. A typical loading curve has a toe region of minimal stiffness, a linear region, and elastic limit. Rotating a MSU beyond the elastic limit can cause a permanent strain to the MSU. [Source: Adapted with permission. Adams M, Bogduk N, Burton K, and Dolan P. The Biomechanics of Back Pain. London: Elsevier Science Limited 2002; Page 133.]

zygapophysial joint osteoarthrosis, spinal stenosis, spondylolisthesis, and segmental instability as a potential sources of lower back pain (1). Moreover, the mechanical failure of the intervertebral disc has been identified as probable common thread among these pathologies (7).

Mechanical failure of the disc is characterized by degenerative changes that include: (1) the nucleus becoming less hydrated and more fibrotic, (2) collagen and elastin fibers becoming more disorganized, (3) nerve and blood vessels beginning to degenerate, and (4) an increase in the necrotic and apoptotic appearance of disc cells. The cumulative effects of these degenerative changes results in the loss of intervertebral disc height, which compromises the integrity of neural disc space and promotes uneven distribution of the loads across the spinal column (15,30,32,61).

The intervertebral disc is kept healthy and nourished through the diffusion of molecules across the vertebral endplates and by blood vessels integrated in the annulus fibrous. However, should there be a decrease in the nutrient supply, perhaps due to a decrease in blood supply or endplate calcification, the optimal internal environment of the intervertebral cells can be disrupted. Events that typically lead to the failure of intervertebral disc cells to maintain the extracellular matrix, particularly the concentrations of collagen and proteoglycan aggrecan aggregates, begin with a decrease in the glucose and oxygen concentrations (62,63). Without glucose and oxygen the disc cells are forced to abandon glycolysis and resort to the production of lactic acid, which has a plethora of negative effect on cells including inactivation of enzymes, the unfolding of proteins, and changing the cell's electrochemistry.

The degradation of the extra cellular matrix results in a significant loss in the proteoglycan aggrecan molecules, and an inability of disc cells to replace the lost aggrecan molecules. Without the aggrecan molecules, which have the ability to attract and hold water molecules over 500 times their own weight, the nucleus looses it hydrostatic pressure, the ability to maintain disc height, and the capacity to transmit the forces to the annulus (30).

Under normal conditions the nucleus is sufficiently hydrated and when loaded the hydrostatic pressure within the nucleus increases. The hydrostatic pressure pushes the contents of the annulus outwards and creates a tensile stress in the annulus, which functions to simultaneously support the load placed on the vertebral body and resist motion (1,23). At lower levels of hydration the load carrying capacity of the disc is reduced. Further, axial loads will no longer be supported by the annulus but instead directly transmitted to the vertebral body below. The increase in the vertebral body load can lead to the deformation of the endplate and overtime end-plate failure. A failed end-plate leaves the subjacent vertebral body prone to fracture (1,23,31,41).

A degenerative disc also alters the load sharing properties between the anterior column and the posterior elements, with the posterior elements increasingly supporting greater loads as the intervertebral disc continues to fail (1,23). Unaccustomed to supporting the increased load, the posterior elements become prone to injury and degeneration. Of particular concern is increased wear and failure of the facet joints,

which often are a source of debilitating pain (31). Shifting the loads often results in high compressive stresses to appear in the posterior annulus in the neutral upright position, whereas the anterior annulus experiences stress shielding. As such, the anterior annulus begins to lose strength and stiffness, and when loaded in flexion its mechanical capability to support the load is reduced. Under the right conditions excessive loading during flexion with a stress shielded annulus could result in a disc herniation.

A loss of intervertebral disc height due to degenerative changes could reduce the lumbar lordotic alignment (1). Increased compressive forces on the spine and loads on the posterior elements may modify the mechanical behavior of adjacent levels and lead to the flat back syndrome, adjacent level disc disease, or lower back pain. In addition, anterior displacement of the global axis of gravity could occur with a loss in the lumbar lordosis. As such the posterior back muscles would be required to exert greater energy to provide stability to the spine.

Furthermore, disc height reduction could create slack in the spinal ligaments such that the motion segment unit becomes unstable during bending (1,23,30). Slack spinal ligaments increase the neutral zone, allowing for greater rotation before providing resistance. Hyper-mobility may lead to the subluxation of the vertebral body, as demonstrated by spondylolithesis. In addition slack ligaments, particularly the posterior longitudinal ligament, could protrude into the vertebral foramen and cause nerve impingement and pain.

A degenerative disc causes a transient period of hyper-mobility for the motion segment unit. During this period the disc is especially susceptible to injuries, such as annular tears and disc herniation. The clinical manifestations during the hyper-mobility phase include episodes of back and leg pain. However, as the disc continues to degenerate the motion segment unit begins to stiffen from increased osteophyte formation and facet arthrosis (23). As the hyper-mobility phase elapses the lower back and leg pain subsides. Unfortunately as one motion segment stiffens, it potentially results in the hyper-mobility of the adjacent segments, thereby accelerating their degeneration (1,23,30). The extent to which this actually occurs is currently the focus of much research and debate.

In assessing clinical instability and quality of motion due to a degenerative disc, several biomechanical parameters are used; including neutral zone, total range of motion, and center of rotation measurements.

Research has shown that range of the neutral zone increases following disc degeneration, trauma, and cyclic loading (39,64,65). The increase in the neutral zone has been associated with a higher overall range of motion and hyper-mobility of the MSU. A reduced neutral zone has been linked to late stage disc degeneration and a loss of motion. The association between ROM and clinical instability is difficult to assess. Fujwara et al. classified disc degeneration from Grade I to Grade V in 110 lumbar spines and concluded that ROM increased for all degenerative Grades, except Grade V, for which ROM decreased (66). Zhao et al. induced instability in lumbar spines by simulating disc dehydration and endplate fracture and demonstrated an increase in ROM for the unstable case as compared to the intact case (39).

Degenerative disc failure also influences the location of the COR of the spine. Gertzbein et al. reported a greater scatter of CORs was detected for spinal segments having morphologic changes cause by disc degeneration (67). Tournier et al. found that flexion and extension ROM tends to be higher when the COR was in its usual area compared to the unusual (41). Zhao et al. demonstrated in a lumbar cadaveric model that the position of the COR migrated from the normal loci after induced spinal instability (39). The degeneration caused the COR to migrate 10.5mm superiorly in flexion and 9.1mm posteriorly in extension from its normal location in the posterior, inferior portion of the vertebral body.

Following identification of clinical instability in the spine, clinicians may prescribe a variety of conservative treatments, including bed rest, pain medication, steroid shots, and physical therapy. When the conservative treatment fails to eliminate the pain and restore the spine to a normal kinematic profile, surgical intervention is required. The current gold standard is spinal fusion, or arthrodesis.

Fusion

Approximately 350,000 spinal fusion surgeries are performed each year, with an average 200,000 involving fusion of the lower lumbar region (the number two most common type of lumbar surgery) (68). The two fold objective for fusion is to eliminate motion and relieve pain by decompressing the neural elements.

Several types of spinal fusion options exist; including a posterior approach, an anterior approach, or a combination of both (31,61). All approaches involve performing a discectomy at the unstable level and adding a bone graft material. The bone graft is used to induce bone growth between two vertebral bodies to effectively create one long bone. Spinal instrumentation is often used in conjunction with the bone graft to provide stability to the operated level until the graft has fused. The use of instrumentation, which includes rod, hooks, pedicle screws, and anterior plates, has been shown to improve fusion rates (31,61).

Spinal fusion has been previously reported to be unsuccessful in 5% to 35% of patients (31). While the exact reason for the high failure rates in spinal fusion vary among experts in the field, it has been suggested that the failure rates are a combination of inadequate surgical technique, excessive stresses across the fusion site, insufficient internal or external stabilization, and stress shielding of the bone graft (31,61). Even with successful bone fusion, there is still the potential concern that immediately after surgery patients may continue to experience pain. This is likely a result of the surgeon failing to properly identify the pain contributors or accurately diagnose the source of the pain. Long term concerns with fusion involve the possible development of adjacent segment disease (ASD) (10,11,12). It has been theorized that the loss of motion at the fused level is transferred to the adjacent segments, causing increased interdiscal pressure, facet loading, and supplementary motion, the result of which is the accelerated disc degeneration. Often the treatment for adjacent level disc disease requires additional surgery.

Several in vitro studies have created a correlation between fusion and adjacent segment disease by showing a significant increase in adjacent level range of motion as compared to the native spine (28,31). DiAngelo et al. examined the amount of adjacent level motion compensation due to a single level cervical fusion and found significant differences in both flexion and extension (53). Likewise, Panjabi et al. in a study comparing adjacent level effects in full lumbar cadaveric spines found a 7.8% and 35.3% increase for the one- and two-level fusion condition as compared to the intact spine (61). Wong et al. in a full lumbar study comparing three total disc replacement devices to a simulated fusion case concluded that in flexion and extension, the simulated fusion condition had a significant loss of motion at the operated level, and that motion was distributed amongst each of the remaining adjacent levels (24).

Similar to in vitro studies, clinical outcome evaluations have reported the effects of fusion on ASD. A prospective randomized study with a minimum follow-up of ten years conducted by Ekman et al. concluded that fusion accelerated changes at the adjacent level with a mean disc height reduction of 15% as compared to natural aging (70). Disc height reduction in adjacent segments after a 360º interbody fusion was likewise analyzed by Schulte et al., who found a 21% and 16% reduction in disc height at the first cephalic and second cephalic adjacent segment, respectively (12). Auerbach et al. made similar conclusions at a two year follow-up when comparing the effects of fusion on range of motion at all non operated levels (71). Changes were most notable at the first cranial adjacent level, with a 12.1% increase in ROM as compared to the intact. Lehmann et al. conducted a retrospective study of 62 patients with a mean follow-up of 33 years following lumbar fusion. Segmental instability was observed at the adjacent levels in 45% of the patients (72).

Since the increase in motion at adjacent levels or a reduced disc height does not necessarily correlate to the presence of adjacent segment disease, nor does it signify correlation with clinical outcome, the previously mentioned studies fail to make firm conclusions on the clinical presence of ASD.

A study by Cheh et al., which determined the presence of radiographic (spondylolisthesis > 4mm, segmental kyphosis > 10º, complete collapse of the disc space) and clinical (spinal stenosis, intractable back pain, sagittal imbalance) adjacent level disease, found that 42.6% of the 188 patients at five years of follow-up developed radiographic ASD, whereas 30.3% of patients were classified with clinical ASD (10). Hayashi et al. conducted a similar study and found that at a four year minimum follow-up that 15 of 32 patients (46.8%) had adjacent segment degeneration, including disc slippage and narrowing (73). Likewise, a study by Yang et al., attempted to define a relationship between ASD and clinical outcome by analyzing disc degeneration at adjacent levels for single, 2-level, and more than 3 level fusion (14). Results from this group at a two year follow-up showed the presence of ASD in 11.6%, 14.5%, and 16.3% of patients, respectively. A one year follow up study conducted by Lee et al. found that of the 1069 patients that underwent lumbar fusion 28 (2.62%) patients needed additional surgery because of ASD (74).

Despite some of trends observed in the clinical investigation of fusion on ASD, critics are quick to voice the limitations presented in such studies. Mainly, there is difficulty in determining the contribution of the natural aging process and rationalizing the correlation between ASD and clinical outcome.

Penta et al. attempted to shed light on the controversy by evaluating the relationship between ASD and fusion length (75). Plain radiographs revealed that 32% of the 52 patients had degenerative changes at a previously normal disc level and that this percentage was not correlated to the length of fusion. Etebar and Cahill et al. attempted to distinguish the contributions of fusion from that of patient history and surgery (13). In a retrospective study of patients undergoing fusion with rigid instrumentation, 14% of 125 patients had ASD. From this patient pool a subset group of patients that were smokers and obese were identified. The researchers concluded that the risk of ASD was higher for patients with rigid instrumentation and additional health problems as compared to patients that had rigid instrumentation alone.

The long-term consequences of spinal fusion on adjacent segment have led some surgeons to seek for alternatives in treating degenerative disc disease. Several alternatives exist including posterior dynamic stabilization systems, nucleus arthroplasty devices, and total disc replacement implants. Aside from biomechanical interventions, a few biological treatment options are being investigated; namely, disc regeneration and intradiscal electrothermal coagulation (76-79). For the purposes of this research a brief introduction will be provided on posterior dynamic stabilization systems and nucleus arthroplasty devices, whereas the majority of the focus will be on total disc replacement devices.

Posterior Dynamic Stabilization

Posterior dynamic stabilization (PDS) devices were initially used in adjunct to fusion to provide stability to the spine while fusion was achieved. However recently there has been a trend to test these as stand-alone devices. PDS devices can be classified into three categories; (1) interspinous spacers, (2) pedicle based dynamic rod devices, and (3) total facet replacement systems. These devices act to decompress the spine and permit controlled, physiological motion.

Interspinous spacers are positioned between the spinous process of adjacent vertebrae and act to directly decompress the neural elements. Furthermore, the spacers keep the vertebrae slightly flexed in its neutral alignment and limit range of motion in extension. As such, they disengage the facet joints and relieve pain. Dynamic rod devices were the derivative of the rigid pedicle rod and screw construct; where the rigid rods were replaced by chords, flexible rods, or mechanically moving rods. As such these devices act to permit controlled motion. In addition to stabilizing the spine, dynamic rods allow load sharing between the anterior and posterior structures of the vertebral body, possibly preventing the onset or minimizing the effects of adjacent segment disease. Total facet replacement systems were designed to functionally restore the facet joints, which have been known to be a source of pain generation during disc degeneration. They

have also been used in adjunct to decompression surgeries where aggressive laminectomies and facetectomies require these devices to restore stability to the region.

Nucleus Arthroplasty

Nucleus Arthroplasty (NA) is an early stage surgical alternative to fusion, where the degenerated nucleus is replaced via an implant. These devices intend to preserve motion and geometry of the intervertebral disc in hopes of preventing the onset or minimizing the effects of adjacent level segment disease as a result of disc degeneration (80).

Currently, over 20 NA devices are currently undergoing research and development. They can be broadly organized into three categories; (1) hydrogels, (2) polymers/synthetics, and (3) mechanical devices (80). Hydrogel devices are flexible and porous, designed to mimic the natural diurnal cycle of the nucleus pulposus by absorbing and releasing water in response to a load. These devices are available in varying sizes, shapes, and axial stiffness to accommodate an assortment of patient anatomies. Polymer/synthetic technologies are a group of devices that deliver the nucleus replacement implant via an injectable apparatus. The injectable implant is initially in a semi-liquid state and solidifies within the disc space. An advantage of this technology over hydrogels is in its ability to custom form/shape to the curvature of the disc space, and thereby potentially reduce implant migration or subsidence. Mechanical devices are in contact with both endplates within the nucleus and transmit forces across the disc space. These devices are composed of various materials and have unique design methodologies to restore disc height and provide motion to the vertebral body.

Total Disc Replacement

Disc arthroplasty holds the promise to alleviate pain from degenerative disc disease by restoring the disc height and preserving motion without compromising vertebral stability. Clinically, total disc replacement devices must successfully provide pain relief, improve the sagittal balance, decompress the spine, and safe guard against adjacent level disc disease (37). Biomechanically, TDR devices must ideally preserve or restore range of motion within normal limits for all modes of loading and transmits forces for proper load sharing with surrounding anatomical structures (37).

A variety of the TDR designs exist each based on a different design modality. However, only two, the Charité Artificial Disc Replacement (DePuy Spine, Inc., Raynham, MA) and the ProDisc-L Artificial Total Disc Replacement (Synthes, Inc., Paoli, PA) have been approved by the Food and Drug Administration (FDA) for implantation in the United States. The MAVERICK lumbar prosthesis (Medtronic Sofamor Danek, Inc, Memphis, TN) and the FlexiCore lumbar prosthesis (Stryker Spine, Allendale, NJ) are two devices presently enrolled in FDAs investigational device trials.

Of all the TDR prostheses mentioned above, three have incorporated a “ball-and-socket” design and one has incorporated a mobile core design for the preservation of

motion. Even within the "ball and socket" devices there are variations in the implementation of this design, which is the source of variation in the magnitude and quality of motion among these implants. For example, some prostheses are unconstrained, allowing for both translation and rotation, where as others are semi-constrained, allowing for rotation with no translation. In addition, these prostheses vary in the placement of the fixed COR. The COR can be placed either midline within the footprint or offset from the center. Also, the COR could be positioned anywhere from within the disc space to some distance away from the endplates of the vertebral body. Table 2-5 highlights the differences amongst the four major arthroplasty devices for the lumbar spine in the United States.

Early clinical findings of TDR's equivalency to fusion in eliminating pain and having a successful clinical outcome have been documented. Herkowitz et al. confirmed the hypothesis that TDR was as effective as an anterior lumbar interbody fusion (ALIF) by observing greater improvements in the visual analogue scale (VAS) and Oswestry Disability Index (ODI) scores (61). A clinical success rate of 63% was observed with the Charité group, as compared to the 56% with the ALIF group. Tropiano et al. reported similar findings with an 8.6 year follow-up with the ProDisc-L TDR (81). Significant improvements in back-pain, radiculopathy, disability, and modified Stauffer-Coventry scores, with no incidence of implant loosening, migration, and failure allowed this group to conclude that the TDR was effective in treating degenerative disc disease. Zieglar et al., Delamarter et al., and Bertagnoli et al. all reached analogous conclusions about the efficacy of TDRs in treating discogenic LBP as compared to fusion (16,82,83).

The ability of TDR devices to prevent or slow the progression of ASD remains unresolved. In vitro studies have indicated that TDR devices do have an influence in alleviating increased motion at adjacent levels as compared to fusion. Cunningham et al. conducted an in vitro cadaveric study comparing the biomechanical effects of the Charité TDR device on the ROM of a lumbar spine as compared to conventional stabilization techniques (17). At the operated level, a slight increase in the ROM of the MSU with the TDR as compared to the intact condition was observed, whereas a significant reduction in ROM was observed with the posteriorly stabilized condition. The adjacent levels showed no significant difference in the ROM compared to the intact condition with TDR, whereas the ROM was increased at the proximal and distal adjacent levels with posterior stabilization. Similar results were found by Wong et al. in a cadaveric lumbar study (L1-S1) comparing three artificial discs, Charité, ProDisc-L, and Maverick, to a simulated fusion construct (32). In flexion-extension motion analysis, the fusion construct demonstrated significantly less motion at the operative level then all the artificial discs. A significant increase in motion was observed at all adjacent levels except the L3-L4 as compared to the Charité and Maverick, and at all levels as compared to the ProDisc-L. In a kinematic analysis of a lumbar cadaveric spine implanted with the ProDisc-L, Demetropoulos et al. found combined flexion-extension ROM was marginally reduced following instrumentation with the TDR; however there were no significant changes in range of motion and interdiscal pressure at the adjacent levels as compared to the intact condition (84).

Table 2-5: **Differences among Total Disc Arthroplasty Devices.**

Parameter	Implant Type			
	Charité	ProDisc-L	MAVERICK	FlexiCore
Material	Metal on Polymer (CoCr with UHMWPE)	Metal on Polymer (CoCrMo with UHMWPE)	Metal on Metal (CoCrMo)	Metal on Metal (CoCrMo)
Constraints	Rotation and Translation	Rotation	Rotation	Restricted Rotation and Translation
COR	Floating Center of Rotation	Midline and Below Inferior Endplate	Posteriorly and Below Inferior Endplate	Midline and Within the Disc Space
Fixation	Ventral and Dorsal Teeth with Hydroxyapatite Coating	Central Keel with Porous Coated Surface	Central Keel with Hydroxyapatite Coating	Ventral and Dorsal Teeth with Titanium Plasma Spray

Clinical data supporting an influence of the ProDisc-L to offset ASD effects have been reported. In an IDE study comparing the effects of ProDisc-L and single level fusion on the relative segmental contribution to the total lumbar ROM, Auerbach et al. concluded that patients with TDRs experienced a slight loss in total ROM from the operative level, which was compensated by the caudal adjacent level. However, with fusion, a significant loss in ROM was attributed to the arthrodesis and motion compensation was observed at all levels, most notably the first cranial adjacent level (71). Furthermore, relative to the preoperative condition, patients with the TDR displayed a significant increase in overall ROM (6.3º), whereas no change was observed in the fusion group. Similar results were found by both Zigler et al. and Delamarter et al., who found an increase in the sagittal plane motion for a ProDisc-L replacement group from the preoperative at the 6-month period, while the fusion group saw a significant decrease in motion (82,84). However unlike Auerbach et al., these researchers reported no significant increases in ROM at the adjacent levels compared to the preoperative values. Huang et al. attempted to correlate ROM measurements to the presence of ASD with the ProDisc-L TDR (85). At a 8.7 year follow-up the presence of ASD was observed in 24% of patients, whose mean range of motion was 1.6º±1.3º; whereas patients without ASD had a mean motion of 4.7º±4.5º.

Immediate post operative clinical results from literature compare favorably to fusion with the advantage of motion preservation and potential avoidance of increased rates of adjacent level disc disease. However, TDR devices are not without limitations and criticism. There is some concern that higher ROM with TDR as compared to the native spine will alter the natural mechanics of the spine which has the potential to introduce stress in the posterior elements and contribute to facet arthrosis and pain (15,18,43,45). This outcome is even more likely if the COR of the implant does not coincide with the inherent COR of the MSU. Without long-term clinical results the answers to these concerns remain unresolved.

Biomechanical Testing Protocols

In the present in study, the objective was to determine the influence of surgical placement of a fixed center of rotation total disc replacement device on the loading mechanics and range of motion of a L4-L5 MSU. The following sections will introduce two typical biomechanical testing protocols used for in vitro spinal evaluations and address their limitation. Finally, a new testing apparatus and protocol developed by this group will be introduced which describes it validity in accomplishing the present objective.

Panjabi et al. had originally coined the terms “flexibility” and “stiffness” testing to describe biomechanical testing under either load or displacement control (23). Under displacement control the spine is rotated and the corresponding load is measured; whereas under load control the spine is loaded and the corresponding rotation is measured. Both protocols have their advantages and presently there is no consensus as to which protocol offers the best method of evaluating spinal behavior.

Pure Moment

Load control involves the application of a known load to spinal tissue, usually by inducing a pure moment, and measuring the motion response in terms of neutral zone and range of motion. The goal of this protocol was to establish a measurement of the structural properties of the spine. Therefore, pure moment was ideal to evaluate intact motion segment units and fusion constructs/instrumentation. Originally pure moments were induced through a cable and pulley system attached to the unconstrained end of a spine. The cables were positioned in the plane of rotation and used as a force couple to apply a constant bending moment. As science advanced the cable and pulley system was replaced by robotic simulators and commercial testing systems.

The primary drawback of the pure moment protocol is that it does not replicate normal physiological loads or physiological motion. The difficulty in measuring physiological loads of the spine non-invasively requires that the magnitude and application of those loads be approximated in the laboratory. This has been typically done through trial and error cadaveric testing, biomechanical analyses, and/or electromuscular measurements. Furthermore, the spine does not experience a constant bending moment across its spinal levels, as induced by the pure moment protocol, but rather experiences a moment distribution as the spine is flexed. While some researchers consider this an advantage of the protocol, it is not physiologic. In addition, the pure moment protocol is limited to applying a pure moment about the geometric center of the spine, which has the potential to over constrain the structure. In reality, the point about which the moment should be induced depends on the mode of bending, posture, and anatomical location of the COR.

Spinal range of motion can be approximated through flexion-extension radiographs and the pure moment protocol can replicate the magnitude of ROM, but fails to replicate the quality of motion. The quality of motion describes how the vertebral bodies rotate and translate in relation to one another and can be expressed by monitoring the locations of vertebral CORs.

Despite its limitations, the pure moment protocol is actively used in the spinal community and has become a standard for testing in several laboratories. It is particularly useful for comparing the effects of different biomechanical devices and may be useful for testing fusion instrumentation. However, in terms of motion preservation devices and devices with variable stiffness properties the pure moment protocol falls short. The motion and load distribution with TDRs cannot be delineated from the net kinetics of the spine. An alternative in vitro testing method is needed for the testing of TDR devices.

Eccentric Loading

Eccentric loading is a displacement control protocol that involves the application of a known displacement and measures the resultant load and moment response. Implementation of this protocol typically involves the application of an eccentric load to

the long axis of the spine to induce a rotation. As the spine rotates, this protocol induces a compressive load and bending moment to spinal segments.

The advantage of the eccentric load protocol over pure moment is that the kinematic profile generated is more representative of in vivo physiologic motion. However, this protocol shares similar drawbacks to pure moment in terms of physiological loading. While the actuator applies a compressive load, it fails to induce shear loads. Furthermore, the application of an eccentric load generates a global moment, which is naturally distributed amongst its structures by the spine. However, the moment distribution is not physiologic. In vivo analyses suggest as a spine is flexed the moment increases as you descend down the vertebral column. However with the eccentric load protocol, as the spine is flexed the moment decreases. Moreover with the displacement control protocol only the applied loads and moments are known. How the spine distributes the loads and moments among the remaining structures remains unresolved.

In regards to the biomechanical testing of spinal implants both the eccentric load protocol and the pure moment protocols are limited in their ability to study the loading mechanics and kinematics requirements of total disc replacement devices. TDR devices typically have a prescribed center of rotation. Rotation about a point other than the COR of the native spine can lead to an overloaded and constrained condition between spinal vertebrae. Current gold standard testing methodologies such as those described above lack the sensitivity to measure changes in spinal kinematics and internal load sharing mechanics with subtle changes in implant COR design and surgical placement with respect to spinal anatomy. With these limitations, a new sophisticated method of implant testing is required. One that is capable of prescribing a rotation about the COR of the implant and is equipped at measuring the resultant loads and moments of the spine.

Fixed Axis

A novel biomechanical testing system was designed and built by Kelly et al. to better test the complex behavior and motion of the human spinal column (86). The testing apparatus, named the Spine Robot, is a custom-designed, multi-axis testing platform designed to replicate physiological loading of a cadaver spine by allowing coupled motion and complex loading patterns. It consists of four programmable axes that can be independently operated under displacement control, force feedback control, or a combination thereof. Using the Spine Robot, the kinematic profile of an intact motion segment unit can be programmed to follow a specified path or rotate about a fixed point in space.

The Spine Robot was used to develop a unique fixed axis testing protocol (21, 86,88). This protocol utilizes a built-in tool transform function to coordinate the movement of three actuators simultaneously to rotate about any anatomical location within spine. Registration of the tool tip to the spine can be accomplished through spinal radiographs and/or through optical tracking systems. This capability of the Spine Robot provides the means to rotate about the COR of a fixed axis motion preservation device. While limited to resolving only the net loads and moments experienced by the spine, the

fixed axis protocol does allow for the measurement of net shear and compressive loads. Furthermore, the use of a six-axis load cell transformed to the point of rotation allows for a more accurate measurement of the spinal mechanics. In addition, the high positional resolution and precise control of the rotational axis by the Spine Robot, in the micrometer range, allows for greater accuracy in simulating the placement of TDR.

CHAPTER 3: METHODS

UT Spine Robot

The Spine Robot (University of Tennessee Biomechanics Laboratory, Memphis, TN), shown in Figure 3-1A, is a custom-designed, multi-axis testing platform designed to better replicate physiological loading of a cadaveric lumbar spine. It consists of four programmable axes that can be operated under displacement control, force feedback control, or a combination thereof. Using the Spine Robot, the kinematic profile of an intact motion segment unit can be programmed to follow a specified path or rotate about a fixed point in space.

The initial tool position of the Spine Robot was known upon powering up and calibration. This position, termed the null tool tip, was defined by the intersection of the rotational axis of the two available rotatory actuators (Figure 3-1B). The coordinated movements of the different actuators combined such that the position and orientation of the tool tip was commanded and controlled within a right-hand Cartesian coordinate frame. The tool tip position could be redefined by the user such that it laid a prescribed distance away from the null location in the X and Z coordinate directions. This feature permitted robotic control of the position and orientation of working tool tips attached to the robotic wrist; a common need in industrial applications.

Figure 3-2 illustrates how the Spine Robot coordinated its movement to rotate about a fixed point in space. A tool transformation of 0mm in X and -50mm in Z from the null tool tip defined the new point of operation for the Spine Robot. Thereafter a pure rotation of the tool tip was programmed, effectively imposing a fixed COR about the tool tip. The vertical distance from the null tool tip to the point of rotation in this example defined the radius for the path of the Spine Robot. In order to get from the start position, labeled 1, to the desired end position, labeled 2, the Spine Robot had to travel a distance of ΔX horizontally, ΔZ vertically, and rotate $\Delta\Theta$ clockwise. These movements were not performed sequentially, but coordinated together by built-in controller functions.

Specimen Preparation

Ten fresh human cadaveric full lumbar spines were procured from the Medical Education and Research Institute (MERI, Memphis, TN). The spines were screened with lateral and anterior-posterior (AP) radiographs using a fluoroscopic c-arm (GE 9600 or 9800, GE Healthcare, Chalfont St. Giles, United Kingdom). Any specimen with gross osteophytes, reduced disc height, abnormal lordosis, pervious surgery, or pathology was excluded. Bone density was not measured. Eight specimens with sufficient tissue quality were identified and used for this study. Two specimens were damaged during testing. Table 3-1, provides the specimen demographics. Spines were double wrapped in plastic bags and stored at -20 degrees Celsius in-between handling. Before use, the spines were thawed for a 24 hour period in a refrigeration system and were kept hydrated with a 0.9% saline solution.

(A)  **(B)** 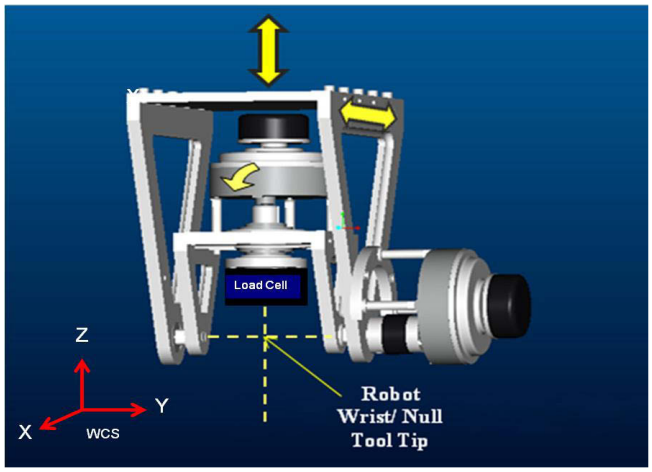

Figure 3-1: UT Spine Robot and Null Tool Tip Location. (A) A multi-axis testing platform designed to better replicate physiological loading and range of motion of human cadaveric spines. (B) The null tool of the Spine Robot was defined by the intersection of the rotatory actuators. All movements were conducted to control the end effect of this position. [Source: Reprinted with permission. Kelly, B. A Multi-axis Programmable Spine Robot for the Study of Multi-body Spinal Biomechanics Using Real-Time Hybrid Force and Displacement Control Strategies. Doctoral Dissertation, University of Tennessee Health Science Center at Memphis, 2005.]

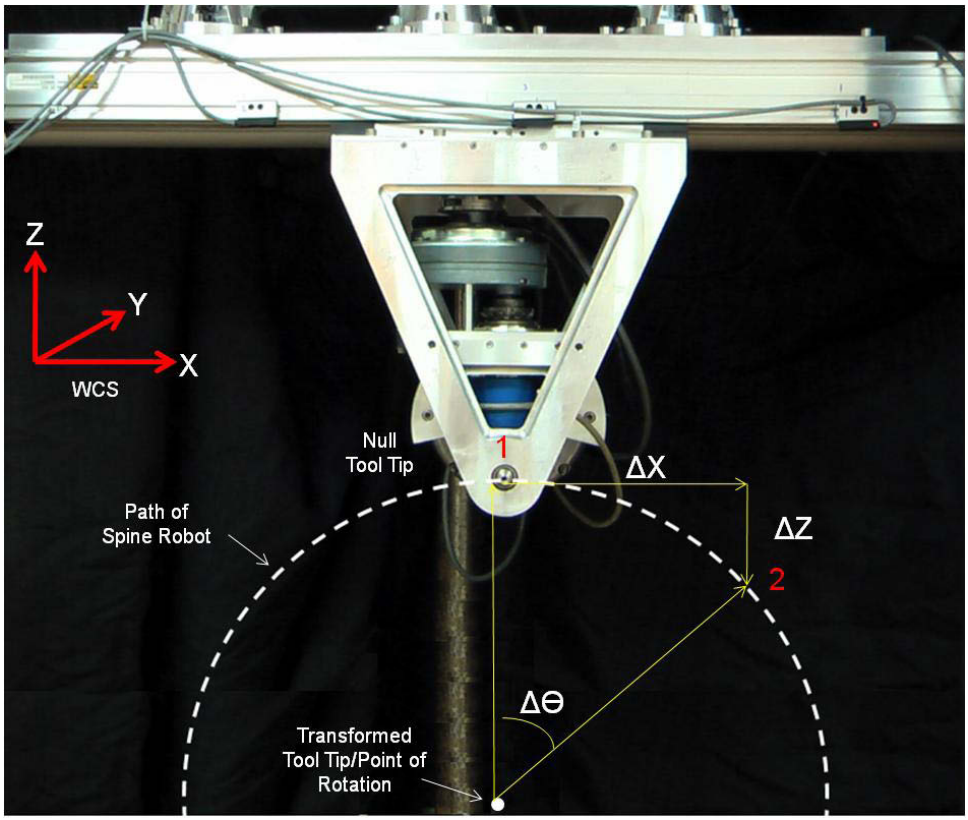

Figure 3-2: Prescribing a Pure Rotation about a Point in Space. The continuous and coordinated movements of three actuators (two translations and 1 rotation) were required prescribe a pure rotation about a point in space. In order to rotate about the transformed tool tip, the Spine Robot had to simultaneously translate in the ΔX and ΔZ directions, while rotating ΔΘ about the pitch (Y) axis, effectively moving from point 1 to point 2 along a circular arc.

Table 3-1: Specimen Demographics.

Specimen Name	Reference Number	Level	Age	Sex	Race	Cause of Death
PD1	518	L4-L5	62	M	CA	COPD
PD2	DRT050687	L4-L5	58	M	CA	Cardiac Death
PD3	DRT060701	L4-L5	67	F	OT	Respiratory Failure
PD4	DRT087036	L4-L5	66	M	CA	Cardiac Death
PD5	UB06J008	L4-L5	52	F	CA	Cardiac Death
PD6	UJ04K007	L4-L5	64	M	CA	Cardiac Death

Full lumbar specimens, L1-Sacrum, were radiographed in their neutral, upright position in order to establish the orientation of the L4-L5 MSU within the multilevel lumbar spine. The neutral alignment of the full lumbar ensured that the proper lordosis of the lumbar spine was maintained. The L4-L5 alignment was preserved when the MSU was disarticulated and potted in a custom potting mold for testing.

Figure 3-3A shows a lateral radiograph of a full lumbar segment positioned in the neutral, upright position in a custom alignment frame. A mounting plate was attached to the L1 vertebral body (red line) and positioned parallel to the horizontal datum plane by a level. The remainder of the lumbar spine was left unconstrained. The radiographic images were imported into Image-J software (Open Source, NIH) and calibrated with a known distance from calipers. The calibrated image was used to determine the L4-L5 disc angle in degrees.

The L4-L5 motion segment unit was disarticulated from the full lumbar spine and cleaned of paravertebral musculature and other soft tissue. Care was taken to preserve the ligamentous structures of the MSU. A curette was used to remove the remaining annular tissue from the superior and inferior endplates and expose the underlying bone. Exposed bone provided a good foundation for fixation as well as the purchase of screws that provided additional fixation in the pot (Figure 3-3B).

Alignment screws and rubber bands were used to temporarily stabilize the motion segment unit in the custom fabricated mounting pots. The MSU was placed upright and positioned centrally within the pot. The MSU was angled such that the harvested lordotic L4-L5 disc angle was maintained. A needle pin placed centrally into the intervertebral disc under radiographic imaging acted as an external reference to help orient the MSU in its neutral alignment. A low melting point bismuth alloy (Small Parts, Miami Lakes, FL) was poured in the mounting pot to create a cylindrical mold. The mold was broken, the specimen was oriented upside down in the alignment frame, and the procedure was repeated. A level was used to ensure that the potted molds remained parallel. The potted MSU was evaluated to make certain that spinal motion was not hindered by the potting material (Figure 3-3C).

Spinal Instrumentation

The Prodisc-L^{TM} (Synthes, West Chester, PA) is a total disc replacement device designed to maintain motion, restore disc height, and provide stability to the lumbar spine. The implant is a three component device, consisting of two colbalt-chrome-molybdenium alloy (CoCrMo) plates and an ultra-high-molecular-weight polyethylene (UHMWPE) core. The polyethylene core snap-locks into the inferior plate and provides a convex-bearing surface for articulation. The superior plate has a highly polished surface that contacts the convex polyethylene inlay.

The upper endplate component is available in 4 angles; 3, 6, 9 and 11 degrees, to accommodate the natural lordosis of the MSU. The lower endplate component has no built-in lordotic angulation. Each component has a large central keel with lateral spikes to

(A)

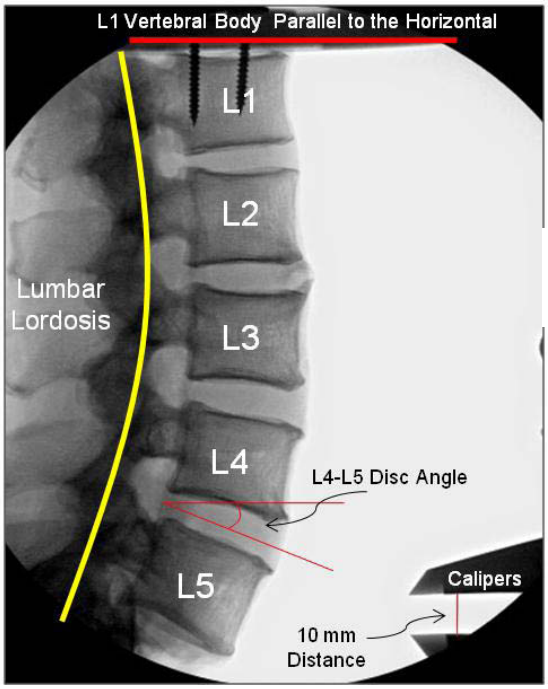

(B)

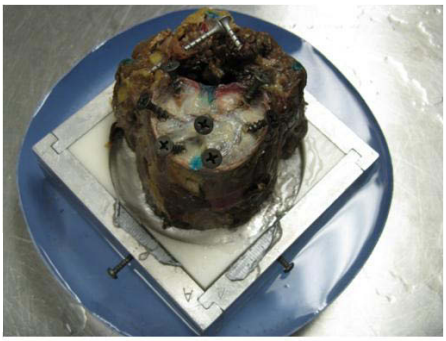

(C)

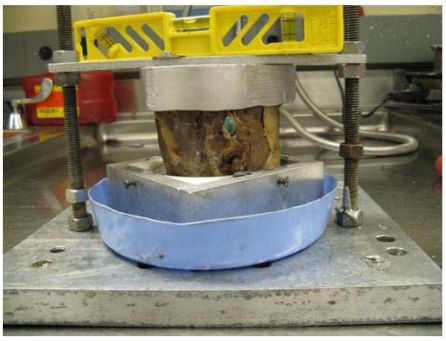

Figure 3-3: Disarticulation and Potting of the L4-L5 MSU in Its Natural Alignment. (A) A calibrated lateral radiographic of the full lumbar spine in its neutral upright alignment was used to determine the L4-L5 disc angle, which was maintained during potting. (B) Wood screws were placed into the endplates and spinous process to provide additional fixation of the vertebral body to the potting material. (C) The L4-L5 MSU was mounted in its natural alignment and centered within the pot. Care was taken to ensure that the pots were parallel to each other and the horizontal datum.

provide immediate fixation and anchorage to the vertebral body. For long term stability the implant surfaces are plasma coated with titanium to enhance bone in-growth.

The fixed COR of the ProDisc-L is intended to permit controlled, predicable movements of the MSU. The COR for this device is located midline within the AP depth of the inferior component and a few millimeters below the endplate of the inferior vertebral body. The axis of rotation can be adjusted vertically with respect to the inferior vertebral body by selection of different polyethylene inlays, whereas the AP placement of the COR can only be adjusted by physical changes in anterior-posterior placement of the implant in the sagittal plane. The polyethylene core or inlay for the ProDisc-L is available in, 10mm, 12mm, and 14mm heights. The COR of the medium implant is positioned 6mm below the endplate with the smallest 10mm inlay height, whereas the COR of the large implant is positioned 8mm below the endplate with the 10mm inlay height (Figure 3-4). With each increase in the inlay height there is a corresponding reduction of 2mm in the COR position below the endplate.

Biomechanically, the implant is a semi-constrained device that allows for 13 degrees of flexion, 7 degrees of extension, 10 degrees of lateral bending and ± 3 degrees of axial rotation around a fixed axis of rotation. Figure 3-5 illustrates the ROM of the device. The ProDisc-L does not allow for AP and lateral translations. The reported range of axial rotation is limited by the anatomy of the MSU and not necessarily the device.

Surgery and Implantation

Surgical discectomy of the MSU was performed by a single spinal surgeon (R. Bertangoli) at the Medical Education and Research Institute. Curettes and rongeurs were used to perform a thorough discectomy. The posterior portion of the annulus and the posterior longitudinal ligament were resected. This allowed for access to the vertebral foreman for the removal of posterior osteophytes and/or herniated materials as well as full remobilization of the motion segment. Lateral aspects of the annulus were preserved to help prevent over-distraction of the segment. Depending on the curvature of the endplates and the presence of osteophytes, endplate remolding was undertaken. Trial implants were used to determine the proper footprint size, lordotic angle, and posterior disc height for the discectomized space. Thereafter, an inserter tool was used to drive the superior and inferior metal plates of the ProDisc-L into the disc space, followed by the polyethylene inlay. A fluoroscopic image was used to position the implant to the appropriate disc depth.

After implantation with the ProDisc-L, there were notable changes in MSU alignment. Tables 3-2 and 3-3 present specimen alignment parameters prior to and post implantation. All measurements were made from lateral radiographs with Image-J software (Open Source, NIH) after the image had been calibrated with a known distance from calipers. Most notably there was a substantial increase in MSU lordotic alignment; increasing from a neutral (0 degrees of lordosis) alignment prior to surgery to the values provided in Table 3-3, column 3. Appendix A presents lateral radiographic images of all test specimens before and after implantation with the ProDisc-L.

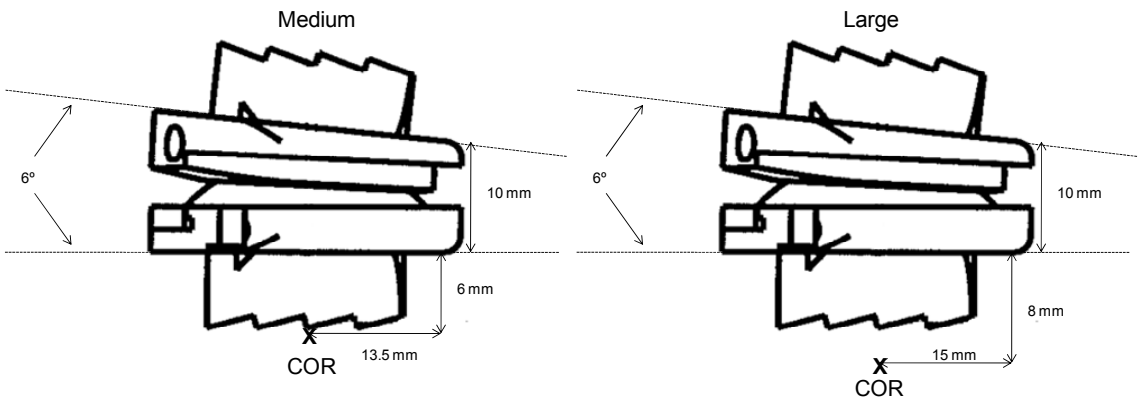

Figure 3-4: **COR Locations of the ProDisc-L with a 10mm Inlay Height.** All MSUs were implanted with a ProDisc-L with a 10mm inlay and 6º lordosis. The CORs of the implant were midline to the AP depth of the inferior component and offset 6mm and 8mm caudally from inferior endplate for the medium and large size implants, respectively.

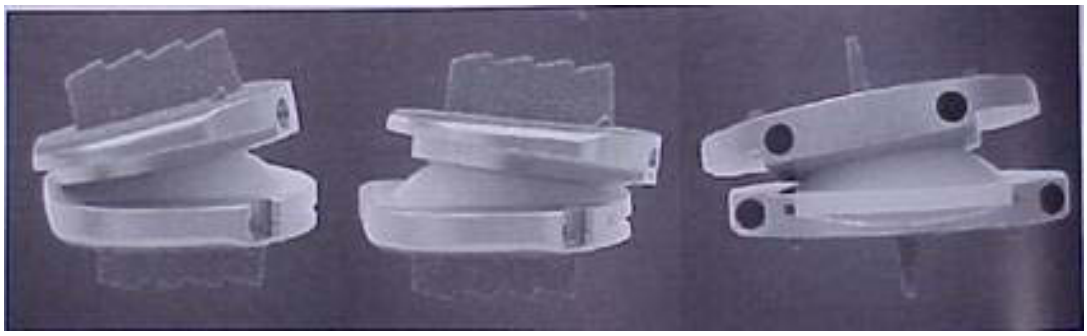

Figure 3-5: ProDisc-L Range of Motion. The ProDisc-L is a semi-constrained device that allows for rotations in all three planes and no translation. The center of rotation of the device is located centrally within the AP depth and offset a few millimeters below the endplate of the inferior plate.

Table 3-2: Harvested Specimen Parameters.

Specimen Name	AP Depth	Posterior Disc Height	Disc Angle*
PD1	33 mm	7.5 mm	8.5°
PD2	35.5 mm	5.5 mm	10°
PD3	35 mm	6.5 mm	8.5°
PD4	35 mm	6.5 mm	7.0°
PD5	39 mm	6.5 mm	6.0°
PD6	37 mm	7.0 mm	7.5°

Note: *Angle created by the intervertebral disc endplates.

Table 3-3: Specimen Parameter after Surgery and Implantation.

Specimen Name	Implant Size*	MSU Lordosis**	Disc Angle***	Endplate Angle Relative to Horizontal †
PD1	L	8.4°	13.0°	14.5° Caudal
PD2	M	6.0°	12.0°	19.5° Caudal
PD3	L	5.0°	12.0°	25.0° Caudal
PD4	M	8.5°	13.5°	16.0° Caudal
PD5	L	9.5°	12.5	15.5° Caudal
PD6	L	6.5°	12.0°	6.5° Caudal

Note: *All implants had a 10mm inlay height and 6° lordosis, **Angle of the upper pot relative to the horizontal datum, ***Angle between the superior and inferior components of the ProDisc-L, †Superior endplate of the inferior vertebral body.

Size selection and placement of the ProDisc-L for each specimen was determined by the spine surgeon's clinical expertise and experience. Each implant was placed posterior to the midline of the intervertebral disc space to disengage the facets, which may have engaged due to the loss in disc height, and decompress the neural space. Furthermore, the posterior positioning better aligned the arc of motion of the proximal vertebra relative to the distal vertebra to the curvature of the facets. This placement would minimize the potential of the facets to separate in flexion and engage in extension. Premature facet engagement or separation may result in a stiffer structure and/or increased loading of posterior elements beyond the normal physiologic range. To achieve the desired placement the largest possible implant footprint size and smallest polyethylene inlay height available with the ProDisc-L were used in each specimen.

The above rationale for the implantation of the ProDisc-L differs from the current approach and education of most surgeons. The majority of surgeons tend place the implant midline and may oversize it. Oversizing ensures that the neural space is decompressed; however, it has the adverse effect of placing the posterior ligaments in tension. No studies presently exist which advocate the placement of the implant midline over a position further posterior. In addition, there are no strict guidelines for the placement of a total disc replacement device.

Harvested radiographs of all MSUs were overlaid with circles by Dr. Bertagnoli highlighting placement of the ProDisc-L using the rationale presented above and are available in Appendix A. In Figure 3-6, the red circle indicates a theoretical ideal placement of the ProDisc-L such that the arc of motion of the proximal vertebra would occur without compression or disarticulation of the facets, resulting in MSU rotations about an unhindered path. The blue and yellow circles represent the arc of motion of the MSU positioned midline and in an anterior most placement respectively. The corresponding colored dots within each circle represent the COR of the implant. The white circle represents the arc of curvature of the facets. Anterior and posterior placed CORs for the specimen in Figure 3-6 were offset 4mm relative to the midline for this specimen.

Table 3-4, shows the difference in the theoretical placement of the ProDisc-L TDR by Dr. Bertagnoli based on harvested radiographs and the actual surgical placement of the ProDisc-L relative to the midline of the disc for each test specimen. On average, an offset of 2.6±1.2mm was observed between anterior-posterior positions relative to the midline for all specimens.

Fixed Axis Protocol

The basic fixed axis testing protocol used here-in consisted of mounting a prepared test specimen within the robotic testing frame in its neutral or post surgical alignment. Each specimen was compressively preloaded to a value of 10N. Anterior-posterior shear and sagittal plane bending moment were actively adjusted to zero values to start. Using the robotic tool tip transformation feature, described previously, a tool tip transform was programmed to a desired location with respect to implant

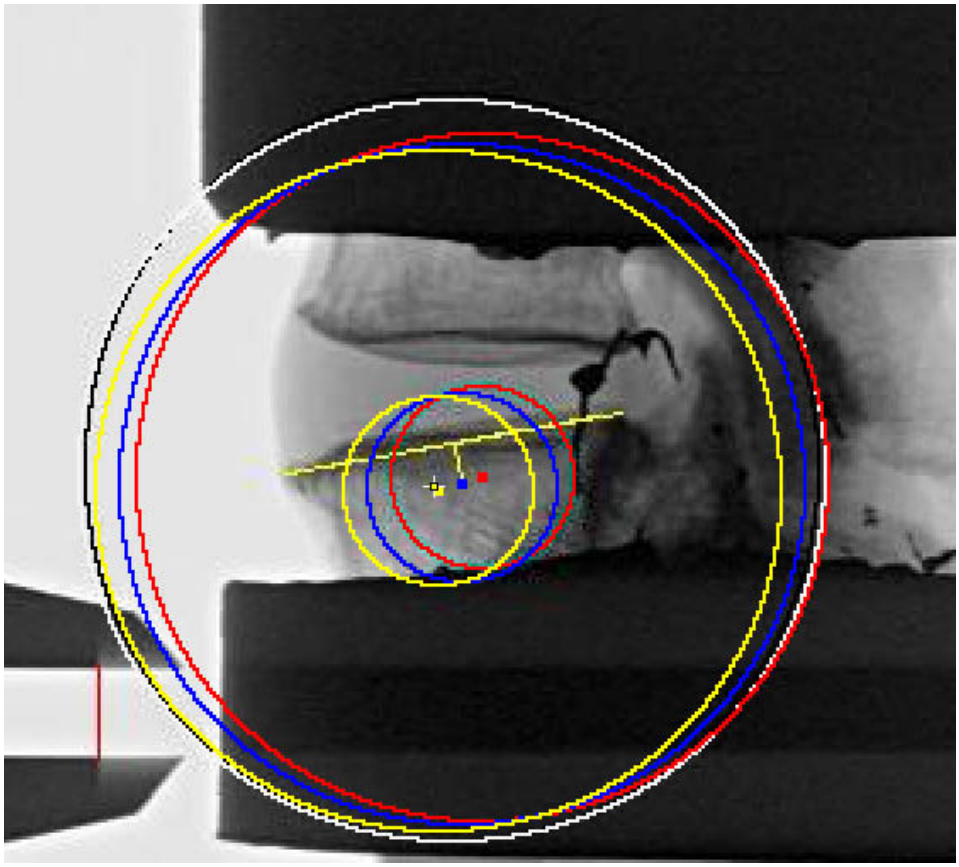

Figure 3-6: **Concentric Circles Determining the Arc of Motion of the Proximal Vertebral Body at Various Placements.** The surgeon's expertise and experience advocates the posterior to midline placement of the ProDisc-L such that the arc of motion of the proximal vertebra is aligned with facet curvature. This would minimize the potential of facet separation in flexion and facet engagement in extension, as well as decompress the neural elements.

Table 3-4: The Theoretical and Actual Placement of the ProDisc-L Implant.

Specimen Name	Theoretical Implant Placement Relative to Midline	Actual Placement Relative to Midline
PD1	1.5 mm Anterior	1.0 mm Posterior
PD2	0.5 mm Anterior	1.5 mm Posterior
PD3	0 mm Midline	2.5 mm Posterior
PD4	1 mm Posterior	3.0 mm Posterior
PD5	0.5 mm Posterior	3.5 mm Posterior
PD6	2.5 mm Posterior	4.0 mm Posterior

geometry/location. Pure rotations of the tool tip location were prescribed in flexion and extension under displacement control at a rotational velocity of 2 degrees per second to an end load limit of 8Nm.

Spinal loads were measured through the use of a six axis load cell. Three orthogonal forces and moments applied to the MSU were measured about a Cartesian coordinate system programmed to be coincident with the tool tip location and hence the selected COR for each test. The load cell, shown in Figure 3-1, was housed in the center of the gimbal, and had a load rating 890N and 444.8N rating along the z axis and both the x and y axes, respectively. It has an accuracy rating to within 1% of the full working range.

Figure 3-7 presents an explanation of the sign conventions used in the fixed axis protocol. A positive axial force value (+Fz) indicated a resultant tensile force normal to the MSU, whereas a negative axial force value (-Fz) signified a resultant compressive force. A positive shear force value (+Fx) represented a net posterior shear and a negative shear force value (-Fx) represented a net anterior shear. A clockwise rotation (flexion) in the sagittal plane created negative moment value (-My), while a positive moment value (+My) was observed during a counter-clockwise rotation (extension).

Spine Conditions

Following instrumentation of test specimens with the ProDisc-L two different specimen conditions were tested; (1) constrained implant spine condition and (2) simulated implant condition tested over a variety of implant sizes and surgical placement variations. Specific details and the rationale behind methods used in each condition are detailed below.

Constrained Implant Spine Condition

An initial goal of this study was to compare the MSU response in terms of mechanics and range of motion to a fixed kinematic rotational input about the COR of the ProDisc-L, both with the implant in place and subsequently about the exact same COR with the ProDisc-L implant removed. This necessitated determination of the COR of the implanted ProDisc-L as accurately as possible such that a robotic tool tip and force frame transform could be performed to the COR location of the implant. A two-fold approach was used to identify the location of the COR of the implanted ProDisc-L. The first step consisted of direct measurement of the COR location from lateral radiographs of implanted test specimens. The second step was an iterative process that attempted to refine the location of the COR by shifting its location by small incremental amounts until a minimal and constant compressive and shear force response was observed over a short range of rotational input about the COR. It was hypothesized that (1) over an initial small range of rotation posterior tissue resistance would be minimal and (2) a COR selection that was coincident with the true COR location of the implant would result in minimal force resistance due to mechanical contact or impingement of spherical bearing surfaces

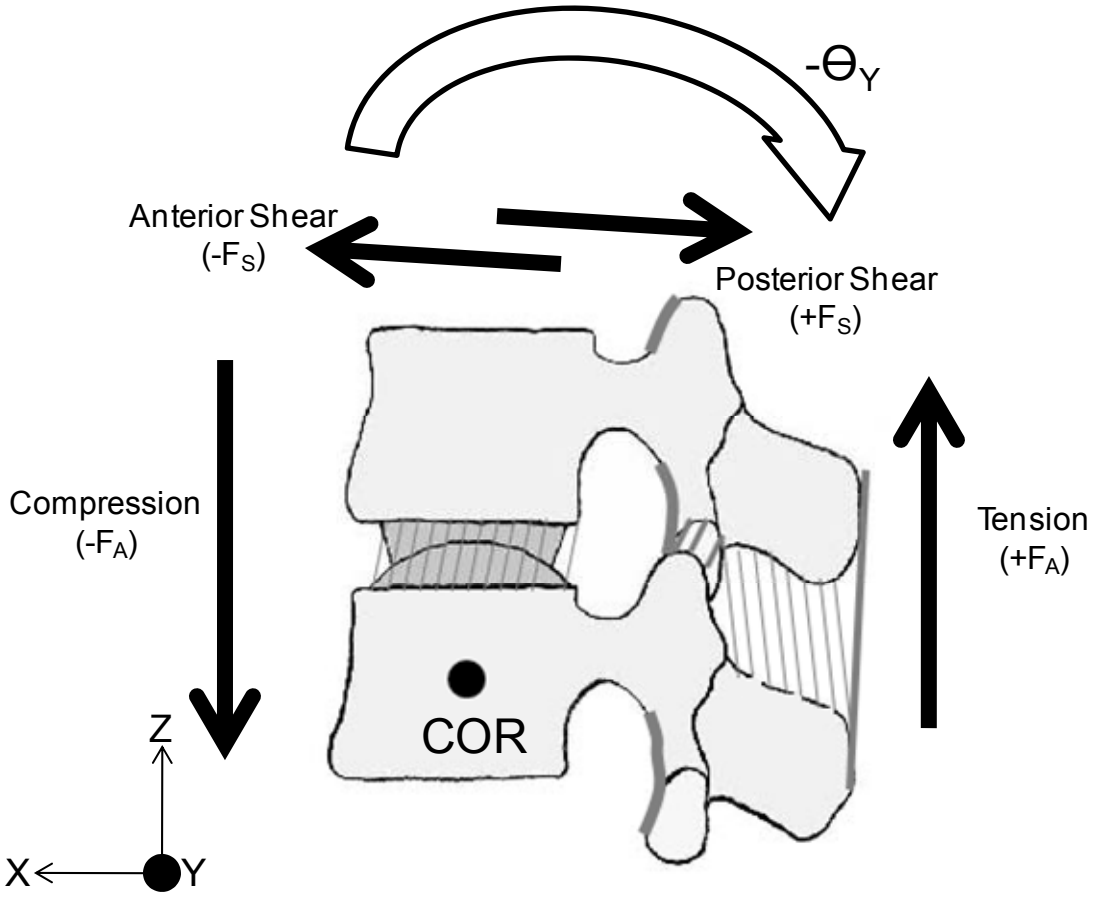

Figure 3-7: **Sign Convention of Test Results.** When the above external forces were applied to the proximal end of an MSU via robotic motion, the six axis force sensor (interposed between the robot and proximal vertebra) recorded forces with the sign conventions given. All spinal forces and moments were measured at the center of rotation of the implant. [Source: Adapted with permission. Huang R. The Implication of Constraint in Lumbar Total Disc Replacement. Journal of Spinal Disorders and Techniques 2003; 16(4): 412-417.]

of the implant itself. Conversely if the programmed point of rotation did not coincide with the true ProDisc-L COR there would be discernable differences in loads due to contact forces resulting from forcing a ball and socket to rotate about a point not coincident with the mechanical COR.

Figure 3-8, shows a schematic that helps identify the position of the implant's COR relative to the location and orientation of the null tool tip of the Spine Robot. The position of the robotic null tool tip was midline and offset 9.76mm caudally from the top edge of the superior pot. The X an Z coordinates of the COR were identified using the measurements presented in Figure 3-4. The X and Z translations from the null tool tip to the COR of the implant were calculated by subtracting the X and Z coordinates of the null tool tip and COR. Thereafter the tool tip location and force sensing reference frame were programmed to be coincident with the selected COR for all tests.

Potential errors in determining the COR location from radiographic analysis including image distortion, measurement and implant mal-alignment in the sagittal plane meant that it was necessary to refine the location of implant's COR using the Spine Robot, which had a positional accuracy in the micrometers.

Using the radiographic COR transforms as a starting point, the MSU was rotated in flexion-extension to an end rotational limit of three degrees. This was followed by an iterative process involving the adjustment of the X and Z tool transforms at 0.25mm increments left-right and up-down from the initial point to fine-tune the true location of the COR. Adjusting the X transform had a noticeable effect on the axial force loading behavior, whereas adjusting the Z transform significantly affected the shear force loading behavior. Figure 3-9A illustrates that shifting the COR cephalic (up, U) increased the posterior shear force, whereas shifting the COR caudal (down, D) increased the anterior shear force. During the onset of rotation the direction of net shear force was unpredictable. It was hypothesized that the orientation of the facets and relative position of the COR with respect to the facets significantly contributed to the orientation of the shear force. Therefore, when analyzing the effects of shifting the tool tip location on shear force, the goal was to maintain a constant shear force over three degrees of rotation.

With respect to anterior-posterior (AP) changes in the tool tip location, Figure 3-9B illustrates that shifting the tool transform anteriorly (to the right, R) increased the net axial force, likely due to increased tensile engagement from the posterior structures. Shifting the tool transform posteriorly (to the left, L) resulted in a net compressive force, likely due to implant contact. Final AP location of the implant COR was honed by finding the inflection point from which axial load shifted from a net compressive to a net tensile force; this point suggested that the implant components were just barely making contact. During these rotations the change in moment was observed to be minimal, less than 0.5Nm over a three degree range of motion.

After finalizing the location of the COR in both the A-P and P-D directions, the MSU was rotated about the selected COR in flexion and extension to a moment end limit of 8Nm. All positional robot data as well as six axis force sensor data were recorded for each test at a sampling rate of 60Hz.

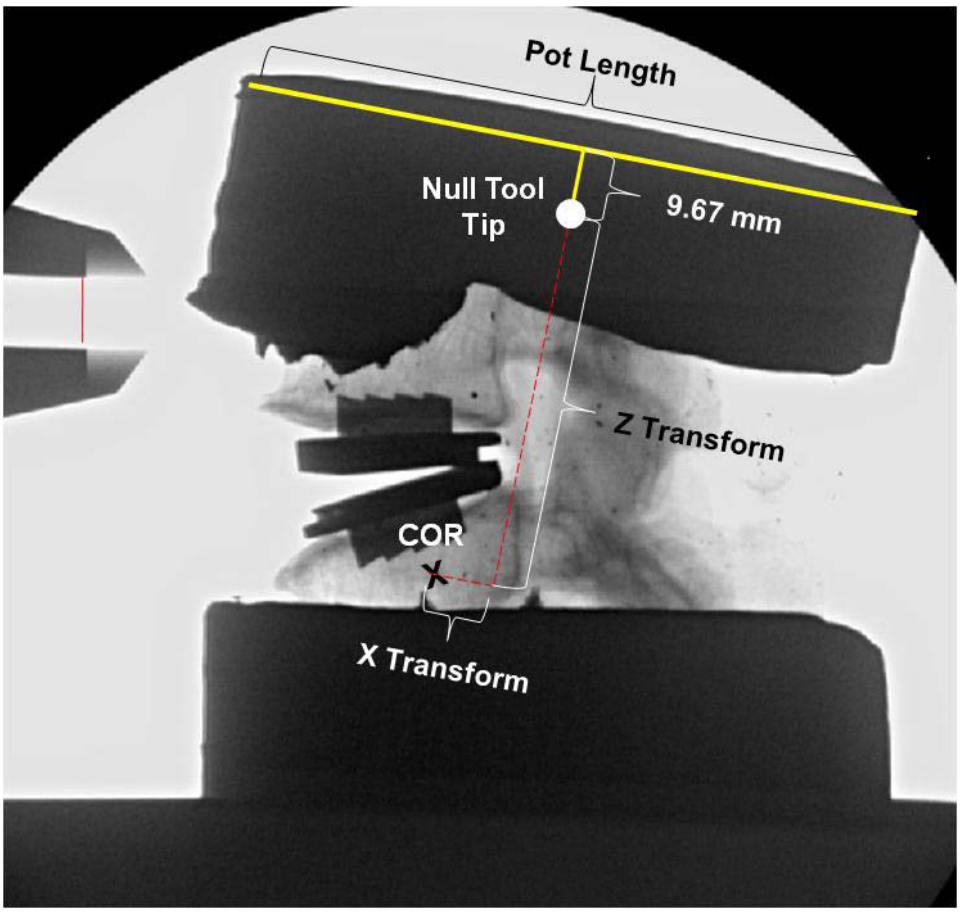

Figure 3-8: **Identifying the COR of the Implant.** A calibrated radiograph allowed for determination of the X and Z transform from coordinated values of the null tool tip and COR. The X and Z transforms from the radiographic image were programmed into the Spine Robot, such that the MSU was rotated about the COR of the ProDisc-L implant.

(A)

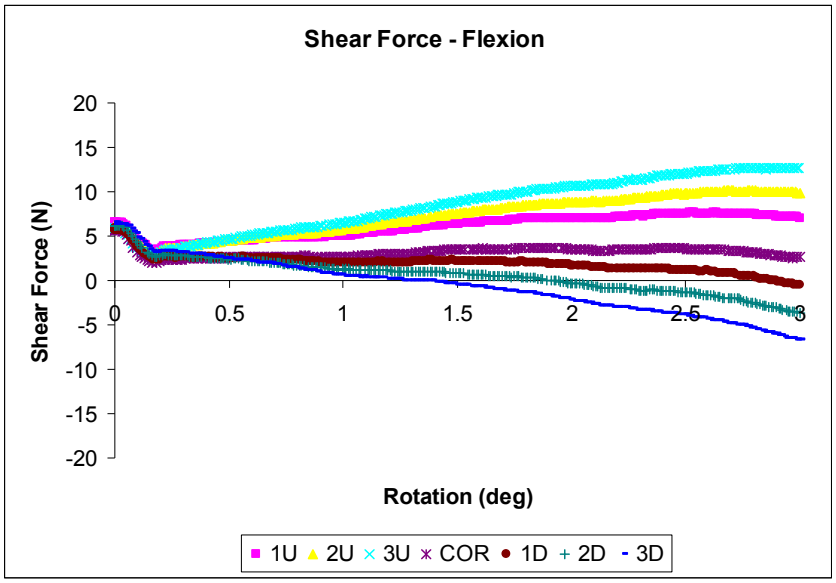

(B)

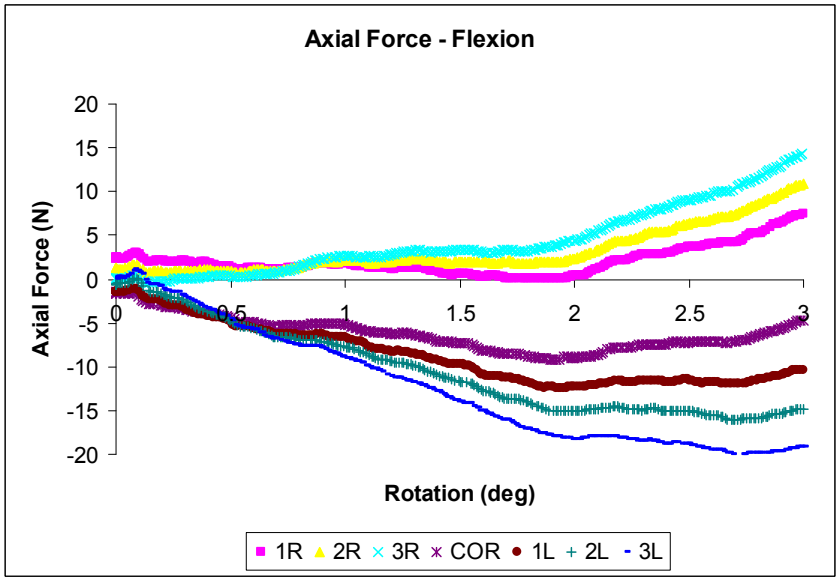

Figure 3-9: Fine-Tuning the COR Location. (A) Adjusting the Z transform alone predominately affected the shear loading profile. Due to the unpredictable orientation of the net shear force during the onset of rotation, the objective was to maintain a constant shear load over the ROM. A positive shear force indicated a posterior shear, while a negative shear force indicated an anterior shear force. (B) Adjusting the X transform affected the axial loading. The goal was to find the inflection point where net axial loading response shifted from a net compressive load to a net tensile load. Tensile forces generated a positive axial force whereas compressive forces generated negative axial force. The radiographic center of rotation (COR) was shifted a total of 3mm up (U, Cephalic)-down (D, Caudal) and left (L, Posteriorly)-right (R, Anteriorly) until the refined COR location was identified.

Following rotational testing of the implanted case about the refined COR location, the ProDisc-L implant was removed from the test specimen while the specimen remained securely fixed within the robotic testing frame. To achieve this, the specimen was distracted slightly to an end load limit of 50N in tension. The insert tool was coupled to the individual components of the implant and used to distract the superior component of the implant from the inferior component. Thereafter, a number 22 scalpel was positioned underneath the polyethylene inlay and forceps were used to extract the inlay from the disc space. Thereafter, the superior component of the ProDisc-L was removed.

Subsequently, the specimen was repositioned to the exact same starting position as tests performed with the implant in place and rotated in flexion and extension to a moment end limit of 8Nm about an identical COR to that of the implant as placed by the surgeon. The axial force, shear force, and stiffness curves with and without the implant were compared. Figure 3-10, show radiographs of a MSU rotated about identical CORs both with and without the implant.

Simulated Implant Condition: Various Sizes and Placements

In order to simulate other possible implant sizes and placements within a given test specimen, thereafter, each MSU was rotated about a series of COR points, arranged in a customized grid pattern as shown in Figure 3-11. The grid pattern consisted of 8 CORs which simulated different placements of both a medium and large size simulated constrained ball and socket device, like the ProDisc-L. The points were aligned in two different planes, 6 and 8mm below and parallel to the inferior endplate. The 6mm plane consisted of 5 points and represented possible COR locations with the medium sized simulated implant; while the 8mm plane consisted of 3 points and represented possible COR locations with the large sized simulated implant. The nomenclature for the 8 point grid system consisted of two letters with an optional plus sign. The first character in the nomenclature identified the plane, L- for the large size implant plane (8mm plane) and M- for the medium size implant plane (6mm plane). The second character identified the position relative to the midline of the disc space; M- for midline, P- for posterior, and A- for anterior. The plus sign signified an additional translation of 1.5mm, which could occur if a large size implant was exchanged for a medium as determined by Equation 3-1, where AP_{large} is the anterior-posterior depth of the large implant (30mm) and AP_{medium} is the anterior-posterior depth of the medium implant (27mm).

$$Aditional\_Translation = \frac{APl\arg e - APmedium}{2} \qquad \text{(Eq. 3-1)}$$

Of the specimens used in this study four were implanted with a large size ProDisc-L and two with a medium size. For the large size placements each grid pattern was dimensionally scaled according to the end plate width of a given specimen. The grid pattern location was first determined by identifying the implanted ProDisc-L COR location based on the surgeon's preference for a posterior most placement of the implant with the largest possible footprint size and the smallest inlay height. From there a large sized implant could optionally be positioned centrally or midline within the disc space or

(A)

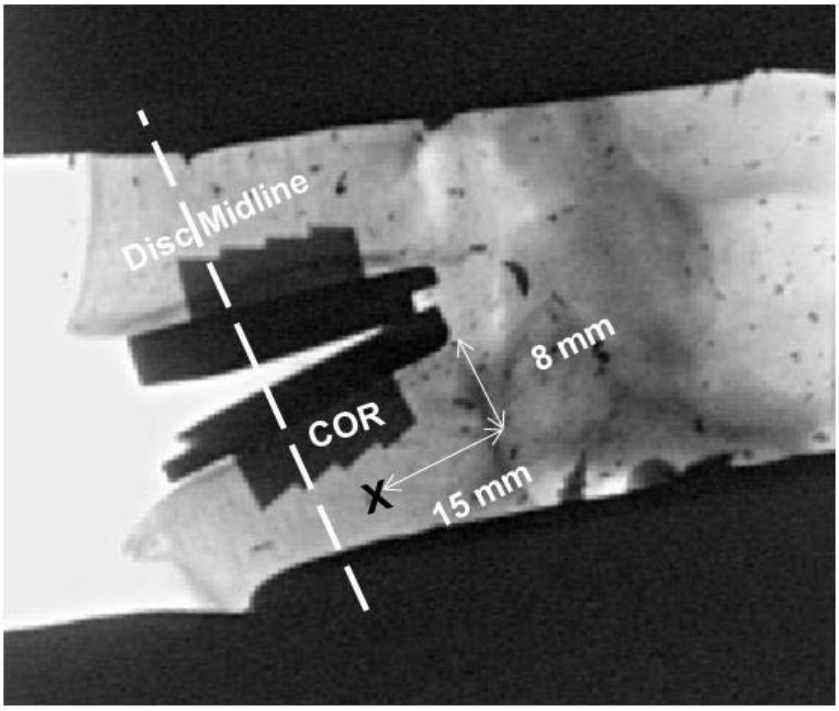

(B)

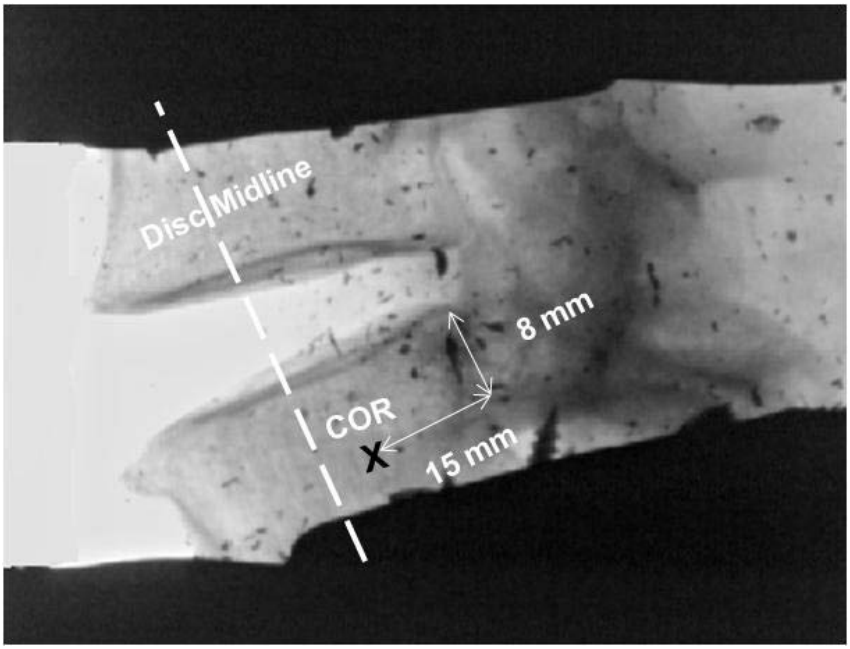

Figure 3-10: **Constrained Implant Simulation.** (A) Lateral radiograph with the COR of the ProDisc-L identified. (B) Lateral radiographs of the same MSU with the implant removed. The MSU was rotated about the COR of the implant and then, with MSU held rigid, the implant was removed and the test was repeated.

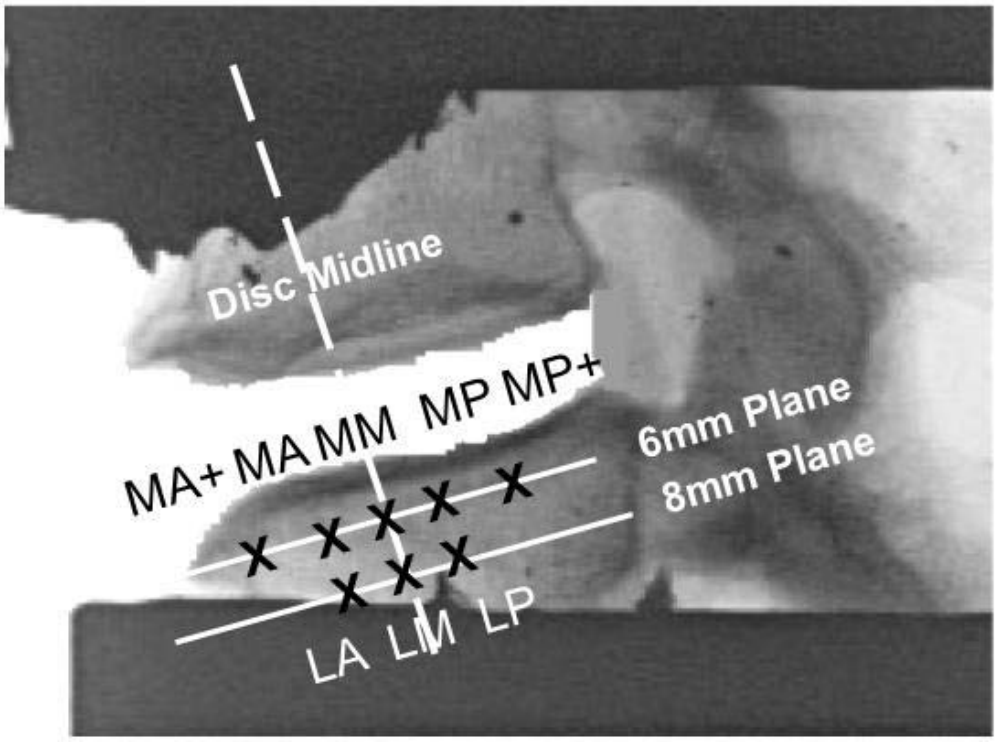

Figure 3-11: **Grid Pattern of Simulated CORs.** A customized grid pattern was based on the surgeon's preference for the posterior placement of the implant with the largest footprint size and the smallest inlay height.

an equivalent distance anterior from the midline as the posterior placement. The offset of the anterior and posterior points relative to the midline of the disc and parallel to the inferior endplate of a given specimen was determined by Equation 3-2 where AP_{disc} is the anterior-posterior depth of the endplate and $AP_{implant}$ is the anterior-posterior depth of the implant.

$$Maximum\_AP\_Offset = \frac{APdisc - APimplant}{2} \quad \text{(Eq. 3-2)}$$

Positioning the implant further posterior than the Maximum AP Offset distance would cause the implant to encroach the vertebral foramen. Positioning the implant further anterior than the Maximum AP Offset would place the implant past the anterior lip of disc space. Simulation of a medium size implant selection and placement for the four test specimens physically instrumented with large size ProDisc-L was performed using 5 COR locations with the midline, anterior and posterior locations similarly spaced as that determined for the large size implant along the 6mm plane. The narrower depth of the medium size implant permitted additional COR locations namely MA+ and MP+, to be considered as per Equation 3-1.

The two specimens physically implanted with medium size implants by the surgeon were dimensionally smaller. For these specimens the COR grid pattern was determined in an identical manner but starting with the posterior most placement of the medium sized implant as preferred by the surgeon. In the case of one test specimen the posterior most placement of the medium sized implant was less than 1.5mm from the midline of the disc with the result that MA+ and MP+ placements were not possible. Similarly with this specimen there was insufficient disc width in the sagittal plane to consider LP and LA simulated COR placements.

For testing and programming of the Spine Robot the simulated COR grid pattern locations for each specimen needed to be transformed into the robot tool tip reference frame to determine X and Z translations of the tool tip for each COR. The transformations are presented in Table 3-5 and were calculated based on disc angle, robot pitch (sagittal plane) angle, and the simulated COR's relative position to the refined COR of the implant. Equations 3-3 and 3-4 below calculated simulated COR positions within the same plane, i.e. the Medium (6mm) or Large (8mm plane), whereas Equations 3-5 and 3-6 calculate simulated COR positions in the alternate plane.

$$X_{COR\_In-Plane\_AP\_Shift} = X_{Implanted\_COR} \pm [AP\_shift * COS(\Theta_d) * COS(\Theta_p)] \quad \text{(Eq. 3-3)}$$

$$Z_{COR\_In-Plane\_AP\_Shift} = Z_{Implanted\_COR} \quad \text{(Eq. 3-4)}$$

$$X_{COR\_Between\_Plane\_Shift} = X_{Implanted\_COR} + (PD\_shift * COS(90 - \Theta_d - \Theta_p) \quad \text{(Eq. 3-5)}$$

$$Z_{COR\_Between\_Plane\_Shift} = Z_{Implanted\_COR} + (PD\_shift * SIN(90 - \Theta_d - \Theta_p) \quad \text{(Eq. 3-6)}$$

Table 3-5: Tool Tip Transforms for Simulated COR Positions.

Implant Type	Specimen Name	Radiograph Implant COR	Fixed Axis Implant COR	Grid Point Placement				
				Anterior +	Anteiror	Midline	Posteior	Posterior +
Medium Size	PD1	(12,-64.5)	(13.75, -60)	(17.88,-58.16)	(16.44, -58.16)	(15.49, -58.16)	(14.53, -58.16)	(13.09, -58.16)
	PD2	(16, -54.5)	(14.5, -56)	N/A	(17.36, -56)	(15.93, -56)	(14.5, -56)*	N/A
	PD3	(12.5, -60.0)	(11, -60)	(17.86, -58.28)	(16.53, -58.28)	(14.28, -58.28)	(12.03, -58.28)	(10.67, -58.28)
	PD4	(9.5, -52.5)	(11, -48)	(16.62, -48)	(15.21, -48)	(13.81, -48)	(12.4, -48)	(11, -48)*
	PD5	(13, -52.5)	(13.7, -50)	(22.62, -48.19)	(21.20, -48.19)	(17.87, -48.19)	(14.54, -48.19)	(13.12, -48.19)
	PD6	(16, -56.0)	(12, -50)	(21.83, -48.05)	(20.35, -48.05)	(16.41, -48.05)	(12.46, -48.05)	(10.98, -48.05)
Large Size	PD1	(12,-64.5)	(13.75, -60)	N/A	(15.67,-60)	(14.71,-60)	(13.75,-60)*	N/A
	PD2	(16, -54.5)	(14.5, -56)	N/A	N/A	(15.18, -57.85)	N/A	N/A
	PD3	(12.5, -60.0)	(11, -60)	N/A	(15.51, -60)	(13.25, -60)	(11, -60)*	N/A
	PD4	(9.5, -52.5)	(11, -48)	N/A	(14.36, -49.78)	(12.90, -49.78)	(11.50, -49.78)	N/A
	PD5	(13, -52.5)	(13.7, -50)	N/A	(20.35, -50)	(17.03, -50)	(13.7, -50)*	N/A
	PD6	(16, -56.0)	(12, -50)	N/A	(19.89, -50)	(15.94, -50)	(12, -50)*	N/A

Note: *Represents the simulated point that coincides with location of the Implant's COR as positioned by the surgeon.

where,

$X_{Implanted\_COR}$ = x tool tip transform of the surgically implanted COR
$Z_{Implanted\_COR}$ = z tool tip transform of the surgically implanted COR
AP_shift = linear anterior-posterior translation along the Medium or Large plane from the implanted COR to the simulated COR
PD_shift = translation of 2mm between Medium (6mm) and Large (8mm) planes
Θ_d = disc angle: angle of the superior endplate of inferior vertebral body with respect to the horizontal
Θ_p = robotic pitch angle: tilt angle of the upper pot with respect to the horizontal datum in the sagittal plane

Note: the z tool tip location moved with robot as the disc space was distracted or reduced in height, and therefore remained effectively unchanged.

Shifting the COR placement in the anterior-posterior plane required an associated height change in the proximal-distal direction, owing to the wedge shaped opening of the disc space itself. Simulating a COR further posterior than the surgically implanted COR of the implant required distraction of the disc space, while simulating a COR more anterior required a reduction in the disc space. The associated height change with AP changes in the implant placement is illustrated schematically in Figure 3-12. Equation 3-7 was used to quantify the amount of height change. When a medium sized implant was simulated there was an additional height increase of 0.16mm, which was the inherent height difference from the peak of the concave component of the superior implant to its keel. The associated height change was accomplished by displacing the vertical actuator upward when simulating a posterior placement of the implant and downward when simulating a more anterior placement. During vertical displacement the relative positions of the remaining actuators were held stationary.

$$delta\_height = AP\_shift * SIN(\Theta_d) \qquad \text{(Eq. 3-7)}$$

where,

AP_shift = linear anterior-posterior translation distance along a disc plane from the implanted COR to the simulated COR
Θ_d = disc angle: angle of the superior endplate of the inferior vertebral body with respect to the horizontal.

Distraction of the disc space placed the posterior ligaments in tension and increased the net sagittal plane bending moment. To alleviate the moment buildup the MSU was rotated in extension at 0.25 degree intervals until sagittal plane moment returned to the baseline value. Thus the associated height change with variations in the AP placement of the COR resulted in changes in the lordotic angle of the MSU to maintain a zero bending load state. The reduction of the disc space had no effect on the sagittal plane moment. Redefining the disc space height and lordotic orientation for the simulated CORs ensured that physical changes to MSU alignment associated with changes in implant sizing or placement were as realistic as possible.

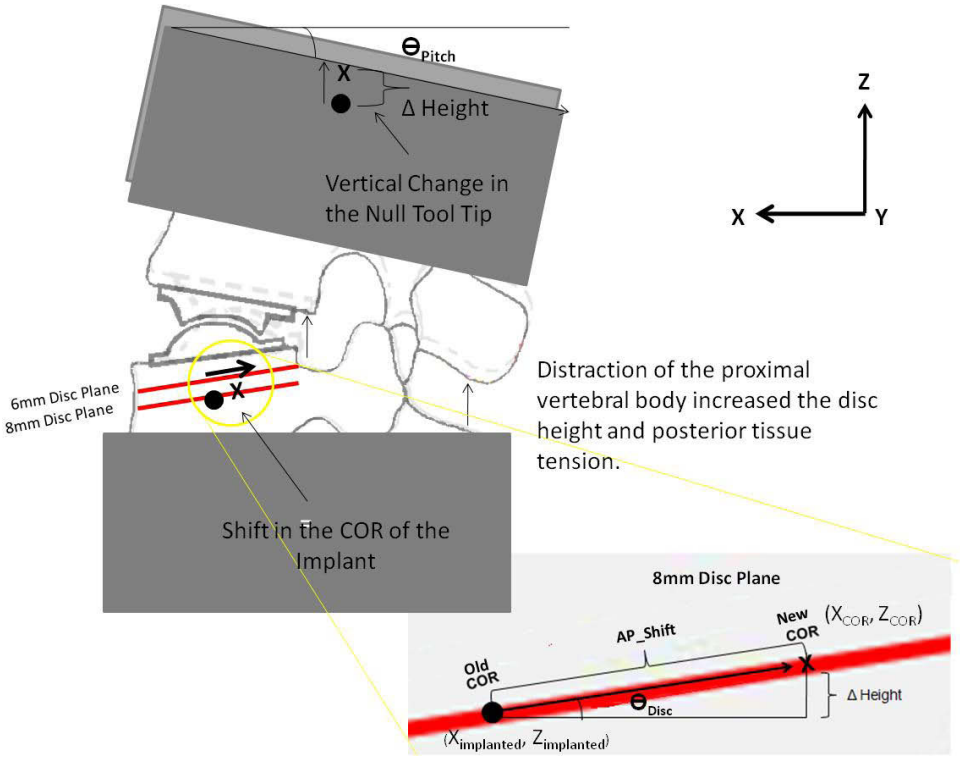

Figure 3-12: Associated Height Change Due to Variations in the AP Placement of the Simulated CORs. An AP translation in the location of the COR had an associated height change in the proximal-distal plane. Positioning the COR posteriorly required a distraction of the disc space, whereas shifting the COR anteriorly required a reduction in the disc space.

Data Measurement

Two sets of positional data were collected. The first set of data consisted of the absolute positions and displacements of all the actuators and was referred to as the joint data. The second set of data consisted of the absolute positions and displacements of the tool tip location itself. Linear displacements were recorded and presented in millimeters whereas all rotation data was collected and reported in degrees.

Force data was collected as net forces (Newtons) and moments (Newton-meter) measured along the three orthogonal axes of a right Cartesian system with the origin programmed to lay coincident with the tool tip of the Spine robot and hence the programmed COR location.

Following data collection and force data analysis all force data was transformed to an anatomical reference frame aligned with the orientation of the superior endplate of the inferior vertebral body such that reported shear force was along the endplate of the disc in the sagittal view and the axial force was perpendicular to the endplate. Sign conventions for each force component were reported in Figure 3-7. The angle of the endplates for each specimen was determined through lateral radiographs. Equations 3-8 and 3-9 were used to transform shear and axial forces from values recorded in the load cell reference frame centered at the COR to values aligned with the endplate and COR planes.

$$F_{Shear\_Endplate} = Fx * \cos(\Theta_T) - Fz * \sin(\Theta_T) \quad \text{(Eq. 3-8)}$$

$$F_{Axia\_Endpalte} = Fx * \sin(\Theta_T) + Fz * \cos(\Theta_T) \quad \text{(Eq. 3-9)}$$

where,

$\Theta_{Total} = \Theta_{Disc}+\Theta_{MSU}$ at the onset of rotation,
$\Theta_{Disc}-(\Theta_{Rotation}-\Theta_{MSU})$ at the end load limit in flexion, and
$\Theta_{Disc}+(\Theta_{Rotaiton}+\Theta_{MSU})$ at the end load limit in extension.
Θ_d = disc angle: angle of the superior endplate of the inferior vertebral body with respect to the horizontal
Θ_{MSU} = robotic pitch angle at the onset of rotation
$\Theta_{Rotaiton}$ = robotic pitch angle at end load limit
F_x= x direction force value recorded from load sensor
F_z = z direction force value recorded from load sensor

Errors in load cell readings due to changes in the orientation of the load cell within the gravitational field caused deviations in the force readings. A protocol reported by Kelly et al. was used to quantify these errors and apply a correction factor. The Spine Robot, mounted with a potting mold of 20N, was programmed to rotate about a point offset 50mm below the null tool tip. Starting at a -15 degree angulation, it was commanded to rotate clockwise 30 degrees at a speed of 1.28 degree of rotation per second. The force and position output was recorded at a sampling rate of 10Hz. Plots of shear and axial forces as a function of rotation revealed second and third order polynomial, as per Equations 3-10 and 3-11.

$$Shear\_Error = (-1\times10^{-05})*\Theta^3 + (-4\times10^{-05})*\Theta^2 + (0.1746)*\Theta \quad \text{(Eq.3-10)}$$

$$Axial\_Error = (-0.0016)*\Theta^2 + (0.0032)*\Theta \quad \text{(Eq. 3-11)}$$

A correction factor of the pot weight had to be applied to the load cell data to determine the true value of the external load acting on the MSU. The top mounting pot applied a net compressive load of approximately 18N to the MSU, which was not seen by the load cell. Assuming the center of gravity was at the center of the mold and acted vertically during rotation, a correction factor as a function of the pitch angle was determined, as described by the Equations 3-12 to 3-14.

$$Shear\_Pot\_Err = -pot.w*\sin(\Theta_p) \quad \text{(Eq. 3-12)}$$

$$Axial\_Pot\_Err = -pot.w*\cos(\Theta_p) \quad \text{(Eq. 3-13)}$$

$$M\_Err = [-pot.w*\sin(\Theta_p)*(\Delta z\times10^{-3})] + [-pot.w*\cos(\Theta_p)*(\Delta x\times10^{-3})] \quad \text{(Eq.3-14)}$$

where,

pot.w = weight of the upper pot in Newtons
Θ_P = angulation of the upper pot of the MSU in degrees
Δx = offset distance of pot weight component relative to the axis of rotation
Δz = offset distance of pot weight component relative to the axis of rotation

Statistics

Statistical analysis was conducted on all data transformed to the disc space using SigmaStat 3.5 (Systat Software Inc., San Jose, CA). The data was indexed (specimen name and condition) and statistical ranking was applied to the data set for non-normal distributions. The shear force, axial force, and range of motion data for both flexion and extension were compared for each test condition at a moment end limit of 8Nm.

A paired student's t-test was conducted for the load response and ROM with and without the implant at P=0.05. Statistical analysis on the simulated CORs was likewise performed for the shear force, axial force, and ROM. Both inter- and intra- plane simulated CORs were compared using a One-Way Repeated Measure ANOVA with a SNK multiple comparison test at a P=0.05. Inter- plane comparison concluded if differences existed between the large and medium size CORs for identical AP placements, whereas intra-plane comparisons determined if differences existed between different AP placements with either the large or medium size implant.

CHAPTER 4: RESULTS

Constrained Implant Compared to a Simulated Ball and Socket Implant

Typical force-displacement and stiffness curves for MSUs rotated with and without the ProDisc-L TDR about the surgically implanted COR are presented in Figure 4-1. The axial loading curves in both flexion and extension show a higher initial load value of approximately 40N for the simulated implant condition over the ProDisc-L condition. The increased tensile force on the load cell was due to internal load sharing between posterior tissue structures in tension and the ProDisc-L implant which acted to structurally support this load in compression. The net load as recorded by load cell was effectively zero in this condition. With the test specimen held securely in the robot frame and with the implant removed, resistance to the posterior tissue tension was provided by the robot frame itself and thus discernable by the six axis load sensor to which the specimen was mounted proximally. On average the simulated implant condition revealed 43±23N of pre-tensioning over all test specimens. Initial shear force values likewise exhibited differences, on average -18±15N over all test specimens prior to testing. However in this case the sign of the change was not always consistent, 4 specimens demonstrated an increase in shear while 2 specimens demonstrated a decrease in shear with the ProDisc-L removed. Differences in the resistive stiffness (slope) and neutral zone can be observed between the two test conditions, which resulted in increased sagittal plane rotation at 8Nm for the simulated implant condition.

The means and standard deviations of peak shear and axial loads over all test specimens for the ProDisc-L and simulated implant conditions in flexion and extension are provided in Figure 4-2. The data was analyzed at a common end limit of load to permit statistical comparison. A paired t-test at P=0.05 was used to compare the differences in the load mechanics and range of motion with and without the ProDisc-L. Data tables are provided in Appendix B.

In flexion, the axial and shear force graphs indicate significantly higher loading and range of motion with the simulated implant as compared to the Prodisc-L condition, with mean values of 432±73N as compared to 116±40N and 8.3±1.1 degrees compared to 6.4±1.1 degrees, respectively. A significantly greater net anterior shear force was observed for the simulated implant with a mean value of -157±73N as compared to the ProDisc-L condition, which had a mean value of -81±25N. During extension, MSUs implanted with the ProDisc-L reported significantly higher net shear and axial forces, as well as less sagittal plane rotation as compared to the simulated implant case. Loading in both conditions exhibited a net posterior shear and compressive force. For the ProDisc-L condition the mean shear and axial forces were 153±19N and -153±33N, respectively. For the simulated implanted condition a net posterior shear force of 96±22N was observed and a mean compressive force of -58±68N. Mean extension range of motion was 2.2 ± 0.6 degrees for the ProDisc-L condition as compared to 2.5 ± 0.8 degrees for the simulated implant condition. Data tables are provided in Appendix B.

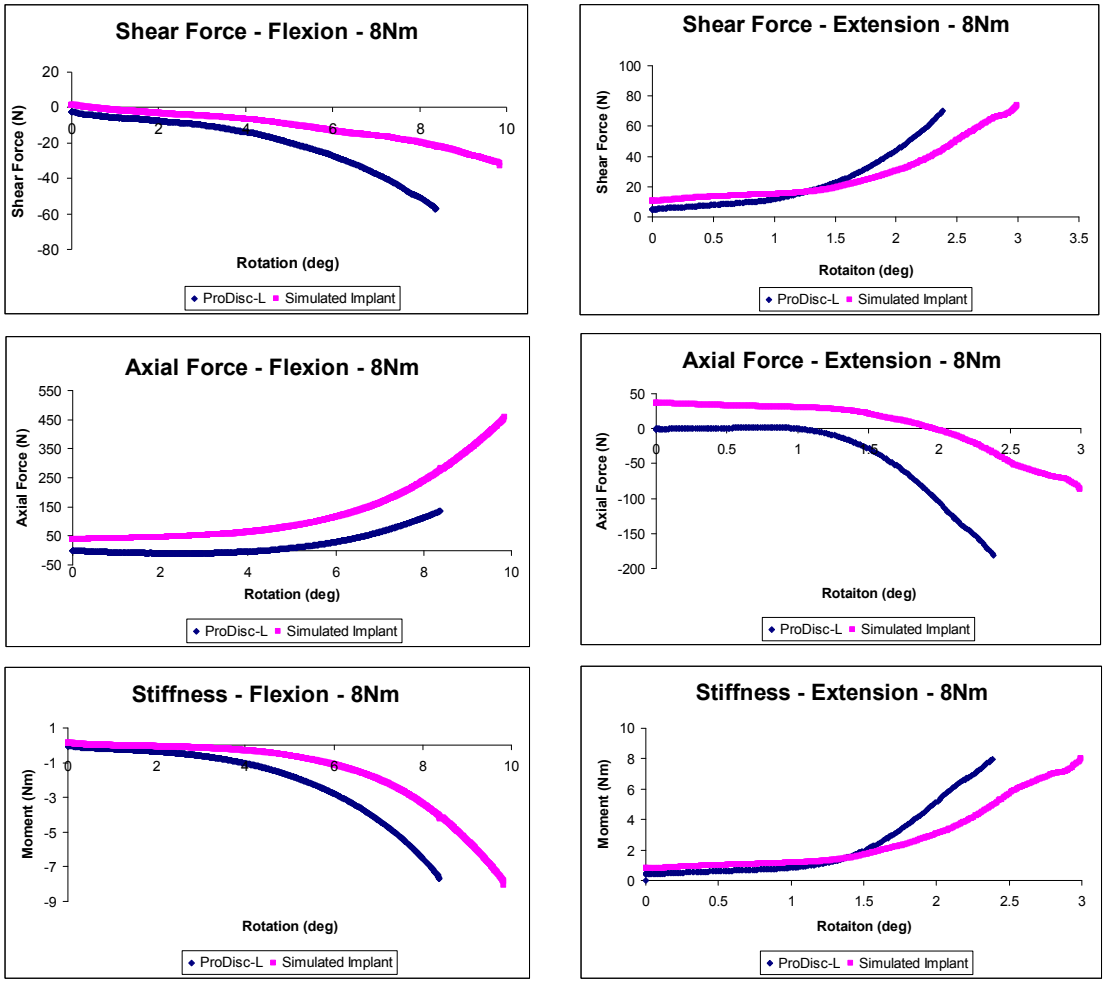

Figure 4-1: **Flexion and Extension Force–Displacement and Stiffness Curves for Specimen PD1 for Rotation about the Same COR with and without the ProDisc-L Implant in Place.**

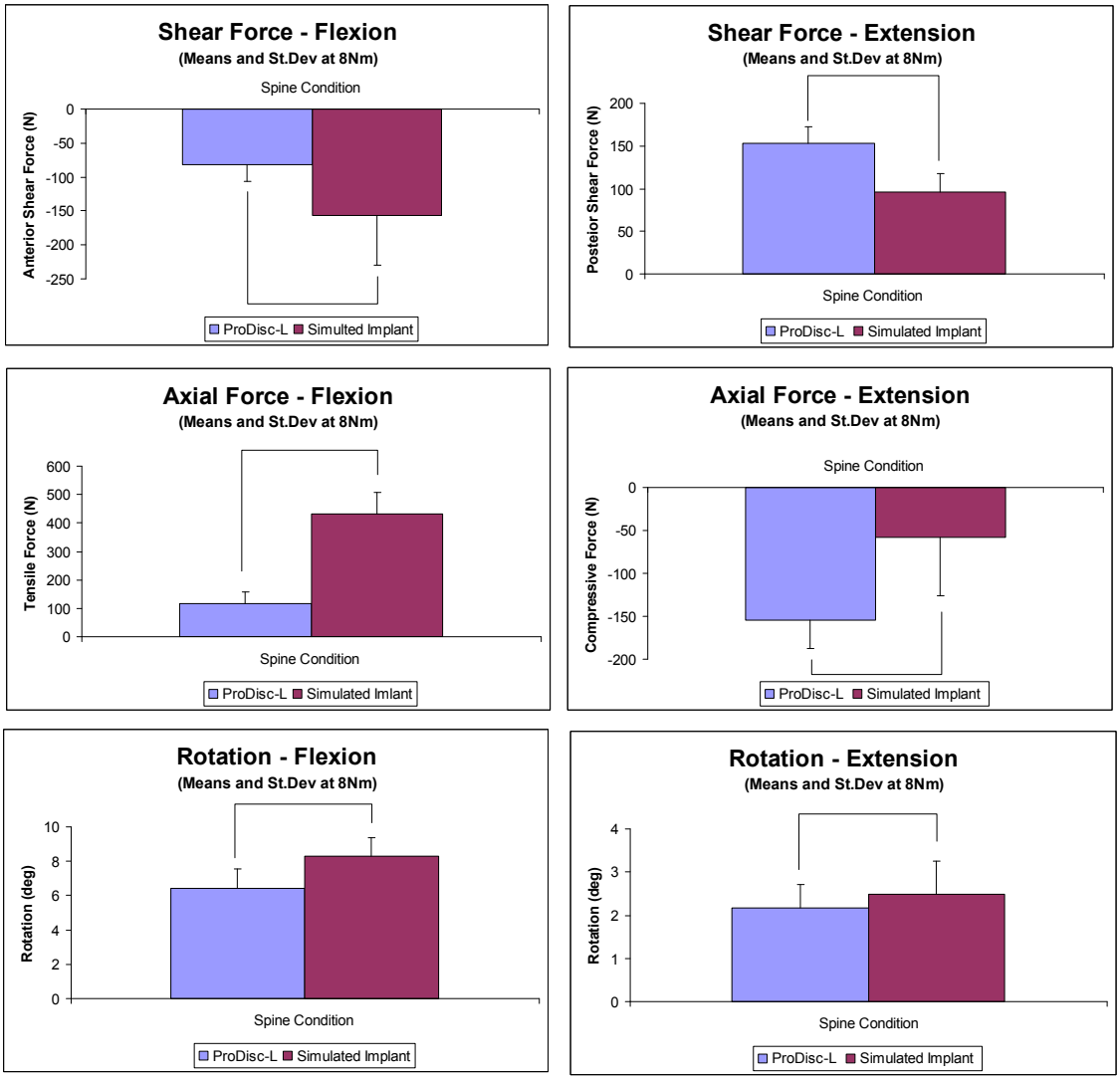

Figure 4-2: **Disc Mechanics and Sagittal Plane Rotation Graphs for MSUs Implanted with and without the ProDisc-L in Flexion and Extension.** The bars represent significant differences between the different spine conditions.

Simulated Ball and Socket Implant: Variations in Sizing and Placement

Effects of Simulated Implant Size: Medium versus Large

Load mechanics and range of motion graphs comparing simulated medium and large size implants at anterior-posterior (AP) placements are provided in Figure 4-3. A one-way RM ANOVA with SNK at P=0.05 was used determine significant differences between the two different simulated implant sizes at equivalent COR placements. Data tables are provided in Appendix B

In flexion, the simulated large implant experienced a significantly greater net anterior shear force for Anterior, Midline, and Posterior placements; approximately 10N greater shear force was observed for the simulated large implant as compared to the simulated medium implant. During extension, no significant differences were observed between the two simulated implant sizes for any AP placement. In flexion, significant differences in the net tensile load were observed between the medium and large size simulated implants for the Posterior and Midline placement with mean values of 439±85N as compared to 445±67N and 373±62N compared to 358±65N, respectively. In extension a significant difference was only observed for the Midline placement; the large simulated implant produced a mean force of -101±57N versus -97±57N for the medium simulated implant. In both modes of bending, no trend was observed that suggested one implant to have consistently higher loads.

Sagittal plane rotation data demonstrated a trend for the simulated large implant to consistently have slightly greater range of motion however, significance was only observed for the Midline placement with 9.0±1.3 degrees of rotation as compared to 8.5±1.3 degrees with a medium simulated implant. During extension, the Midline and Posterior placements showed significant differences in mean sagittal plane rotation; 2.0±0.6 degrees for the large versus 2.1±0.7degrees for the medium and 2.7±0.7degrees for large compared with 2.6±0.1 degrees for medium respectively. No trend was observed between range of motion and different size implants.

Effects of Simulated Implant Placement

Figure 4-4 shows the load mechanics and range of motion graphs comparing center of rotation placements for simulated large and medium size implants. Significant differences are reported between each AP placement and the placement with a star next to the extended line. For example the significant differences observed in the net shear force with the large simulated implant in flexion reports that the LP placement was significantly different from both the LM and LA placements. No significant differences were observed between the LM and LA COR placements. A one-way, repeated measures ANOVA with a SNK multiple comparison test at P=0.05 was used to determine statistical differences. Data tables are presented in Appendix B.

During flexion with the large and medium size simulated implants, the net anterior shear force increased as the COR was positioned posteriorly. For the large size

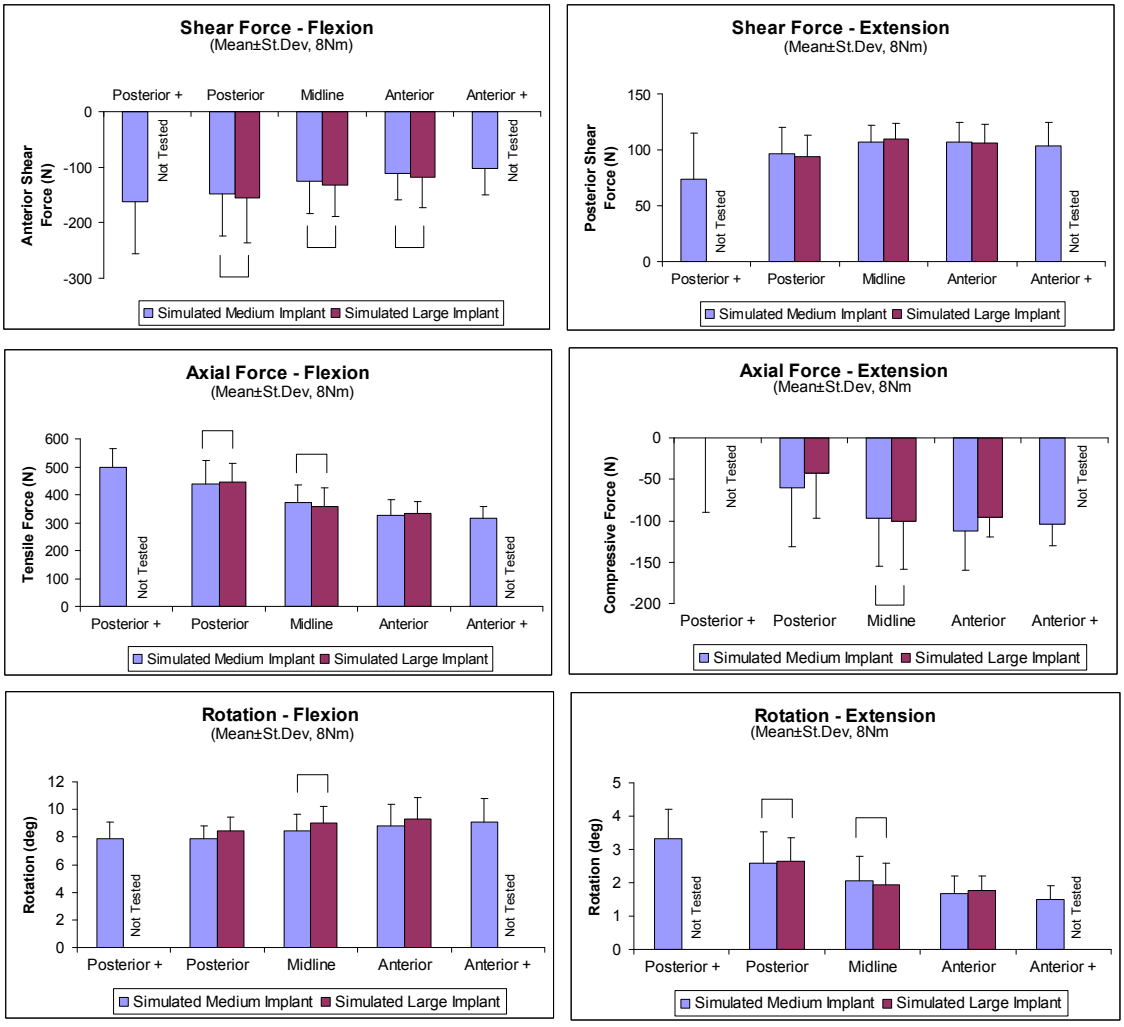

Figure 4-3: **Influence of Simulated Implant Size on Load Mechanics and Sagittal Plane Rotation at Identical AP Placements in Flexion and Extension.** The bars represent significant differences between the two simulated implant sizes.

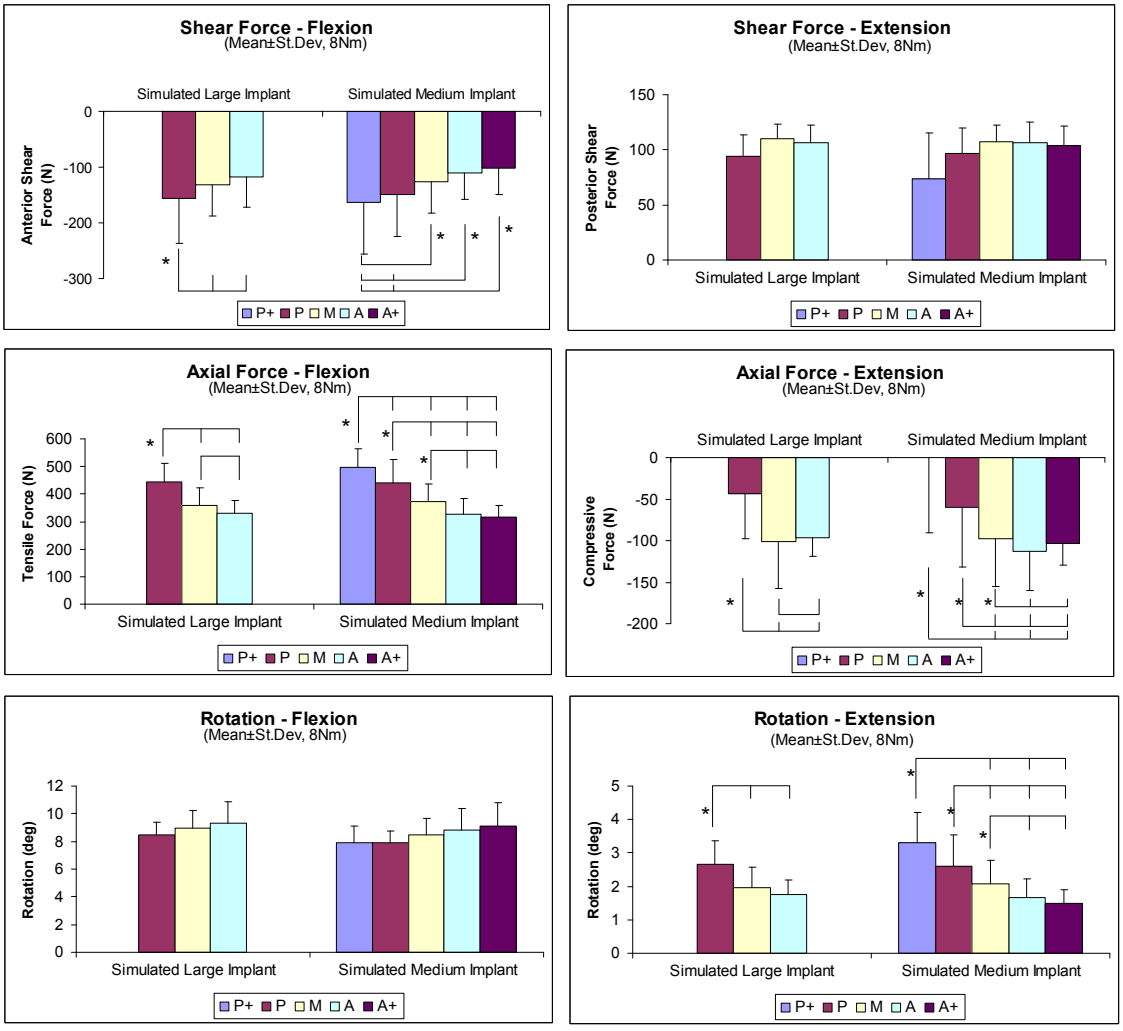

Figure 4-4: **Influence of AP Placement on Load Mechanics and Sagittal Plane Rotation for the Medium and Large Size Simulated Implants in Flexion and Extension.** Significant differences within a group were reported relative to the COR placement associated with the longest bar that has an associated star (*).

implant, significant differences were observed between the Posterior (LP) and both the Midline (LM) and Anterior (LA) COR placements, while for the medium size implant significant differences were typically observed between posterior and anterior placements; where MA+ was significantly different form MP and MP+, MA was significantly different from MP and MP+, and MM was significantly different from MP+. In extension no significant differences were observed in the shear force with either the simulated medium or large size implant.

Axial force was observed to increase as the COR was moved anterior to posterior for both simulated implant sizes during flexion. Significant differences were observed between all COR placements with the simulated large size implant and for all placements for the simulated medium size implant except between simulated placements MA and MA+. During extension significant differences occurred between all three simulated placements for the large size implant, while for the simulated medium size implant, significant differences were observed for all COR placements except between the MP vs. MP+ and MA vs. MA+ positioned CORs. For both simulated sizes axial forces tended to be highest at Midline and Anterior COR locations as opposed to Posterior.

With respect to sagittal plane rotation no significant differences were observed during flexion between any COR placements with both simulated implant sizes, though there appeared to be a slight trend to indicate small steady increases in ROM with the anterior placement of the COR. During extension, there was a trend observed for significantly increased ROM with the posterior placement of the COR. With the large size implant, significant differences were observed between the LP and both LM and MA placements. With the simulated medium size implant, significant difference were seen between all CORs except between the two posterior most (MP+ vs. MP) and two anterior most (MA+ vs. MA) COR placements.

CHAPTER 5: DISCUSSION

It was originally envisioned in this study that comparison of fixed axis rotational data for rotation about an identical COR both with and without the ProDisc-L implant in place would serve as a validation step from which other COR could be simulated. What was learned, however, was that it is not possible to get equivalent loading behavior and range of motion between the two test conditions. The discrepancy in the results can be attributed to a number of factors including tissue pre-tensioning due to surgical placement of the implant itself, implant contact dynamics, constraint parameters, and potential implant mal-alignment.

The effect of tissue pre-tensioning as seen in flexion-extension data in Figure 4-1, was prevalent in all test specimens with a mean axial pre-tension value of 46N over all test specimens. In all cases tensioning of the posterior tissues was initially carried by the implant when in place yielding a net zero starting external loading value. However once the implant was removed, posterior tissue pretension was revealed by an increase in tensile force experienced by the six axis load cell to which the test specimen was coupled and mechanically supported by proximally. The six axis load cell can only resolve net external loads that are acting on the system. Since, the loading sharing between the posterior structures and the implant was an internal load, it confounded comparisons of ProDisc-L versus simulated implant comparisons by altering in an unknown manner both axial and shear loads between the two conditions throughout the full range of rotational movement.

Once mounted within the robotic testing frame and placed under kinematic control of the Spine Robot, the implanted ProDisc-L no longer served the purpose of guiding MSU movement, but rather had a precise movement imposed upon it. This movement was intended to match the COR of the implant exactly, however even a slight mal-alignment between the programmed tool tip and implant COR likely resulted in contact between the implant surfaces that introduced new unknown forces into the test results. Such implant contact dynamics were absent in the simulated implant condition and their involvement could not be predicted. However their presence had a significant impact on the loading behavior of the MSUs. As an example the axial force curve presented in Figure 4-1 indicated the presence of a compressive contact force between implant bearing surfaces that acted in such a way as to reduce the net posterior tissue tensile resistance seen by the load cell, and contributed to the overall net moment by acting in tandem with posterior tissues as a force couple. This result is entirely plausible if implant contact forces occurred anterior to the implant's COR. The consequence of this hidden contact force was a reduction of two degrees in the range of motion. During extension, a similar scenario likely occurred in which contact between implant components generated additional axial and shear forces posterior to the implant COR that further resisted segmental rotation. It is entirely possible that the posterior most edges of the components of the ProDisc-L became engaged during extension and contributed to the net forces generated by the posterior structures. This idea is visually and qualitatively reinforced by the radiographic image in Figure 3-10A, which shows these regions to be in close proximity prior to any extension movement. Posterior positioning of the implant as

preferred by the surgeon resulted in an average increase in specimen lordosis of 7.3±1.7degrees over the harvested intact alignment. Lastly, the protocol used to fine tune the location of the COR with the implant in the MSU had other potential limitations. Mal-alignment of the ProDisc-L in the frontal and transverse planes had the potential to offset the true location of the COR in the sagittal plane.

Thus with respect to ProDisc-L versus simulated implant comparisons it was believed that tests with the ProDisc-L implant in place as a load bearing and potentially constraining structure, as compared to the simulated implant condition where the MSU motion was supported and guided by the robot, were significantly different scenarios from which it was unrealistic and unfeasible to expect MSU mechanics and range of motion in response to fixed COR testing to produce identical results.

In spite of the above conclusion, data from the study demonstrated that the Spine Robot was able to simulate a constrained ball and socket type, like the ProDisc-L, by assuming a pure rotation about a fixed center of rotation with no compressive load. The simulated TDR condition had the capability of demonstrating the motion response of an idealized ProDisc-L and its influence on resulting loading mechanics and range of motion of the MSU as determined by the remaining surrounding native tissue. A key point to be discerned from the results of tests conducted herein was that the force response of the posterior tissue elements quantifies the minimal amounts of load that the ProDisc-L implant would have to endure to perform its function during flexion-extension rotation to an end load limit of 8Nm.

In flexion, greater MSU forces in both the axial and shear directions were observed as the COR was positioned more posteriorly. A more anteriorly located COR would inherently produce a longer lever arm from the COR location to the line of application of the net resultant posterior tissue resistance force, requiring less tissue force to generate a given moment value. As the COR was moved more posterior, the lever arm shortened and required more posterior tissue force to generate the same moment value. In theory a posterior shift should be accompanied by a greater flexion range of rotation since the posterior tissues would need to stretch or become displaced further to generate greater resistance. However, this finding was not observed in the sagittal plane rotational data presented in Figure 4-4, which indicated that the posterior placement of the COR decreased the ROM. Because more posterior placements of the simulated implant required greater disc space distraction to physically accommodate the device, posterior positioning of the COR increased the tensile preloading of the posterior ligaments. This likely had the effect of placing the MSU on a stiffer portion of the stiffness curve as illustrated in Figure 5-1, where the red dots represent loading conditions at the onset of rotation for different COR placements. Positioning the COR anteriorly reduced the tension in the posterior ligaments and thereby increased the neutral zone of rotation.

While the resultant combination of axial and shear force magnitudes varied with different simulated COR placements in flexion, the resultant force angle and the anatomical location of the resultant force did not. Using force and moment data as well as dimensional data from sagittal plane radiographs, the average resultant force magnitude, orientation, and location were determined. For both the medium and large size simulated

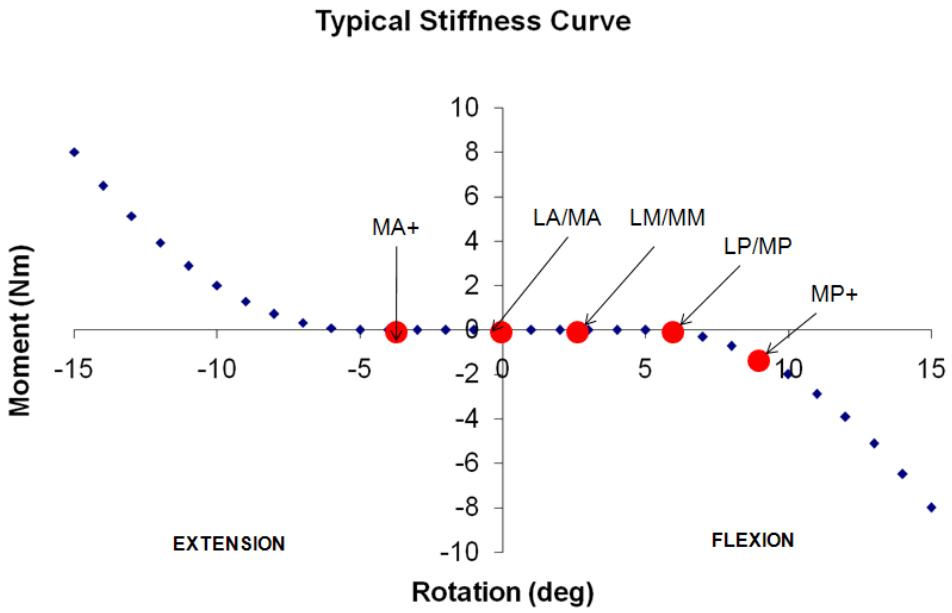

Figure 5-1: **Possible Changes in MSU Stiffness at Various AP Placements.** The anterior positioning of the COR increased the neutral zone ROM for flexion and decreased it for extension.

CORs, the resultant force angle was angled approximately 250 degrees as shown in Table 5-1. Taking into account that the average offset distance for the posterior and anterior points relative to midline were approximately 2.5mm, and 1.5mm between the posterior (MP and MP+) and anterior (MA and MA+) most points, it can be concluded the resultant force vector for each simulated point was located around the same anatomical location. In fact, the variation in the location of the resultant force vector between different simulated points was less than the standard deviation of the resultant force vector location within the same simulated point. This suggests that at the end limit of load, the same posterior structures were recruited.

In extension, MSU ROM significantly increased while axial compressive resistance force measured tended to be highest at the midline and anterior COR locations. Following the above discussed interrelationship between resistance force and lever arm length it would be similarly expected in extension that a more posterior COR would result in a higher observed posterior resistance force. However, in the posterior most COR locations for both the large and medium size simulated implant locations the axial force recorded was minimal. Referring to Table 5-1 it is seen that unlike flexion, the average resultant force vectors changed in magnitude, orientation and location with A-P changes in COR placement. More posterior COR locations tended to: (1) change the angle of the resultant force from a more posterior-distal directed force to purely a posterior oriented force (as viewed/experienced by the proximal vertebral body) and (2) to move the vector itself to a more posterior location away from the COR. This would have the effect of increasing the lever arm between the resultant force vector and COR, requiring less force to achieve the 8Nm moment end limit.

It is plausible that the increased ROM with a more posterior COR was the result of reduced facet resistance to rotation either through an uncoupling of the facet joints due to increased disc space separation with more posterior placement of the implant, and/or an improved alignment of the imposed rotation with the articulating surfaces of the facet joints themselves. However, it is difficult to make concluding statements about the behavior and contact of posterior structures without knowing the contributions from the annular tissue which was preserved during surgery. With extension motion, tensile loading from the annulus could have reduced the net external compressive loads generated by the posterior structures; which would have been even greater with the posterior positioning of the COR, potentially explaining the trend in observed in Table 5-1. It was difficult to determine if the increase in the computed lever arm length between the net resultant force and COR was from tissue structure contact at a position more posterior (for example spinous process contact) or an artifact of the annular tissue contribution.

Limitations of the study included potential errors in the measurements of COR locations from radiographic images due to image distortion, magnification, out of plane views and point selection. Such errors had the potential to affect the placement of the true location of the center of rotation of the implant and instill bias in location of the simulated CORs. Test specimens were constrained in the sagittal plane. All simulations of the ProDisc-L assumed a prefect ball and socket device that maintained full bearing surface contact at all times; however, in vivio, this may not be the case. Lastly, the

Table 5-1: Resultant Force Data at Various Simulated CORs.

Mode of Bending	COR Placement	Resultant Force Magnitude (N)	Resultant Force Angle (deg)	Distance from COR (mm)
Flexion	LP	(477.9 ± 60.5)	(250.3 ± 9.9)	(17.1 ± 2.2)
	LM	(386.6 ± 55.5)	(249.1 ± 9.4)	(21.3 ± 3.3)
	LA	(356.2 ± 34.8)	(250.2 ± 9.7)	(22.8 ± 2.3)
	MP+	(531.9 ± 58.3)	(251.5 ± 10.3)	(14.7 ± 2.6)
	MP	(468.9 ± 82.1)	(250.7 ± 9.1)	(17.6 ± 3.2)
	MM	(398.3 ± 54.6)	(250.8 ± 8.9)	(20.6 ± 2.9)
	MA	(349.7 ± 47.5)	(250.8 ± 8.6)	(23.4 ± 3.1)
	MA+	(335.4 ± 36.5)	(251.8 ± 8.9)	(24.4 ± 2.6)
Extension	LP	(114.2 ± 19.4)	(19.2 ± 9.9)	(72.6 ± 14.5)
	LM	(153.0 ± 15.4)	(39.8 ± 13.8)	(55.8 ± 12.2)
	LA	(144.8 ± 16/2)	(41.8 ± 9.6)	(56.6 ± 6.9)
	MP+	(113.1 ± 25.0)	(0.15 ± 51.8)	(73.9 ± 14.3)
	MP	(127.4 ± 41.9)	(23.3 ± 34.8)	(68.2 ± 18.6)
	MM	(149.3 ± 45.2)	(39.5 ± 14.7)	(57.2 ± 12.5)
	MA	(157.6 ± 40.5)	(-44.9 ± 11.4)	(53.6 ± 10.8)
	MA+	(148.4 ± 23.6)	(44.8 ± 9.8)	(55.4 ± 8.6)

Note: The net resultant forces measured on the proximal vertebral body. The Cartesian coordinate system was oriented to coincide with the L4-L5 disc angle, where the shear force was along the superior endplate of the inferior vertebral body and the axial force was perpendicular to the endplate.

response of the native tissues to simulated COR placements considered only passive response from the spine. No effort was made to simulate muscle activity or the effects of external loads.

CHAPTER 6: CONCLUSION

The original approach undertaken in this study to validate loading mechanics and range of motion of the lumbar MSU with a simulated implant as compared to the ProDisc-L device proved unfeasible and invalid. However, the fixed rotational axis testing protocol was able to simulate a constrained ball and socket device and determine the influence of implant size selection and surgical placement on the load mechanics and range of motion on remaining surrounding tissue. The results of this study suggested that both the medium and large size implant (with 10mm inlay height and 6 degree lordosis) will equally tend to further distract the intervertebral disc space and provide significantly increased range of motion in extension at the expense of increased loads on posterior ligaments in flexion with the posterior placement of the TDR.

The long term effects of increased tissue tension on the posterior ligaments are presently unknown and one should be cautious in clinically interpreting the results of this study. In flexion there was a trend for increased range of motion of approximately 0.5 degrees with selection of the large size implant over the medium at identical placements, with significance occurring at the Midline placement. A trend also existed for slightly reduced motion in flexion with increasing posterior placement of the implant for the both the medium and large size implants. The trend was without significance and may have been an artifact due to unforeseen and uncontrolled differences in neutral zone range of motion between different tests. Future studies should incorporate a consistent method of neutral zone identification and start position with respect to sagittal plane rotation.

The data presented herein measured the effects of COR placement on remaining native MSU tissue only. It would be of considerable interest to correlate the findings of the current study with clinical data, measurements, and outcomes from patients who have had the ProDisc-L implanted by Dr. Bertagnoli.

For future work, the use of a multi-axis load cell at region of the disc space to measure directly the loads experienced by the implant in response to external loading is suggested. Alternately the UT Spine Robot could be programmed to apply known external loads to the MSU with the ProDisc-L in place. The resulting path of the MSU in response to the load could be recorded and played back with the implant removed. The differences in axial and shear force data between these two tests would represent the force carried by the ProDisc-L for the given external load conditions. With respect to the current study the spared annular tissue from the lateral portions of the vertebral body could be removed and specimens retested to determine their contributions to both the load mechanics and range of motion. This data would be of significant clinical interest to surgeons who currently question the biomechanical benefit of sparing annular tissue in such procedures. It would also answer the question as to whether or not tissue contact and net tissue resistance moves more posterior with posterior TDR placement in extension. This data would provide further insight on the influence of COR placement with the MSU as a whole. It would likewise be beneficial to perform tests under video fluoroscopy to better determine the behavior of the implant and posterior structures in various modes of bending.

LIST OF REFERENCES

1. Adams M., Bogduk N., Burton K., and Dolan P. The Biomechanics of Back Pain. London: Elsevier Science Limited, 2002.

2. Deyo R., Mirza S., and Martin B. Back Pain Prevalence and Visit Rates: Estimates from U.S. National Surveys, 2002. Spine 2006; 31(23): 2724-2727.

3. Croft PR., Papageorgious AC., Thomas E., et al. Short-term Physical Risk Factors for New Episodes of Low Back Pain: Prospective Evidence from South Manchester Back Pain Study. Spine 1999; 24: 1556-1561.

4. Freburger J., Holmes G., Agans R., et al. The Rising Prevalence of Chronic Low Back Pain. Archives of Internal Medicine 2009; 169(3):251-258.

5. Volinn, E. The Epidemiology of Low Back Pain in the Rest of the World: A Review of Surveys in Low- and Middle-Income Countries. Spine 1997; 22(15): 1747-1754.

6. Hills E. (2009, November 19). Mechanical Low Back Pain. Retrieved February 10 2010, from EMedicine website: http://emedicine.medscape.com/article/310353 - overview.

7. de Kleuver M., Oner FC., and Jacobs, WCH. Total Disc Replacement for Chronic Low Back Pain: Background and a Systematic Review of Literature. European Spine Journal 2003; 12: 108-116.

8. de Schepper E., Damen J., van Meures JB., et al. The Association between Lumbar Disc Degeneration and Low Back Pain: The Influence of Age, Gender, and Individual Radiographic Features. Spine 2010; 35(5): 531-536.

9. Pye SR., Reid DM., Adams JE., et al. Radiographic Features of Lumbar Disc Degeneration and Self-Reported Back Pain. Journal of Rheumatology 2004; 31(3): 753-758.

10. Cheh G., Birdwell K., Lenke L., et al. Adjacent Segment Disease Following Lumbar/Thoracolumbar Fusion with Pedicle Screw Instrumentation: A Minimum 5-Year Follow-up. Spine 2007; 32(2): 2253-2257.

11. Levin D., Hale J., and Bendo J. Adjacent Segment Disease Following Spinal Fusion for Degenerative Disc Disease. Bulletin of the NYU Hospital for Joint Diseases 2007; 65(1): 29-36.

12. van Tulder MW., Assendelft WJ., Koes BW., et al. Spinal Radiographic Findings and Nonspecific Low Back Pain. A Systematic Review of Observational Studies. Spine 1997; 22(4): 427-434.

13. Etebar S. and Cahill D. Risk Factors for Adjacent-Segment Failure Following Lumbar Fixation with Rigid Instrumentation for Degenerative Instability. Journal of Neurosurgery. Spine 1999; 90: 163-169.

14. Yang J., Lee J., and Song H. The Impact of Adjacent Segment Degeneration on the Clinical Outcome After Lumbar Spinal Fusion. Spine 2008; 33(5): 503-507.

15. Errico T. Why a Mechanical Disc? The Spine Journal 2004; 4(6S): 151S-157S.

16. Bertagnoli R. and Habbicht H. The ProDisc-L Lumbar Prosthesis. Interactive Surgery 2008; 3(4): 209-213.

17. Cunningham B., Gordon J., Dmitriev A., et al. Biomechanical Evaluation of Total Disc Replacement Arthroplasty: An In Vitro Human Cadaveric Model. Spine 2003; 28(20S): S110-S117.

18. Huang R., Tropiano P., Marnay T., et al. Range of Motion and Adjacent Level Degeneration after Lumbar Total Disc Replacement. The Spine Journal 2006; 6(3): 242-247.

19. Tropiano P., Huang R., Girardi F., et al. Lumbar Total Disc Replacement: Seven to Eleven-Year Follow-up. The Journal of Bone and Joint Surgery 2005; 87: 490-496.

20. Lee C. and Goel V. Artificial Disc Prosthesis: Design Concepts and Criteria. The Spine Journal 2004; 4(6): 290S-218S.

21. Zufelt, NA. A Kinematics-Based Testing Protocol to Study the Mechanics of the Human Lumbar Spine. Master's Dissertation, University of Tennessee Health Science Center at Memphis, 2008.

22. Ullrich P. (2007, May 25). Lower Back Anatomy. Retrieved February 15 2010, from Spine-Health website: http://www.spine-health.com/conditions/lower-back-pain/lower-back-anatomy.

23. White A. and Panjabi M. The Clinical Biomechanics of the Spine. New York: J.B. Lippincott Company, 1990.

24. Rhoades R. and Tanner G. Medical Physiology 2ed. Philadelphia, PA: Lippincott Williams and Wilkins, 2003.

25. Gray, H. Gray's Anatomy 15ed. New York, NY: Barnes & Nobles, 1995.

26. DePalma, A. and Rothman, R. The Intervertebral Disc. Philadelphia, PA: W.B. Saunders Company, 1970.

27. Gilad I. and Nissan M. Sagittal Evaluation of Elemental Geometrical Dimensions of Human Vertebrae. Journal of Anatomy 1985; 143: 115-120.

28. Pintar F., Yoganandan N., Myers T., et al. Biomechanical Properties of Human Lumbar Spine Ligaments. Journal of Biomechanics 1992; 25: 1351-1356.

29. Gillard D. (2005) Basic Disc and Lumbar Anatomy. Retrieved February 10 2010, from ChiroGeek.com website: http://chirogeek.com/000_Disc_Anatomy.htm#T2 _Weighted_Axial.

30. Raj P. Intervertebral Disc: Anatomy-Physiology-Pathophysiology-Treatment. Pain Practice 2008; 8(1): 18-44.

31. Benzel, E. Spine Surgery: Techniques, Complication Avoidance, and Management 2ed. Philadelphia, PA: Elsevier Churchill Livingstone, 1999.

32. Wong, P. Biomechanical Comparison of Lumbar Disc Replacements. Master's Dissertation, University of Tennessee Health Science Center at Memphis, 2009.

33. Rundell S., Auerbach J., Balderston R., et al. Total Disc Replacement Positioning Affects Facet Contact Forces and Vertebral Body Strains. Spine 2008; 33(23): 2510-2517.

34. Pearcy M., Portek I., and Shepherd J. Three Dimensional X-ray Analysis of Normal Movement in the Lumbar Spine. Spine 1984; 9: 294-297.

35. Pearcy M. and Tibrewal S. Axial Rotation and Lateral Bending in the Normal Lumbar Spine Measured by Three-Dimensional Radiography. Spine 1984; 9: 582-587.

36. Dvorak J., Panjabi M., Chang D., et al. Functional Radiographic Diagnosis of the Lumbar Spine: Flexion-Extension and Lateral Bending. Spine 1991; 16(5) 562-571.

37. Yue Y., Bertagnoli R., McAfee P., et al. Motion Preservation Surgery of the Spine: Advanced Techniques and Controversies. China: Saunders Elsevier, 2008.

38. Bogduk N. Clinical Anatomy of the Lumbar Spine and Sacrum. Sydney: Churchill Livingstone, 2005.

39. Zhao F., Pollintine P., Hole, B. et al. Discogenic Orgins of Spinal Instability. Spine 2005; 30(23): 2621-2630.

40. Schneider G., Pearcy M., and Bogduk N. Abnormal Motion in Spondylolytic Spondylolisthesis. Spine 2005; 30(10): 159-164.

41. Tournier C., Aunoble S., Huec C., et al. Total Disc Arthroplasty: Consequence for Sagittal Balance and Lumbar Spine Movement. European Spine Journal 2007; 16: 411-421.

42. Dimnet J., Fischer L., and Carret J. Radiographic Studies of Lateral Flexion in the Lumbar Spine. Journal of Biomechanics 1978; 11:143-150.

43. Rousseau M., Bradford D., Bertagnoli R., et al. Disc Arthroplasty Design Influences Intervertebral Kinematics and Facet Forces. The Spine Journal 2006; 6: 258-266.

44. Crisco J., Chen X., Panjabi M., et al. Optimal Marker Placement for Calculating the Instantaneous Center of Rotation. Journal of Biomechanics 1994; 27(9): 1183-1187.

45. Schmidt H., Heuer F., Claes L., et al. The Relation between the Instantaneous Center of Rotation and Facet Joint Force: A Finite Analysis. Clinical Biomechanics 2007; 23: 270-278.

46. Cossette J., Farfan H., Robertson J., et al. The Instantaneous Center of Rotation of the Third Lumbar Intervertebral Joint. Journal of Biomechanics 1971; 4: 149-153.

47. Haher T., Bergman M., O'Brien M., et al. The Effect of the Three Columns of the Spine on the Instantaneous Axis of Rotation in Flexion and Extension. Spine 1991; 16: S312-S318.

48. McCane B., Abbott H., and King T. On Calculating the Finite Center of Rotation for Rigid Planar Motion. Medical Engineering and Physics 2004. 27(1): 75-79.

49. Challis, J. Estimation of the Finite Center of Rotation in Planar Movements. Medical Engineering and Physics 2001; 23(3): 227-233.

50. Hipp J. Errors in Assessing Intervertebral Rotation from Flexion/Extension X-Rays using Manual Line Drawn Methods. Retrieved February 21, 2010, from Medical Metrics, Inc website: http://www.medicalmetrics.com/pdfs/ Measurement_Errors___Hipp.pdf.

51. Panjabi M. Centers and Angles of Rotation of Body Joints: A Study of Errors and Optimization. Journal of Biomechanics 1979; 12: 911-920.

52. Buckley J., Metzger M., Bradford D., et al. How Accurately Can We Measure the Instantaneous Axis of Rotation? Retrieved June 23, 2008, from The Dynamics of the Human Spine website: http://www.me.berkeley.edu/spine/papers/SAS_IAR_ theory_v3.pdf.

53. DiAngelo DJ. et al. Effect of Single Level Cervical Fusion on Adjacent Segment Compensation. Spine Journal 2004; 4(5): S6-S7.

54. Woltring H., HuHuiskes R., and De Lange A. Finite Centroid and Helical Axis Estimation from Noisy Landmark Measurement in the Study of Human Joint Kinematics. Journal of Biomechanics 1985; 18: 379-389.

55. Pearcy M. and Bogduk N. Instantaneous Axes of Rotation of the Lumbar Intervertebral Joints. Spine 1988; 13: 1033-1041.

56. Lim M., Loder R., Huang R., et al. Measurement Error of Lumbar Total Disc Replacement Range of Motion. Spine 2006; 31: E291-297.

57. Taylor M., Hipp J., Gertzbein S. et al. Observer Agreement in Assessing Flexion-Extension X-rays of the Cervical Spine: with and without the use of Quantitative Measurements of Intervertebral Motion. Retrieved February 21, 2010, from Medical Metrics, Inc website: http://www.medicalmetrics.com/pdfs/ Observer_Agreeement___Taylor.pdf.

58. Cakir B., Richter M., Puhl W., et al. Reliability of Motion Measurements after Total Disc Replacement: the Spike and Fin Method. The European Spine Journal 2006; 15: 165-173.

59. Lee S., Draper E., and Hughes S. Instantaneous Center of Rotation and Instability of the Cervical Spine: A Clinical Study. Spine 1997; 22(6): 641-647.

60. Zhao K., Yang C., Zhao C. et al. Assessment of Noninvasive Intervertebral Motion Measurements in the Lumbar Spine. Journal of Biomechanics 2005; 38(9): 1943-1946.

61. Herkowitz H., Dvorak J., Bell G., et al. The Lumbar Spine 3ed. New York, NY: Lippincott Williams and Wilkins, 2004.

62. Horner H., Phil M., and Urban J. Volvo Award Winner in Basic Science Studies: Effect of Nutrient Supply on the Viability of Cells from the Nucleus Pulposus of the Intervertebral Disc. Spine 2001, 26(23): 2543-2549.

63. Bibby S., Jones D., Ripley R., et al. Metabolism of the Intervertebral Disc: Effects of Low Oxygen, Glucose, and PH on Rates of Energy Metabolism of Bovine Nucleus Pulposus Cells. Spine 2005; 30(5):487-497.

64. Boos N. and Aebi M. Spinal Disorders: Fundamentals of Diagnosis and Treatment. Switzerland: Springer, 2008.

65. Panjabi M. The Stabilizing System of the Spine: Neutral Zone and Instability Hypothesis. Journal of Spinal Disorders 1992; 5:390-396.

66. Fujwara A., Lim T., An H., et al. The Effect of Disc Degeneration and Facet Joint Osteoarthritis on the Segmental Flexibility of the Lumbar Spine. Spine 2000; 25(23): 3036-3044.

67. Gertzbein S., Seligman J., Holtby R., et al. Centrode Patterns and Segmental Instability in Degenerative Disc Disease. Spine 1985; 10: 257.

68. (2007) Low Back Pain. Retrieved February 20, 2010, from American Academy of Orthopedic Surgeons website: http://orthoinfo.aaos.org/topic.cfm?topic=A00348.

69. Panjabi M. et al. Multidirectional Testing of One- and Two- Level ProDisc-L Versus Simulated Fusion. Spine 2007; 32(12): 1311-1319.

70. Ekman P., Moller H., Shalabi A., et al. A Prospective Randomized Study on the Long-term Effect of Lumbar Fusion on Adjacent Disc Degeneration. European Spine Journal 2009; 18(8): 1175-1186.

71. Auerbach J., Jones K., Milby A., et al. Segmental Contribution Toward Total Lumbar Range of Motion in Disc Replacement and Fusion: A Comparison of Operative and Adjacent Levels. Spine 2009; 34(23): 2510-2517.

72. Lehmann T., Spratt K., Tozzi J., et al. Long-term Follow-up of Lower Lumbar Fusion Patients. Spine 1987; 12(2): 97-104.

73. Hayashi T., Arizono T., Fujimoto T., at al. Degenerative Change in the Adjacent Segments to Fusion Site after Posterolateral Lumbar Fusion with Pedicle Screw Instrumentation: A Minimum 4-year Follow-up. Fukuoka Igaku Zasshi 2008; 99(5): 107-113.

74. Lee CS., Hwang CJ., Lee SW., et al. Risk Factors for Adjacent Segment Disease after Lumbar Fusion. European Spine Journal 2009; 18(11): 1637-1643.

75. Penta M., Sandhu A., and Fraser R.D. Magnetic Resonance Imaging Assessment of Disc Degeneration 10 Years after Anterior Lumbar Interbody Fusion. Spine 1995; 20(6): 743-747.

76. Ruan DK. et al. Experimental Intervertebral Disc Regeneration with Tissue-Engineered Composite in a Canine Model. Tissue Engineering 2010. [ahead of print].

77. Sato M. et al. An Experimental Study of the Regeneration of the Intervertebral Disc with an Allograft of Cultured Annulus Fibrosus Cells using a Tissue-Engineering Method. Spine 2003; 28(6): 548-553.

78. Rozen D. et al. Interdiscal Electrothermal Coagulation and Percutaneous Neuromodulation Therapy in the Treatment of Discogenic Low Back Pain. Pain Practice 2005; 5(3): 228-243.

79. Biyani A. et al. Intradiscal Electrothermal Therapy: A Treatment Option in Patients with Internal Disc Disruption. Spine 2003; 28(15S): S8-S14.

80. Davis RJ. and Girardi FP. (eds). Nucleus Arthroplasty Technology in Spinal Care Voluem I: Fundametntal. Minneapolis, MN: Raymedica, LLC, 2006.

81. Tropiano P., Huang R., Girardi F., et al. Lumbar Total Disc Replacement: Seven to Eleven-Year Follow-up. Journal of Bone and Joint Surgery 2005; 87: 490-496.

82. Zigler J. Lumbar Spine Arthroplasty using the ProDisc II. The Spine Journal 2004; 4: 260S-267S.

83. Delamarter R., Fribourg D., Kanim L., et al. ProDisc Artificial Total Disc Replacement: Introduction and Early Results from the United States Clinical Trials. Spine 2003; 28(20S): S167-S175.

84. Demetropoulos C., Sengupta D., Knaub M., et al. Biomechanical Evaluation of the Kinematics of the Cadaver Lumbar Spine Following Disc Replacement with the ProDisc-L Prosthesis. Spine 2010; 35(1): 26-31.

85. Huang R., Girardi F., Cammisa F., et al. Correlation Between Range of Motion and Outcome After Lumbar Total Disc Replacement : 8.6 Year Follow-up. Spine 2005; 30(12): 1407-1411.

86. Kelly, B. A Multiaxis Programmable Spine Robot for the Study of Multibody Spinal Biomechanics Using Real-Time Hybrid Force and Displacement Control Strategies. Doctoral Dissertation, University of Tennessee Health Science Center at Memphis, 2005.

87. Davis RJ., Girardi FP., Cammisa FP., and Hutton WC. (eds). Nucleus Arthroplasty Technology in Spinal Care Volume II: Biomechanics and Development. Minneapolis, MN: Raymedica, LLC, 2006.

88. Sander EJ. Kinematic Demands of Nucleus Arthroplasty Technology. Master's Dissertation, University of Tennessee Health Science Center at Memphis, 2008.

89. Dooris A., Goel V., Grosland N., et al. Load Sharing Between Anterior and Posterior Elements in a Lumbar Motion Segment Implanted with an Artificial Disc. Spine 2001; 26(6): E112-E129.

90. Back Anatomy. Retrieved April 23, 2010 from BigBackPain.com website: http://www.bigbackpain.com/back_anatomy.html.

91. Huang R. The Implication of Constraint in Lumbar Total Disc Replacement. Journal of Spinal Disorders and Techniques 2003; 16(4): 412-417.

APPENDIX A: MSU RADIOGRAPHS

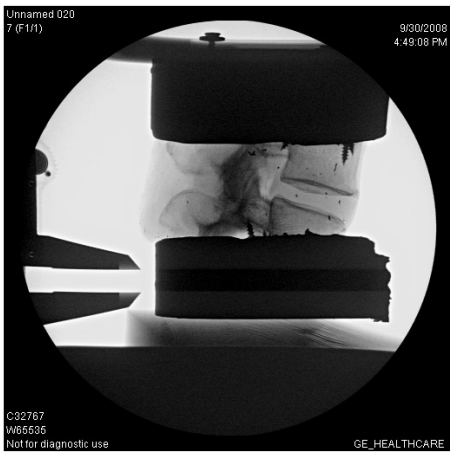

Specimen: PD1

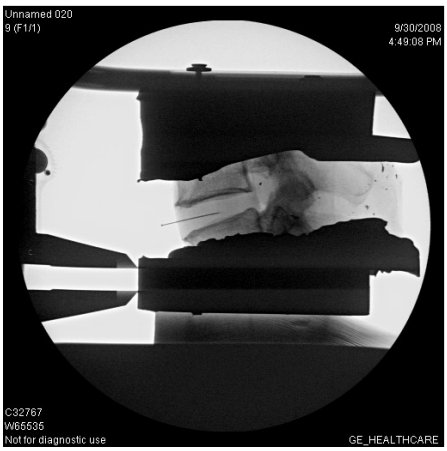

Specimen: PD4

Specimen: PD2

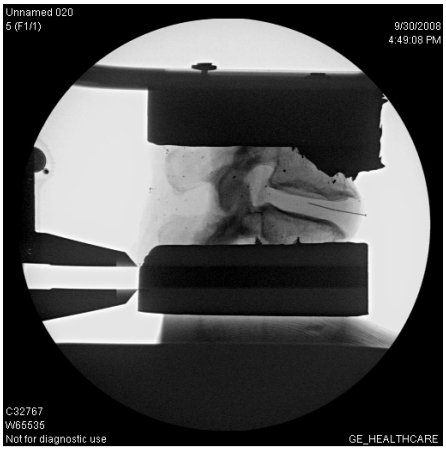

Specimen: PD5

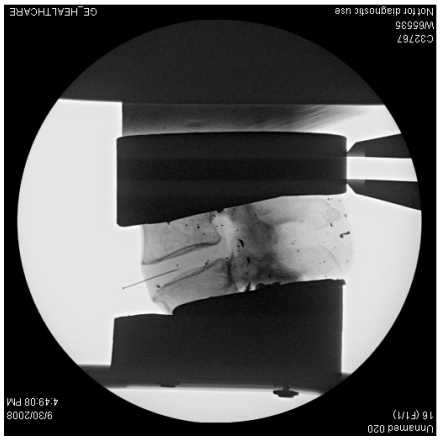

Specimen: PD3

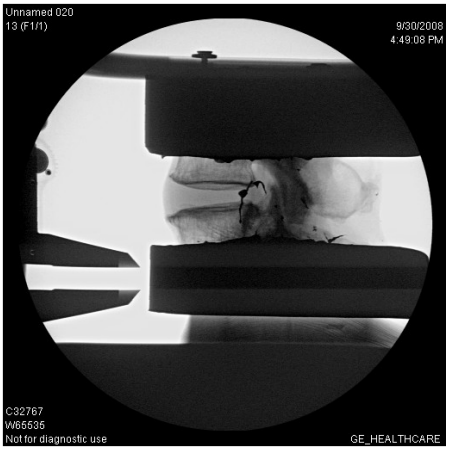

Specimen: PD6

Figure A-1: Harvested MSUs.

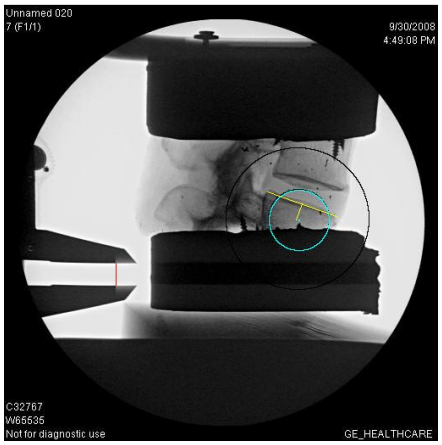

Specimen: PD1

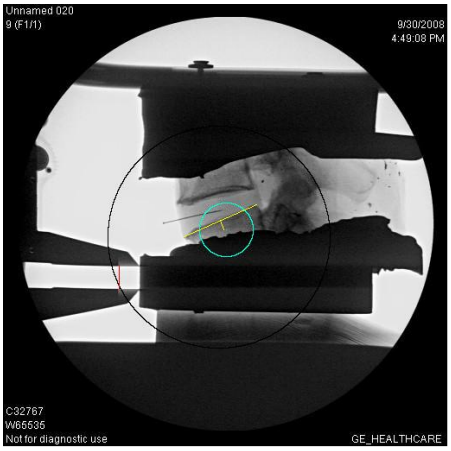

Specimen: PD4

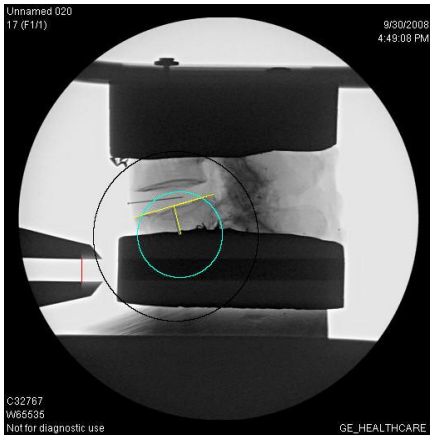

Specimen: PD2

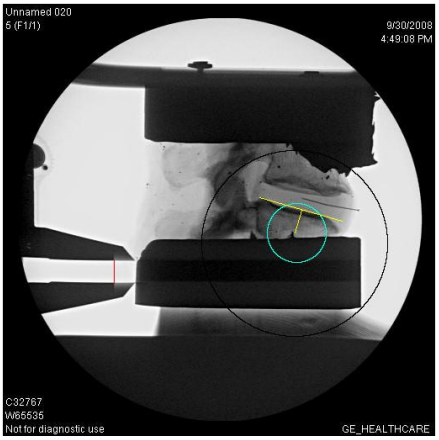

Specimen: PD5

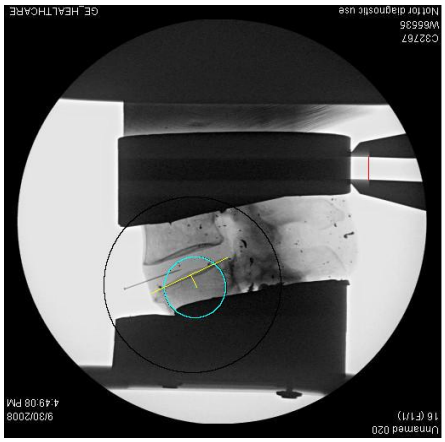

Specimen: PD3

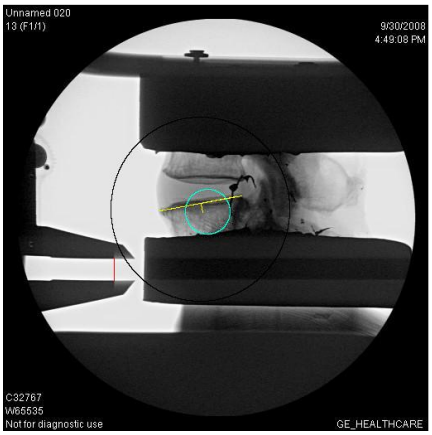

Specimen: PD5

Figure A-2: Harvested MSUs Highlighting the Ideal Placement of the Pro-Disc-L Relative to the Facet Curvature.

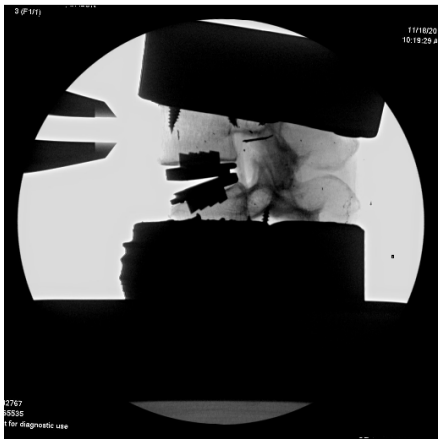

Specimen: PD1

Specimen: PD4

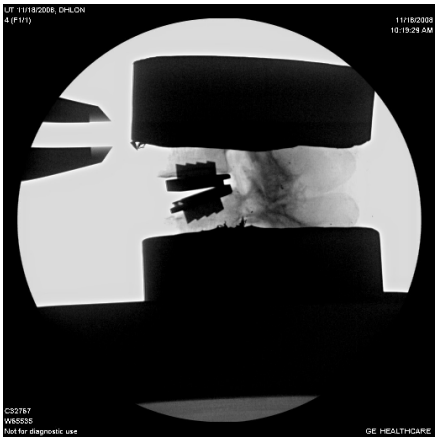

Specimen: PD2

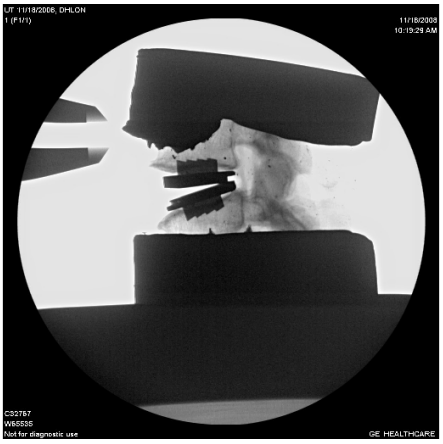

Specimen: PD5

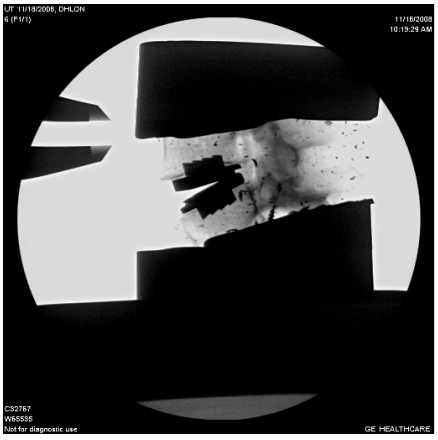

Specimen: PD3

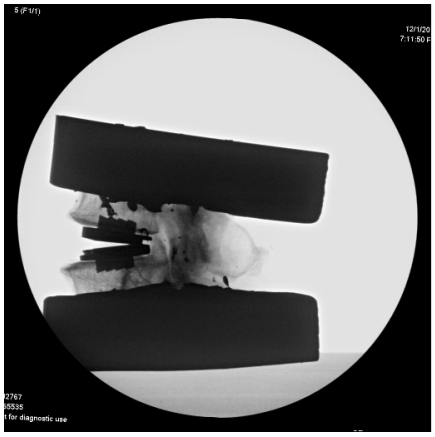

Specimen: PD6

Figure A-3: MSUs Implanted with ProDisc-L TDR.

APPENDIX B: TABULATED DATA

Table B-1: ProDisc-L versus Simulated Implant Data in Flexion.

Condition	Specimen Name	Fx	Fy	Fz	Mx	My	Mz	Pitch
ProDisc-L	518	-90.5	16.9	119.6	5.7	-7.8	0.2	8.4
	UB06J008	-106.9	22.1	166.9	1.3	-8.1	0.7	6.4
	DRT060701	-82.6	-44.6	44.8	3.5	-8.0	0.5	5.1
	UJ04K007	-45.9	51.3	128.2	1.8	-8.0	0.7	6.7
	DRT087036	-57.6	18.2	118.5	3.1	-8.0	3.6	6.2
	DRT050687	-104.1	12.6	121.5	-3.8	-8.0	-2.0	5.8
	Average	-81.3	12.7	116.6	1.9	-8.0	0.6	6.4
	St. Dev	24.8	31.3	39.7	3.2	0.1	1.8	1.1
Simulated Implant	518	-135.8	-19.7	438.6	5.6	-8.1	2.0	9.8
	UB06J008	-188.8	28.6	413.9	-0.1	-8.1	1.0	7.7
	DRT060701	-247.4	-39.7	475.4	-1.1	-8.0	0.2	9.1
	UJ04K007	-32.8	36.3	542.0	-0.2	-8.0	1.4	8.8
	DRT087036	-195.6	16.8	402.4	0.6	-8.0	1.9	7.3
	DRT050687	-142.3	13.9	325.5	-2.6	-8.0	-1.6	6.9
	Average	-157.1	6.0	433.0	0.3	-8.0	0.8	8.3
	St. Dev	73.2	29.5	72.9	2.8	0.0	1.3	1.1

Table B-2: ProDisc-L versus Simulated Implant Data in Extension.

Condition	Specimen Name	Fx	Fy	Fz	Mx	My	Mz	Pitch
ProDisc-L	518	141.9	4.9	-136.1	-0.3	8.0	0.3	2.4
	UB06J008	169.6	6.8	-168.2	1.9	8.1	0.5	3.0
	DRT060701	167.7	-29.9	-102.8	3.0	8.0	0.8	2.0
	UJ04K007	122.6	47.8	-196.3	-0.1	8.2	1.8	2.4
	DRT087036	170.2	16.0	-145.0	1.0	8.1	2.8	1.7
	DRT050687	149.7	12.2	-176.2	1.8	8.0	0.2	1.4
	Average	153.6	9.6	-154.1	1.2	8.1	1.1	2.2
	St. Dev	19.2	24.9	33.2	1.3	0.1	1.0	0.6
Simulated Implant	518	104.6	-8.0	-46.2	1.9	8.0	1.4	3.0
	UB06J008	107.4	6.3	-48.0	0.1	8.0	0.3	3.5
	DRT060701	66.6	-30.7	48.0	0.9	8.0	0.2	2.5
	UJ04K007	80.1	53.0	-88.3	-0.9	8.0	1.7	2.7
	DRT087036	89.9	6.0	-52.0	-0.1	8.0	1.9	1.9
	DRT050687	128.1	5.3	-162.5	2.2	8.0	0.1	1.4
	Average	96.1	5.3	-58.2	0.7	8.0	0.9	2.5
	St. Dev	21.9	27.4	68.3	1.2	0.0	0.8	0.7

Table B-3: Simulated Implant Data for the Large Size Implant at Various AP Placements in Flexion.

Grid Point	Specimen Name	Fx	Fy	Fz	Mx	My	Mz	Pitch	Magnitude	Direction (rad)	Direction (deg)
LP	518	-135.8	-19.7	438.6	5.6	-8.1	2.0	9.8	459.1	1.3	72.8
	UB06J008	-188.8	28.6	413.8	-0.1	-8.1	1.0	7.7	454.9	1.1	65.5
	DRT060701	-251.5	-39.7	473.2	-1.1	-8.0	0.2	8.6	535.9	1.1	62.0
	UJ04K007	-34.2	36.3	540.4	-0.2	-8.1	1.4	8.8	541.5	1.5	86.4
	DRT087036	-170.2	13.2	360.1	0.5	-8.0	1.5	7.4	398.3	1.1	64.7
	DRT050687	N/A	N/A	N/A	N/A	N/A	N/A	N/A	N/A	N/A	N/A
	Average	-156.1	3.8	445.2	0.9	-8.1	1.2	8.5	477.9	1.2	70.3
	St. Dev	80.1	32.5	67.3	2.7	0.0	0.7	1.0	60.5	0.2	9.8
LM	518	-131.3	-21.2	405.8	5.5	-8.1	1.8	10.2	426.5	1.3	72.1
	UB06J008	-149.3	30.7	336.9	-0.7	-8.1	1.0	8.8	368.5	1.2	66.1
	DRT060701	-195.4	-29.3	368.9	-1.4	-8.0	0.0	10.8	417.5	1.1	62.1
	UJ04K007	-25.4	30.3	447.9	-0.1	-8.2	1.2	7.9	448.6	1.5	86.7
	DRT087036	-148.1	8.3	329.7	0.6	-8.0	1.2	8.7	361.5	1.1	65.8
	DRT050687	-140.0	14.4	262.0	-2.5	-8.0	-1.3	7.6	297.0	1.1	61.9
	Average	-131.6	5.5	358.5	0.2	-8.1	0.7	9.0	386.6	1.2	69.1
	St. Dev	56.6	25.5	64.7	2.8	0.1	1.1	1.3	55.5	0.2	9.4
LA	518	-125.8	-21.8	381.7	5.4	-8.1	1.8	10.3	401.9	1.3	71.8
	UB06J008	-124.5	29.0	284.9	-0.8	-8.1	0.9	9.4	310.9	1.2	66.4
	DRT060701	-171.7	-26.7	315.5	-1.5	-8.0	-0.3	11.2	359.2	1.1	61.4
	UJ04K007	-24.6	27.5	372.4	-0.1	-8.1	1.2	7.3	373.2	1.5	86.2
	DRT087036	-140.5	2.1	305.0	0.8	-8.0	1.0	8.4	335.8	1.1	65.3
	DRT050687	N/A	N/A	N/A	N/A	N/A	N/A	N/A	N/A	N/A	N/A
	Average	-117.4	2.0	331.9	0.8	-8.1	0.9	9.3	356.2	1.2	70.2
	St. Dev	55.3	26.3	42.8	2.7	0.0	0.7	1.5	34.8	0.2	9.7

Table B-4: Simulated Implant Data for the Medium Size Implant at Various AP Placements in Flexion.

Grid Point	Specimen Name	Fx	Fy	Fz	Mx	My	Mz	Pitch	Magnitude	Direction (rad)	Direction (deg)
MP+	518	-140.2	-19.2	501.8	5.7	-8.0	2.0	9.2	521.0	1.3	74.4
	UB06J008	-203.3	29.1	475.4	0.4	-8.1	1.3	6.8	517.0	1.2	66.8
	DRT060701	-265.1	-43.9	524.0	0.0	-6.4	0.7	6.5	587.3	1.1	63.2
	UJ04K007	-18.2	34.2	586.7	0.0	-8.0	1.2	8.7	586.9	1.5	88.2
	DRT087036	-188.7	16.8	405.7	0.6	-8.0	1.9	8.3	447.4	1.1	65.1
	DRT050687	N/A	N/A	N/A	N/A	N/A	N/A	N/A	N/A	N/A	N/A
	Average	-163.1	3.4	498.7	1.3	-7.7	1.4	7.9	531.9	1.2	71.5
	St. Dev	92.5	33.7	66.3	2.4	0.7	0.5	1.2	58.3	0.2	10.3
MP	518	-128.5	-18.5	462.2	5.5	-8.1	1.9	9.2	479.7	1.3	74.5
	UB06J008	-183.6	27.7	428.1	0.2	-8.1	1.2	7.1	465.8	1.2	66.8
	DRT060701	-251.1	-39.5	505.1	-0.8	-8.0	0.5	8.3	564.1	1.1	63.6
	UJ04K007	-22.0	33.1	549.9	0.2	-8.0	1.2	8.3	550.3	1.5	87.7
	DRT087036	-164.0	17.4	363.3	0.4	-8.0	1.7	7.7	398.6	1.1	65.7
	DRT050687	-142.3	13.9	325.5	-2.6	-8.0	-1.6	7.0	355.3	1.2	66.4
	Average	-148.6	5.7	439.0	0.5	-8.0	0.8	7.9	469.0	1.2	70.8
	St. Dev	75.4	28.5	84.8	2.7	0.1	1.3	0.9	82.1	0.2	9.1
MM	518	-122.0	-20.0	427.3	5.4	-8.1	1.8	9.5	444.4	1.3	74.1
	UB06J008	-141.5	30.3	348.7	-0.4	-8.2	1.1	8.2	376.3	1.2	67.9
	DRT060701	-194.3	-31.9	393.9	-1.1	-8.1	0.1	10.3	439.2	1.1	63.7
	UJ04K007	-21.2	28.4	449.5	0.3	-8.1	1.1	7.3	450.0	1.5	87.3
	DRT087036	-140.8	15.5	335.5	0.5	-8.0	1.5	8.2	363.9	1.2	67.2
	DRT050687	-136.7	13.9	284.8	-2.5	-8.0	-1.4	7.2	315.9	1.1	64.4
	Average	-126.1	6.1	373.3	0.4	-8.1	0.7	8.4	398.3	1.2	70.8
	St. Dev	57.0	25.9	61.7	2.7	0.1	1.2	1.2	54.7	0.2	8.9
MA	518	-116.4	-20.6	405.0	5.4	-8.1	1.7	9.7	421.4	1.3	74.0
	UB06J008	-113.7	28.6	293.4	-0.6	-8.1	1.0	8.9	314.7	1.2	68.8
	DRT060701	-160.7	-24.9	330.7	-1.5	-8.0	-0.1	11.1	367.7	1.1	64.1
	UJ04K007	-21.6	25.9	372.8	0.2	-8.1	1.1	6.7	373.4	1.5	86.7
	DRT087036	-124.8	6.6	308.0	0.7	-8.0	1.1	9.1	332.3	1.2	67.9
	DRT050687	-129.1	14.7	258.1	-2.3	-8.0	-1.2	7.4	288.6	1.1	63.4
	Average	-111.1	5.1	328.0	0.3	-8.0	0.6	8.8	349.7	1.2	70.8
	St. Dev	46.9	23.0	53.7	2.7	0.0	1.1	1.6	47.5	0.2	8.6
MA+	518	-108.8	-20.6	373.6	5.3	-8.1	1.6	9.8	389.1	1.3	73.8
	UB06J008	-106.2	28.4	276.7	-0.7	-8.2	1.0	9.2	296.4	1.2	69.0
	DRT060701	-148.7	-23.1	295.5	-1.5	-8.1	-0.3	11.3	330.8	1.1	63.3
	UJ04K007	-22.1	25.1	350.2	0.2	-8.1	1.1	6.5	350.9	1.5	86.4
	DRT087036	-122.3	2.0	284.7	0.8	-8.0	0.9	8.7	309.9	1.2	66.7
	DRT050687	N/A	N/A	N/A	N/A	N/A	N/A	N/A	N/A	N/A	N/A
	Average	-101.6	2.3	316.1	0.8	-8.1	0.9	9.1	335.4	1.3	71.8
	St. Dev	47.5	24.3	43.1	2.6	0.1	0.7	1.7	36.5	0.2	9.0

Table B-5: Simulated Implant Data for the Large Size Implant at Various AP Placements in Extension.

Grid Point	Specimen Name	Fx	Fy	Fz	Mx	My	Mz	Pitch	Magnitude	Direction (rad)	Direction (deg)
LP	518	104.6	-8.0	-46.2	1.9	8.0	1.4	3.0	114.3	0.4	23.9
	UB06J008	108.9	6.3	-49.1	0.1	8.1	0.3	3.5	119.5	0.4	24.3
	DRT060701	66.6	-30.7	48.0	0.9	8.0	0.2	2.5	82.1	-0.6	-35.8
	UJ04K007	81.1	53.3	-89.5	-0.9	8.1	1.7	2.8	120.8	0.8	47.8
	DRT087036	108.9	8.4	-78.7	-0.4	8.1	1.4	1.6	134.4	0.6	35.8
	DRT050687	N/A	N/A	N/A	N/A	N/A	N/A	N/A	N/A	N/A	N/A
	Average	94.0	5.9	-43.1	0.3	8.1	1.0	2.7	114.2	0.3	19.2
	St. Dev	19.2	30.8	54.2	1.1	0.0	0.7	0.7	19.4	0.6	32.3
LM	518	104.4	-8.2	-52.3	1.9	8.0	1.3	2.7	116.8	0.5	26.6
	UB06J008	115.6	9.1	-92.4	-0.8	8.1	0.3	2.4	148.0	0.7	38.6
	DRT060701	115.5	-13.9	-49.3	-0.6	8.2	-0.1	1.8	125.6	0.4	23.1
	UJ04K007	86.0	51.8	-109.6	-1.4	8.1	1.8	2.3	139.3	0.9	51.9
	DRT087036	111.4	6.4	-94.6	-0.4	8.0	0.9	1.4	146.1	0.7	40.3
	DRT050687	126.6	6.3	-206.6	2.4	8.2	0.3	1.1	242.3	1.0	58.5
	Average	109.9	8.6	-100.8	0.2	8.1	0.8	1.9	153.0	0.7	39.8
	St. Dev	13.8	23.1	57.2	1.5	0.1	0.7	0.6	45.4	0.2	13.8
LA	518	104.3	-8.0	-56.6	1.9	8.1	1.2	2.4	118.6	0.5	28.5
	UB06J008	110.2	11.3	-101.8	-0.9	8.1	0.4	1.4	150.0	0.7	42.7
	DRT060701	123.9	-17.9	-99.5	-1.6	8.1	-0.5	1.9	159.0	0.7	38.8
	UJ04K007	80.2	49.3	-115.6	-1.5	8.2	1.9	1.7	140.8	1.0	55.2
	DRT087036	112.5	4.1	-107.6	-0.3	8.1	0.6	1.4	155.7	0.8	43.7
	DRT050687	N/A	N/A	N/A	N/A	N/A	N/A	N/A	N/A	N/A	N/A
	Average	106.2	7.7	-96.2	-0.5	8.1	0.7	1.8	144.8	0.7	41.8
	St. Dev	16.2	25.8	23.0	1.4	0.1	0.9	0.4	16.2	0.2	9.6

Table B-6: Simulated Implant Data for the Medium Size Implant at Various AP Placements in Extension.

Grid Point	Specimen Name	Fx	Fy	Fz	Mx	My	Mz	Pitch	Magnitude	Direction (rad)	Direction (deg)
	518	105.8	-9.8	-36.0	2.0	8.0	1.4	3.7	111.8	0.3	18.8
	UB06J008	88.1	4.4	-2.8	1.2	8.1	0.3	4.3	88.1	0.0	1.8
	DRT060701	1.1	-38.1	155.0	2.1	8.0	0.8	3.3	155.0	-1.6	-89.6
	UJ04K007	82.8	49.9	-64.9	-0.3	8.1	1.5	3.3	105.2	0.7	38.1
MP+	DRT087036	91.1	6.1	-52.8	-0.1	8.1	2.0	1.9	105.3	0.5	30.1
	DRT050687	N/A	N/A	N/A	N/A	N/A	N/A	N/A	N/A	N/A	N/A
	Average	73.8	2.5	-0.3	1.0	8.1	1.2	3.3	113.1	0.0	-0.2
	St. Dev	41.5	31.9	89.9	1.1	0.0	0.6	0.9	25.0	0.9	51.8
	518	106.3	-9.5	-46.9	2.0	8.1	1.3	3.2	116.1	0.4	23.8
	UB06J008	102.8	5.9	-47.7	0.2	8.1	0.3	3.8	113.3	0.4	24.9
	DRT060701	59.5	-31.3	57.5	1.2	8.0	0.1	2.7	82.8	-0.8	-44.0
	UJ04K007	80.7	52.1	-83.8	-0.7	8.1	1.6	3.0	116.3	0.8	46.1
MP+	DRT087036	102.1	8.0	-78.4	-0.3	8.1	1.6	1.6	128.7	0.7	37.5
	DRT050687	128.1	5.3	-162.5	2.2	8.0	0.1	1.4	206.9	0.9	51.7
	Average	96.6	5.1	-60.3	0.8	8.1	0.9	2.6	127.4	0.4	23.3
	St. Dev	23.6	27.4	71.5	1.2	0.0	0.8	0.9	41.9	0.6	34.8
	518	105.9	-8.6	-52.1	1.9	8.1	1.3	2.9	118.1	0.5	26.2
	UB06J008	111.8	7.8	-89.6	-0.7	8.0	0.3	2.6	143.3	0.7	38.7
	DRT060701	111.0	-14.9	-41.6	-0.5	8.1	-0.1	2.0	118.5	0.4	20.5
	UJ04K007	80.5	51.1	-109.0	-1.2	8.1	1.8	2.4	135.5	0.9	53.6
MP+	DRT087036	109.0	7.8	-89.9	-0.4	8.0	1.1	1.4	141.3	0.7	39.5
	DRT050687	125.6	5.9	-202.9	2.3	8.1	0.3	1.1	238.7	1.0	58.2
	Average	107.3	8.2	-97.5	0.2	8.1	0.8	2.1	149.2	0.7	39.5
	St. Dev	14.8	23.1	57.5	1.5	0.0	0.7	0.7	45.2	0.3	14.7
	518	104.5	-8.3	-55.2	1.9	8.0	1.2	2.6	118.2	0.5	27.9
	UB06J008	107.5	9.8	-99.2	-0.8	8.1	0.4	1.6	146.3	0.7	42.7
	DRT060701	123.6	-18.9	-102.1	-1.7	8.1	-0.5	1.6	160.3	0.7	39.6
	UJ04K007	73.9	47.8	-113.3	-1.3	8.1	1.9	1.9	135.3	1.0	56.9
MP+	DRT087036	108.4	4.6	-104.4	-0.4	8.0	0.7	1.4	150.4	0.8	43.9
	DRT050687	122.8	7.0	-200.2	2.2	8.3	0.4	1.0	234.8	1.0	58.5
	Average	106.8	7.0	-112.4	0.0	8.1	0.7	1.7	157.6	0.8	44.9
	St. Dev	18.0	22.7	47.6	1.7	0.1	0.8	0.5	40.5	0.2	11.4
	518	103.3	-8.1	-60.4	1.8	8.0	1.1	2.1	119.6	0.5	30.3
	UB06J008	105.3	10.7	-105.1	-0.9	8.1	0.4	1.1	148.8	0.8	44.9
	DRT060701	129.9	-22.3	-127.5	-2.2	8.1	-0.9	1.3	182.0	0.8	44.5
	UJ04K007	71.4	46.3	-113.9	-1.4	8.1	1.9	1.7	134.5	1.0	57.9
MP+	DRT087036	108.9	3.8	-113.2	-0.3	8.0	0.4	1.3	157.1	0.8	46.1
	DRT050687	N/A	N/A	N/A	N/A	N/A	N/A	N/A	N/A	N/A	N/A
	Average	103.8	6.1	-104.0	-0.6	8.1	0.6	1.5	148.4	0.8	44.8
	St. Dev	20.9	25.7	25.7	1.5	0.0	1.0	0.4	23.6	0.2	9.8

VITA

Braham Kanwal Singh Dhillon was born in Thatha, Punjab (India) on October 28, 1983. He emigrated to the United States in 1989. Upon moving to Memphis, TN, Braham attended Kirby High School, where he graduated as valedictorian in 2002. Thereafter, he attended Vanderbilt University in Nashville, TN and received his Bachelor's of Engineering degree in Biomedical Engineering in 2006. After a semester of traveling and finding himself, Braham decided to return to engineering and enrolled in the Graduate Program in Biomedical Engineering and Imaging at the University of Tennessee Health Science Center. Under the guidance of Dr. Brain Kelly, Braham earned his Master of Science Degree in Biomedical Engineering in the spring of 2010.